REVIEW

Functional Fibers and Functional Fiber-Based Components for High-Power Lasers

Xiao Chen[1] · Tianfu Yao[1] · Liangjin Huang[1] · Yi An[1] · Hanshuo Wu[1] · Zhiyong Pan[1] · Pu Zhou[1]

Abstract

The success of high-power fiber lasers is fueled by maturation of active and passive fibers, combined with the availability of high-power fiber-based components. In this contribution, we first overview the enormous potential of rare-earth doped fibers in spectral coverage and recent developments of key fiber-based components employed in high-power laser systems. Subsequently, the emerging functional active and passive fibers in recent years, which exhibit tremendous advantages in balancing or mitigating parasitic nonlinearities hindering high-power transmission, are outlined from the perspectives of geometric and material engineering. Finally, novel functional applications of conventional fiber-based components for nonlinear suppression or spatial mode selection, and correspondingly, the high-power progress of function fiber-based components in power handling are introduced, which suggest more flexible controllability on high-power laser operations.

Keywords High-power laser · Laser fiber · Passive fiber-based component · Functional fiber · Functional fiber-based component

Introduction

Dated from the invention of telecom fiber in 1966 [1, 2], scientists around the world have strived to reduce the propagation loss of silica-based optical fiber as a means to further expand its capability and accessibility [3–7]. The advanced low-loss fiber has sustained optical communication systems to transmit a tremendous amount of information around the world. Furthermore, the optical fiber is not only adopted as a transmission medium, but also for passive components employed in the optical communication system, providing an unparalleled platform for low-loss laser transmission and fiber-based devices.

Although it is a commonplace topic that dates back to the very first fiber designs, high-power laser operation by using this kind of cylindrical waveguide has seen an explosion in activity over the past decades, which is fueled by the superiorities over bulk solid-state lasers for high laser gain, low-loss power delivery, large surface-area-to-volume ratio, and compact system integration. Fiber lasers, however, developed unprosperous because of the limitations imposed by contemporary technology before the invention of double-cladding fiber. Tremendous progress was achieved thanks to the maturity of low-loss optical fiber fabrication technology [4, 5, 8] and the availability of high-brightness semiconductor lasers [9–11]. Remarkably, since the invention of the first cladding-pumped fiber laser exploiting double-cladding neodymium-doped (Nd-doped) fiber [12], the power record of fiber laser has been improved profoundly to 10 kW with a nearly-diffraction-limited beam quality in 2009 [13]. In the past few years, IPG Photonics Inc. announced that single-mode continuous-wave (CW) fiber laser systems of over 20 kW [14] and multimode laser modules of up to 500 kW [15] were commercially available in the market. Besides, benefiting from the versatile energy-level configurations of rare-earth doped fibers, the spectrum range of fiber lasers has covered from the ultra-ultraviolet to the mid-infrared region. Such high output power levels and broadband spectrum operation combined with superior heat dissipation capability lead to a rising scope of fiber laser applications. However, the rapid development implies both opportunities and challenges for high-power fiber lasers (HPFLs), while both

✉ Liangjin Huang
   hlj203@nudt.edu.cn

✉ Pu Zhou
   zhoupu203@163.com

1   College of Advanced Interdisciplinary Studies, National University of Defense Technology, Changsha 410073, China

the optical fiber and the fiber-based components require advanced design and manufacturing.

For optical fibers employed in high-power laser applications, the traditional thin cylindrical structure with a large surface-area-to-volume ratio leads to much attention on parasitic nonlinearities, which limit further power scaling of fiber lasers. Among those, two of the most problematic nonlinearities are nonlinear effects [16–19] (e.g., stimulated Raman scattering (SRS), stimulated Brillouin scattering (SBS) and four-wave mixing effect) and transverse mode instability (TMI) [16, 20–25]. On the one hand, the approaches to mitigate nonlinear effects involve backward pumping [26], seed spectrum filtering [27], temporal stabilizing [28], and novel fiber designs [29–35]. From the point of novel fiber design, routines on modified waveguide structures to enlarge mode area, as well as optimized material compositions to reduce the gain coefficients g_R (Raman gain coefficient) and g_B (Brillouin gain coefficient) [36, 37], have been performed to improve the thresholds of both SRS and SBS effects. On the other hand, the mechanism for suppressing TMI is associated with the minimization of high-order-modes (HOMs) generation, equalizing to ensure an effective single-mode operation through imposing high differential loss on HOMs. Similarly to the efforts to suppress nonlinear effects, approaches for TMI suppression can also be achieved by utilizing either special fiber structures (trench-assisted fibers [34, 38–42] and resonance-coupled fibers [29, 43–45], etc.) or an appropriate choice of fiber materials [37] by combining elements with negative and positive values of thermo-optic coefficient dn/dT.

Besides, it is of great importance to build all-fiberized formats for lasers and amplifiers, where all bulk optical components are replaced with passive fiber-based components. All-fiber construction makes the laser system simpler, more robust, immune to external factors, and more convenient to maintain a good beam quality as the signal laser is confined tightly in the high-index core zone during the amplification process. Driven by the demands of existing and possible applications, the operating power of all-fiberized laser source has reached multi-kilowatt level with an excellent good beam quality. In this case, the design and fabrication of passive fiber-based components become more challenging since they have to provide high coupling efficiency at very high-power levels.

Modern scientific and industrial applications put forward higher requirements for fiber lasers, especially for the demands involving multi-parameter manipulation of high-power output. Confined to this framework, laser fibers and fiber-based devices have been expanded from their responsibilities to more diverse dimensions. The traditional function of optical fibers is providing active amplification or passive transmission for signal laser, but some burgeoning subjects seem to extend their functions to spatial or spectral filtering.

Numerous cross-sectional designs have been proposed to tailor the transverse-mode output, driving the fiber in the form of a transverse beam shaper to obtain robust single-mode output or higher-order customized output, even with very large core diameters.

On the other hand, inner-fiber modulation within the fiber core is also feasible by introducing dimensional variation along the longitudinal direction. Specially, some passive components began to break their original definition of laser manipulation. For example, the function of fiber grating has gradually evolved to spatial filtering rather than merely providing intracavity resonance, which induces new interest in the functional integration of intracavity devices. Some passive components that have traditionally been considered to operate only at low-power levels, such as mode converters or fiber filters, are manifesting emerging prospects for high-power outputs although regulation is applied only at low-power levels. More confidently, advances in fabrication processes have pushed them toward higher power handling capabilities.

In this review, as shown in the overview diagram of Fig. 1, the recent advances in HPFLs and passive fiber-based components serving high-power operations are briefly summarized at first, which are accompanied by pointing out the limitations of parasitic nonlinearities. Then, the concept of **"functionalization"** is introduced to combine the research progress of laser fibers and fiber-based components. Note that all of these improvements based on conventional fibers or devices are designed to eliminate or alleviate the effects of parasitic nonlinearities in fiber lasers. Irrespective of whether parasitic nonlinearities can be completely eliminated or not, most of the functional fibers or fiber-based components point out a new way for the future development of modern fiber lasers. The "functionalization" mentioned here is derived from the ability to functionalize the HPFLs operations, usually referring to the selective control for its spatial mode, spectrum, or linewidth regime. Although the importance of further developments in conventional fibers and devices should be extensively noted, this review highlights the significance of bilateral considerations regarding the future development of laser fibers and fiber-based components. We have tried to make this review comprehensive, but our choices of topics and emphasis will inevitably reflect our own viewpoints and biases.

Brief Overview of High-Power Laser Fibers and Fiber-Based Components

The advent of high-power fiber laser has been a revolutionary force in many applications and quickly replaced other types of bulk lasers. Rare-earth-doped silica fibers have

become ubiquitous as a laser gain medium due to unparalleled advantages of better efficiency, minimum thermal impairment, and high gain extraction. Fiber lasers employing different rare-earth dopants have covered a wide spectrum range of laser emission up to now. Progress in the power handling of fiber-based components for HPFLs, focusing through higher damage threshold and stable reproducibility raise interest in high-power laser generation and propagation. In this section, the enormous potential of laser fibers for broadband spectral coverage is discussed in different wavebands. In addition, the latest advances in the power handling capacity of typical fiber-based components are listed one by one.

Enormous Potential of High-Power Rare-Earth Doped Laser Fibers

Snitzer is credited with pioneering fiber laser development in the 1960s and beyond. His earlier research indicated that using rare-earth doped material for laser amplification within a fiber was possible [116]. On this basis, the successful development of low-loss optical fiber opened the door to creating "new" lasers using various rare-earths elements, such as Ytterbium (Yb), Erbium (Er), Thulium (Tm), Holmium (Ho), Praseodymium (Pr), Dysprosium (Dy), etc.. that could be doped into the glass host readily. The steady advances in optical fiber lasers have been foreseen by the pioneers in optical fiber and lasers 60 years ago, including Maiman (laser) [117], Snitzer (fiber laser) [116, 118], and Kao (optical fiber) [1]. Invention of double-cladding fibers [12] and the rapid deployment of high-power pump modules

triggered unprecedented power scaling of fiber lasers. Thanks to the unique advantages on high-power operation, compact size, long lifetime and uniform fabrication methods, fiber lasers have become indispensable and integrated themselves into a variety of applications, particularly in the fields of defense, industrial cutting, telecommunications and surgery. Figure 2a summarizes the energy level transitions of representative rare-earth ions. As can be seen, given the large number of optical transitions offered by rare-earth-doped materials, high-power laser fibers have demonstrated significant wavelength coverage from the deep-ultraviolet to the mid-infrared region. Along with the continuous expansion of applications, demand on the output power of fiber laser grows synchronously. Because of the various fiber material properties and different readiness levels of the corresponding components in the specialty fibers, fiber lasers with different rare-earth dopants have experienced different development trends. Here, to declare the enormous potential of high-power rare-earth doped laser fibers, several developed fiber lasers with power records based on different dopants are listed for a glance.

Records for Laser Fibers Operating at 1–2 μm (Near-Infrared Region)

Regarding the power scalability of fiber lasers, the Yb^{3+} ion amongst rare-earth dopants has been a choice of gain dopants for output power and the highest slope efficiency near 1 μm in the form of Yb-doped fibers. There are a few reasons related to this success. First, the quantum efficiency of Yb-doped fiber laser is close to 100% due to the low
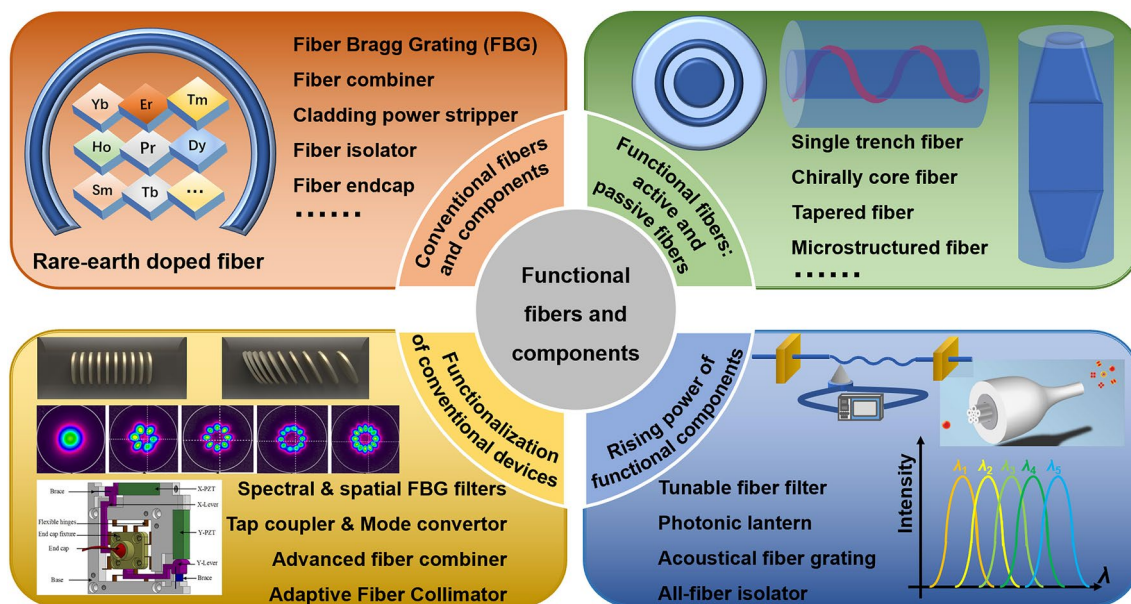

Fig. 1 An overview of the main subjects discussed in this review

energy difference between the pump photon and the laser photon. Second, due to the simplest energy level structure of Yb^{3+} ions between $^2F_{5/2}$ a $^2F_{7/2}$, as illustrated in Fig. 2a, the possibilities of any amphibolous energy transfer, any quenching process and any excited state absorption processes are reduced. Therefore, the doping concentration of Yb^{3+} ions could be very high in Yb-doped fibers. Moreover, the Yb^{3+} ion possesses a broadband absorption spectrum spanning from ~ 850 to ~ 1080 nm, especially the high absorption section in the range of 915–980 nm. This high quantum efficiency in conjunction with the available pump sources enables the power level of the Yb-doped fiber laser to exceed multi-kilowatts with near-diffraction-limited beam quality.

Power records of HPFLs are mostly realized by Yb-doped fibers operating at ~ 1 µm. In recent 20 years, the recording power of CW ytterbium-doped fiber lasers (YDFLs) with diffraction-limited beam quality has experienced an exponential increase. In Fig. 2b and c, the power evolution trends of some representative results for all-fiber laser oscillators and amplifiers operating at ~ 1 µm are summarized, respectively. In 2009, IPG Photonics reported the first cascaded pumped Yb-doped fiber amplifier with an output power of 10 kW operating at a near-diffraction-limited profile [13]. They further increased the maximum power to 20 kW [14], which dominates the maximum power record of near single-mode fiber lasers up to now, although this record can be dated to 10 years ago. Commercial multimode products with 100 kW [119] or even 500 kW [15] power levels are also available at present. It should be noted that functional fibers, e.g., confined fibers and tapered fibers, have played a key role for high-power laser generation in recent years, as illustrated in Fig. 2b and c. As can be seen, the power level that functional fibers can reach is very close to conventional step-index laser fibers. For example, the highest power record of fiber oscillator is created by functional confined fibers at present [59], as depicted by the data sample of 8 kW in Fig. 2b. For fiber amplifiers employing functional laser fibers, the power level of ~ 8 kW or even ~ 10 kW is also achievable with beam quality maintenance [68]. Consequently, the pivotal potential of functional fibers discussed in this review should not be ignored. Furthermore, fiber lasers operating at special wavelengths (e.g., 980 nm, 1007 nm, 1018 nm, and 1150 nm) have also attracted significant interest since they are very useful for nonlinear frequency conversion and efficient pumping on other rare-earth (e.g., Er^{3+}, Tm^{3+}, Ho^{3+}) doped fibers which have absorption bands located in this range. For example, IPG Photonics reported a 1.3 kW 1018 nm fiber laser with the beam quality M^2 less than 1.1 [120]. Recently, the efficiency of Yb-doped all-solid photonic bandgap fiber laser operating at approximately 978 nm has been improved to more than 60% with a recording power of 151 W and an excellent beam quality [121].

Er-doped fibers have an emission waveband spanning from ~ 1480 to ~ 1620 nm which is located in the transparency band of atmospheric window. In the field of optical communication, Er-doped fibers have constituted the cornerstone of long-distance optical fiber networks and become a necessary component in modern systems due to their emission window overlapping the lowest loss region (~ 1550 nm) in silica fibers. However, compared with Yb-doped fibers, the power scaling of Er-doped fiber laser is limited by smaller absorption cross section and lower doping concentration of Er^{3+} ion. Generally, the doping concentration of Er^{3+} ion is limited by clustering effect. Moreover, the power of multimode pump LD for Er-doped fibers is lagging behind their counterparts for Yb-doped fibers. In Fig. 2d, the power scaling schedule of Er-doped or Er-Yb-co-doped laser fibers for ~ 1.5 µm operation is illustrated for a glance. To date, the highest power achieved by pure Er-doped large-mode-area fiber was 656 W with a relatively multimode operation (M^2 ~ 10.5) [95]. To overcome the clustering effect, the co-doping strategy is often adopted to improve the laser efficiency by incorporating Yb^{3+} ions into the host glass. As a result, a new record of 302 W single-mode output from a fiber amplifier with a charming optical efficiency of 56% has been demonstrated [96]. Other issues for Er-doped fibers are that the possible up-conversion mechanism may lead to unwanted emission in the visible waveband, and the possible non-radiative relaxation would generate excess heat load. In this case, employing cascade pumping strategy is a technical means to achieve further power enhancement. However, during the fabrication process, the concentration ratio of Er^{3+} and Yb^{3+} ions should be carefully balanced.

Fiber laser sources working at 2 µm cover a wide spectrum of application fields, including the "eye-safe" lidar, free-space communications for satellites and material processing, etc. Particularly, Tm^{3+} and Ho^{3+} ions are the most successful fiber dopants that provide high optical gain at ~ 2 µm, corresponding to the transitions of $^3F_4 \rightarrow {}^3H_6$ (Tm^{3+}) and $^5I_7 \rightarrow {}^5I_8$ (Ho^{3+}) in Fig. 2a. Compared with conventional Yb-doped fibers, core mode area of fibers at 2 µm is four times that of the core mode operating at ~ 1 µm, thus indicating a prominent advantage in mitigating the nonlinear effects. In Fig. 2e, the power scaling schedule of Tm-doped laser fibers for ~ 1.5 µm operation is illustrated for a glance. On the basis of cladding-pump technology, high-power multimode LDs at 790 nm and highly Tm-doped fibers, the output power of HPFLs exploiting Tm-doped fibers has exceeded the power level of Er-doped fibers gradually and a kilowatt-level output [102] has been achieved as early as 2010, representing the highest CW output power produced by Tm-doped fiber reported publicly currently. In 2018, a Tm-doped chirped pulse amplifier system with a record average power of up to 1150 W and the peak power of more than 5 GW was demonstrated, which brings exciting prospects for
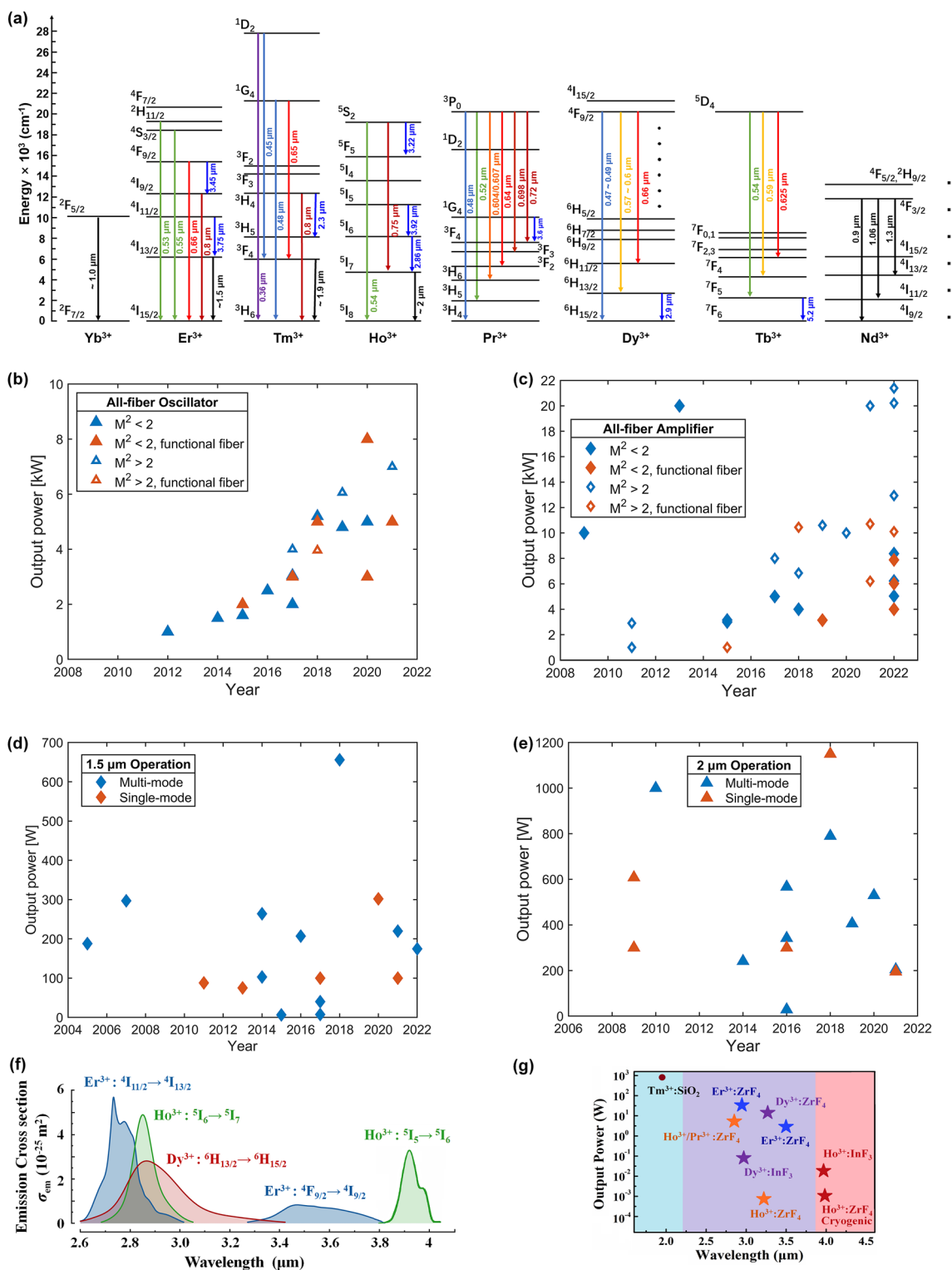
Fig. 2 **a** Schematical diagram of energy level transitions for some representative rare-earth ions. **b–e** Power evolution trends of some representative results for **b** all-fiber laser oscillators operating at ~ 1 μm [46–63], **c** all-fiber laser amplifiers operating at ~ 1 μm [13, 14, 16–19, 35, 64–83], **d** all-fiber Er-doped lasers and Er-Yb-co-doped lasers operating at ~ 1.5 μm [78–99], **e** all-fiber Tm-doped lasers operating at ~ 2 μm [94–113]. **f** Emission cross sections of Er^{3+}, Ho^{3+} and Dy^{3+} ions in mid-infrared waveband [114]. **g** Recent progress of mid-infrared fiber lasers operating at 3–5 μm; Reproduced with permission from Ref. [115], Copyright 2018, Optical Society of America. (© 2018 Optical Society of America under the terms of the OSA Open Access Publishing Agreement)

the generation of multi-kilowatt laser based on Tm-doped fibers [108]. Being a growing technology, the development of 2 µm fiber lasers is hindered by several factors. For instance, the availability of specialty fibers, the key fiber components, suitable high-power pumping LDs and thermal threat on the fiber polymer coatings [122]. There were several works published recently to address or overcome some of the limitations, including Tm/Ho co-doping of silica fibers [123] or pumping the Ho-doped fiber with an in-band Tm-doped fiber laser [124]. Benefits from the availability of high-power Tm-doped pumping sources at 1.95 µm, recent experiments have demonstrated the single-mode Ho-doped fiber laser providing 407 W of output power [125, 126]. Nevertheless, there is still a lot of room for the further breakthrough of 2 µm fiber lasers and the rare-earth doped fibers with excellent optical properties in this waveband.

Mid-infrared Laser Fibers

Mid-infrared fiber lasers operating at 3–5 µm have essential applications in the fields of remote sensing communication, spectral analysis, national defense. Generally, fluoride glass is the preferred medium for 3–5 µm mid-infrared fibers due to its lower phonon energy [127], broader infrared window and higher solubility for rare-earth ions. Limited by host materials and the rare-earth doping technique, the main dopants that can generate 3–5 µm emission are the trivalent Er^{3+}, Ho^{3+} and Dy^{3+} ions, whose energy levels can be seen in Fig. 2a. Figure 2f shows the emission cross sections of Er^{3+}, Ho^{3+} and Dy^{3+} ions in ZrF_4–BaF_2–LaF_3–AlF_3–NaF (ZBLAN) glass at 2.6–4 µm waveband, corresponding to different energy transitions that include 2.6–3.0 µm and 3.3–3.8 µm for Er-ZBLAN fibers, 2.7–3.05 µm and 3.8–4 µm for Ho-ZBLAN fibers, 2.6–3.3 µm for Dy-ZBLAN fibers. At present, Er-, Ho- and Dy-doped ZBLAN fibers have been widely employed for the generation of 3–4 µm mid-infrared lasers.

Thanks to recent developments of high-quality double-cladding fluoride fibers, high-power InGaAs pumping sources and mature application of grating writing technology, ~ 3 µm mid-infrared fiber lasers employing Er-ZBLAN fibers have been developed rapidly in recent years [122–132]. Through the all-fiberized monolithic fiber laser adopting Er-ZBLAN fiber, robust single-mode operation with an average power of 20 W at 2.825 µm was demonstrated in 2011 [129], showing a slope efficiency of 35.4%. To release the thermal load in the laser cavity, Vincent et al. optimized the grating writing process to reduce the loss at the pump and signal wavelength simultaneously, which further increased the output power of mid-infrared laser to 30.5 W at ~ 2.9 µm [130]. In 2018, a high concentration Er-ZBLAN fiber was reported to generate ~ 2.82 µm laser with a maximum output power of over 41 W [133], which is the

highest power record for mid-infrared fiber lasers operating at near 3 µm at present. As for further power scaling, if the co-doping of Pr^{3+} ion [132, 134] and the tandem pumping strategy using 1.6 µm/2.7 µm lasers [135] are introduced, higher laser efficiency and broader coverage of output wavelength are expected theoretically.

Compared with Er-doped fibers, the energy transition of Ho^{3+} ion has a relatively longer emission range (2.7–3.05 µm) and a lower absorption in the pumped excited state. In 2015, a co-doped Ho/Pr-ZBLAN fiber, pumped by a high-power Raman laser at 1.15 µm, achieved a maximum power of 7.2 W at ~ 2.9 µm [136], which is supposed as the highest mid-infrared output obtained by Ho-doped fiber lasers. Indeed, laser efficiency of Ho-doped fibers at ~ 2.9 µm is passively limited by the dynamics of energy levels in the excited state, and gain saturation effect when the pumping power reaches a certain level. To solve this problem, researchers mainly adopt cascade pumping and co-doping of Pr^{3+} ion, currently.

As for the mid-infrared region beyond 3 µm, the output power, efficiency and beam quality of mid-infrared fibers are still lagging behind other bands [115, 137, 138]. Figure 2g summarizes the recent progress of mid-infrared fiber lasers operating at 3–5 µm; as can be seen, the corresponding output power and efficiency decrease when the wavelength gets longer. In light of current reports, energy transitions that can generate mid-infrared wavelengths longer than 3 µm mainly include $^4F_{9/2} \rightarrow {}^4I_{9/2}$ for Er-doped fibers, $^6H_{13/2} \rightarrow {}^6H_{15/2}$ for Dy-doped fibers, and $^5S_2 \rightarrow {}^5F_5$ or $^5I_5 \rightarrow {}^5I_6$ for Ho-doped fibers. To further improve the output power and laser efficiency in the future, advanced rare-earth doped fibers with new compositions could be considered to expand the mid-infrared emission band.

Visible Laser Fibers

Visible lasers, including the emission waveband from the deep-ultraviolet to the deep-red region, have claimed their critical roles in laser guide star, optical communication, optical imaging spectroscopy and other scientific fields. Before the visible fiber lasers are well developed, nonlinear frequency conversion employing optical crystals is the dominant technology to obtain high-power visible lasers. The emergence of visible fiber lasers largely depends on the success of pump sources and rare-earth doped fibers with abundant transition in the visible region, as the energy levels of Pr^{3+} and Dy^{3+} show in Fig. 2a. At present, visible rare-earth dopants in active fibers mainly concentrate on the Pr^{3+}, Dy^{3+}, Tb^{3+} and Sm^{3+} ions, etc. [139], among which Pr-doped fibers have attracted the highest level of attention due to its wide emission range covering the blue, green, red and orange wavebands. Additionally, Dy^{3+} and Tb^{3+} ions are also potential candidates because of their supplementation

in yellow light emission. Similar to mid-infrared ZBLAN fibers, rare-earth doped fibers operating at visible waveband mainly adopt the fluoride host with lower phonon energy [127], which effectively reduce the non-radiative transition rate of upper energy and improve the visible emission efficiency.

Before the maturity of commercial blue LDs, up-conversion mechanism was the main approach to generating visible laser by converting the near-infrared pump light to visible laser output [139]. As early as 1997, an eccentric double-cladding Pr/Yb-ZBLAN fiber with inner/outer-cladding diameters of 5/125 μm has been employed to generate the red laser emission of up to 1.02 W [140]. To improve the pump absorption, a Pr/Yb-ZBLAN fiber with a larger core diameter of 35 μm, pumped by 850 nm light after beam shaping, was used to obtain a 2.06 W red laser at 635 nm, corresponding to a laser efficiency of 45% [141].

The Nobel Prize in Physics in 2014 awarded the breakthrough of high-power blue light diode [142], which profoundly reflects the significance of visible light laser in future development and has largely promoted the commercialization of blue LDs. As a consequence, the mainstream for direct generation of visible fiber lasers shifted to the down-conversion strategy. In 2009, a waterproof Pr-doped aluminum-fluoride fiber pumped by GaN blue light LD was reported to realize both single wavelength and tunable output at 482 nm, 523 nm, 605 nm, 637 nm and 719 nm [143]. To improve the output power and laser efficiency, Fujimoto et al. further introduced optical coating to reduce the cavity loss and to increase the coupling efficiency of pump power into Pr-doped fiber through extending the core diameter and finally achieved a visible laser output of 645.7 mW [144] and 598 mW [145] at the red band and the green band, respectively. Soon afterward, fundamental studies based on Pr-doped waterproof fluoride fibers in the visible waveband have been increasing remarkably and the output power in the red, green and blue bands has reached over 1.0 W. In 2019, a 2-W single-mode visible laser oscillator (@638 nm) based on the waterproof Pr-doped fiber was reported [146]. Up to now, the highest power record for visible fiber lasers reaches 2.3 W at 635.5 nm [141–149], corresponding to a single-mode spatial mode and a narrow linewidth of 0.16 nm. Further optimization on the laser cavity could result in higher output power approaching the 10-W level according to simulation results. As for the emissions of other colors, the output power of CW fiber laser remains at a relatively lower level, especially for yellow light where the energy level of Pr^{3+} ion is hard to cover. In 2021, the first compact watt-level high-power yellow fiber laser was presented, in which a piece of Dy-ZBLAN fiber was adopted as the gain medium. The maximum output power of 1.12 W at 575 nm was obtained at a pump power of 4.20 W provided by a 450-nm pumping source, which yields a maximum efficiency of 33.6% [150].

Breakthrough of Fiber-Based Components

In addition to the double-cladding fiber and high-power LD technology, high-power pump combination components and laser output devices also support the significant success of compact HPFLs based on all-fiberized structure, which gradually become the key technical units limiting further improvement of HPFLs. General fiber systems are mainly divided into fiber oscillators or amplifiers according to their actual structures, of which the fiber amplifiers have a more complex configuration. Figure 3 concisely represents the basic architecture of a laser system based on the Main Oscillation Power Amplification (MOPA) scheme, consisting of a seed oscillator module and a high-power amplifier module separated by an isolator. The main fiber components contain fiber combiners, fiber grating, isolator, cladding power stripper and output endcap, etc. In this section, the current progress of these key components serving high-power operations is reviewed for a glance.

Fiber Bragg Grating (FBG)

FBG is a kind of Bragg grating with periodic refractive index distribution inscribed directly in the few-mode fiber, which provides effective feedback to certain longitudinal and transverse modes in the laser resonator. Thanks to the development of advanced grating inscribing technology in double-clad photosensitive fibers, high-quality FBGs with stable reproducibility have replaced traditional free-space mirrors for in-cavity resonators, realizing an important step towards the all-fiber integration of fiber lasers. Beyond providing resonance feedback, FBG also has the unique advantage of customizing bandwidth and central wavelength, enabling high freedom in tailoring the longitudinal modes or selecting spatial modes through the oscillation process.

All-fiberized oscillators exploiting dual-end FBGs were developed unprecedentedly in recent years. Since 2015, the power record created by Fujikura Inc. experienced a dramatic increase [48, 51, 52, 59]. To date, the directly generated single-mode laser power from monolithic fiber oscillator based on dual-end FBGs has exceeded ~8 kW [59], where a piece of specially designed active fiber plays a key role. In 2016, Yang et al. demonstrated a 4-kW single-mode monolithic all-fiber oscillator based on the dual-end FBGs inscribed in commercial 25/400 μm Yb-doped fiber as well as the bidirectional pump scheme [55]. Later, the output power was further boosted to exceed 5.2 kW [54] by employing a similar system configuration and remaining the dual-end FBGs. Through writing FBG with femtosecond pulses into one port of the gain fiber, a spatially structured fiber oscillator with an output power of 8 kW was constructed [57]. This achievement demonstrates the prospect of FBGs inscription with femtosecond laser in improving
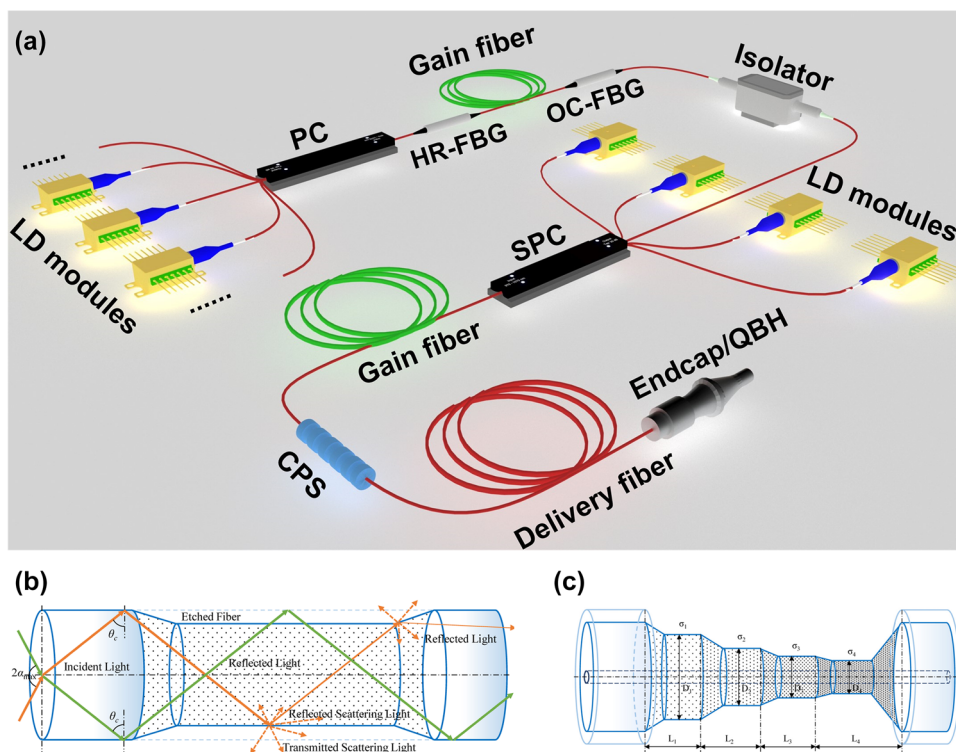
Fig. 3 a Schematical diagram of the conventional fiber amplifier with some key components annotated. PC, pump combiner. HR-FBG, high reflectivity fiber Bragg grating. OC-FBG, output coupler fiber Bragg grating. SPC, signal-pump combiner. CPS, cladding power stripper. QBH, quartz block head. **b** and **c** Schematic of the leakage guidance for cladding power in CPSs. **b** Basic principle of CPS for cladding power stripping by destructing the total reflection condition through the traditional hydrogen-carrying method and increasing the reliability of FBG resonators [58, 61, 62].

chemical etching process; Reproduced with permission from Ref. [151], Copyright 2017, Optical Society of America. (© 2017 Optical Society of America under the terms of the OSA Open Access Publishing Agreement). **c** Segmented corrosion method for modified CPS fabrication; Reproduced with permission from Ref. [151], Copyright 2017, Optical Society of America

Due to the improvements of key components including large-mode-area fibers and FBGs, single-stage all-fiber laser oscillator with an increasing output power is becoming more attractive in industrial applications. Compared with the MOPA scheme, monolithic fiber oscillators exploiting dual-end FBGs have many advantages, including a more compact configuration, resistance to backward transmitted light and higher mode instability threshold, etc. Relevant studies show that the gap between fiber oscillators and MOPA amplifiers is gradually eliminated in terms of output power and beam quality. Ideally, FBG-based fiber oscillators have enormous potential and are promising to achieve a power level that is basically equal to MOPA configurations or even higher.

High-Power Fiber Combiner

The injected pump power scaling determines the power level fiber lasers can reach. Advances in fiber combiners allow higher pumping injections, more compact HPFL configurations, and impose a profound effect on beam quality fidelity. Among all the passive fiber-based components, the issue of enhancing power handling capacity is the most essential and challenging task for fiber combiners. Therefore, a higher power handling capacity of combiners with higher pump power injection is always what people pursue. Depart from the structures of MOPA amplifier and monolithic oscillator, fiber combiners can be divided into two main types, including the signal-pump combiners (SPCs) and the pump combiners (PCs), respectively. Table 1 summarizes the recent progress (including both publications and commercial products) of SPCs and PCs with high-power pump injection capacities over 2 kW. Generally speaking, the technical scope and fabrication complexity of SPCs are relatively larger than PCs; hence the brief overview of power scaling advances in this section mainly focuses on SPCs. Most of the fabrication processes or technical details are similar for both the SPCs and PCs, and more details on the fabrication techniques or research progress can be found in other review articles [152, 153].

At present, SPCs with high transmission efficiency, repeatable production and compact package have been

widely employed in fiber amplifiers as the end-pumping combiner. Fabrication of end-pumping SPCs is generally based on the taper-fused fiber bundle (TFB) technology. To fabricate an SPC through the adiabatic tapering process, multiple pieces of pumping fibers are tightly arranged and drawn into a constant tapering waist that matches with the delivery fiber. A $(6+1)\times1$ SPC fabricated by Gu et al. has been demonstrated with a remarkable power handling ability of over 3 kW. The launching efficiency for both signal and pumping beam reaches 98% and the measured M^2 of signal output is ~ 2.8 [162]. More recently, researchers released their self-made SPC utilized for backward pumping applications with a power handling of over 5 kW, the transmission efficiencies for signal laser and pumping light are 95.5% (together with negligible M^2 deterioration) and 98.2%, respectively [164]. Commercial SPCs tend to develop products with more pump branches, and the $(24+1)\times1$ SPCs with a 6.48 kW power handling capacity released by ITF Inc. are already on sale [166]. Breakthrough of SPCs indicates further compactness of the kilowatt-level HPFLs, which means that fewer LD-pumping modules or amplifier stages are sufficient to supply the required pumping injection.

As the power of the guided laser gets higher, output delivery fiber of SPCs with an increased core diameter is more favored to prevent local nonlinear effects, which, however, inevitably decreases the core diameter and the mode field of signal fiber with the tapering of fiber bundles, leading to a mismatch between the signal fiber and the output fiber. Although the thermal core expansion technology [167] has been well developed to adapt fibers with different mode

fields, the fusion-induced insert loss and beam quality degradation are adverse to high-power transmission. In this way, the application of non-tapering fabrication approach represents an important direction for SPCs to minimize the mode field mismatch.

As the tapering-induced fusion loss gets more prominent at higher power level, the side-pumping combiners, as an alternative candidate for end-pumping SPCs, has seized the historical opportunity for high-power applications. Side-pumping combiners have significant advantages in preserving signal beam quality, maintaining an uninterrupted signal core and equipping an unlimited number of pump ports. For side-pumping combiners, the launching of pumping light into the central signal fiber depends on several pieces of coreless intermediate fibers, the fabrication process is known as taper-fused method [168]. After the procedures of cleaving and moderate polishing, tapered section of the coreless intermediate fiber is spliced with the signal fiber, whose outer cladding is pre-processed to expose the inner cladding. The tapered intermediate fiber enables an increasing numerical aperture (NA) of pumping light and facilitates the coupling of pumping light into the inner cladding of signal fiber, a 2-kW diffractive-limited output has been realized through a pair of taper-fused $(2+1)\times1$ side-pumping combiners [169]. After further optimization, the maximum power handling of a single launching port was scaled to 2730 W recently [170, 171], demonstrating a vigorous potential of total pumping injection over 5 kW. Owing to the higher sensitivity to the injected NA, the working capacity of a single side-pumping combiner is limited to below 3 kW when it comes to pure LD pumping. Additionally,

Table 1 Representative publications or commercial products of SPCs and PCs with high-power pump handling capacity of over 2 kW

Types	Year	Architecture	Pump handling (kW)	Pump/signal transmission
PCs	2013 [154]	7×1	3.01	99.4%/null
	2015 [155]	7×1	3.81	98.4%/null
	2016 [156]	7×1	4.72	99.4%/null
	2019 [157]	7×1	3.218	98%/null
	2020 [158]	19×1	3.125	98.6%/null
	Accessed online [159]	7×1	2.8	Null/null
		19×1	2.66	Null/null
		31×1	4.34	Null/null
SPCs	2016 [160]	$(6+1)\times1$	9.95	99%/null
	2018 [161]	$(6+1)\times1$	2.9	94.8%/null
	2019 [162]	$(6+1)\times1$	3.068	98.1%/>97%
	2021 [163, 164]	$(6+1)\times1$	5.05	98.2%/95.5%
	Accessed online [165]	$(18+1)\times1$	2.5	>95%/>85%
		$(36+1)\times1$	2.5	>93%/>85%
	Accessed online [166]	$(6+1)\times1$	2.4	Null/>89%
		$(18+1)\times1$	3.6	
		$(24+1)\times1$	6.48	

the tandem pumping strategy allows higher pumping injection with respect to LD sources. For example, a recording implementation has coupled a maximum pumping power of 5600 W at 1018 nm by using a $(3+1)\times 1$ combiner [172]. A previous report also depicted a $(2+1)\times 1$ combiner with the maximum input of over 2800 W [173]. Moreover, as the pumping light is coupled via the side of the signal fiber, the side-pumping combiner does not occupy the input and output ends; thus people can achieve a distributed multi-port pump structure [174]. Furthermore, compared with the end-pumping combiner, the higher backward pump isolation of the side-pumping combiner can protect LDs effectively in counter-pumping or bi-directional pumping schemes.

The incoherent combination of HPFLs based on the signal-power combiner is another straightforward solution to address the power scaling limitation of single-channel fiber laser. Using this kind of fiber-based device, IPG Photonics has realized a multi-channel single-mode laser combination with the beam quality of $M^2 = 33$ and the output power of up to 50 kW in 2009 [175]. In 2012, high brightness beam combination with a total power of 17 kW, a beam quality of $M^2 = 5.84$ [176] and an output of 31.5 kW, a beam quality of $M^2 = 8.77$ [177] were realized, respectively. In the following year, a new power record of 100 kW multimode combination was created [119]. In view of other participants of the HPFLs industry, commercial laser systems have revealed a general pump injection capacity of over 20 kW for signal-power combiners [13, 14, 178], suggesting a powerful potential for industrial processing. Recently, a series of industrial achievements about "Core Technology and Industrialization of 100 kW Fiber Laser with High Beam Quality" have been fermenting [179, 180].

Further development of fiber combiners depends on the continuous optimization of optical post-processing platforms. At the same time, the flexible design and mass production is an ongoing topic. While the HPFL has sustained its fundamentals of long-term growth and strong resilience in terms of power scaling, it should be noted that both the strengthening handling capacity and a better beam quality of fiber combiners need persistent attempts.

Cladding Power Stripper (CPS)

As the output power of HPFLs employing cladding-pumped schemes goes up to several kilowatts, the residual pumping light caused by incomplete absorption may pose a thermal-induced threat to the stable operation of HPFLs. CPS acts as the core device to filter out the unwanted light, ensure the output beam quality and protect the operation of HPFLs from catastrophic points fusion or backward light leaking into the cladding. In principle, it helps to leak the cladding light by destructing the total reflection condition through a chemical, optical or mechanical process, as illustrated in

Fig. 3b. Given the upward power level of HPFLs, which is compounded by a growing amount of cladding light that needs to be dissipated, quite a number of forceful designs to retrieve the contradiction between power removal ability and temperature accumulation for CPS have been demonstrated.

By employing the chemical etching together with the polymers recoating technique [181], Poozesh et al. reported a CPS with the hundred-watt stripping ability. Since then, targeted 100-watt stripping for CPS has achieved great progress [151, 176–184]. The traditional CPS generally removes the cladding light in a short length of fiber, which may result in high local temperature under a cladding light power of 1 kW, thus disrupting the stable operation of the laser source. To ease thermal issues, the stripping distance in CPS has to be elongated to reduce the leakage power density and hence reduce the local temperature. By introducing the segmented etching process, as portrayed in Fig. 3c, local thermal load can be released through a cascaded power stripping. Several organizations have achieved higher power handling levels of 150 W [182], 438 W [183] and 670 W [151], respectively. Recently, Yan et al. realized a power handling capability of around 1.187 kW with a total length of 1.5 m by combining a fiber-etched CPS with a cascaded polymer-recoated one [185]. However, considering the excessive length of CPS is not conducive to nonlinear suppression, another report revealed a possible solution of 1.01 kW by employing continuous gradient chemical etching, in which a CPS of only 150 mm was utilized [186]. The highest power extraction experimentally demonstrated recently showed a cladding power stripping ability of up to 2.16 kW through merely 200 mm of package length [187, 188]. These advances in CPSs indicate the feasibility to meet the requirements of 10-kilowatt-level applications.

The polymer-free scheme offers another solution to avoid high local temperature. For instance, a unique format of CPS was reported to handle a 150-W power stripping by exploiting soft metal materials [189]. In addition, the CPS without outer polymers was experimentally tested with a 500-W striped power [190]. Taking advantage of the optical machining technology, structured surface manipulation for CPS was supposed to be another prospective method. In this way, the microstructure high-power CPS with a power handling capacity of 350 W has been presented [191]. Recently, more and more groups attempted to apply laser surface processing technique to CPS for inner cladding power extraction, such as the CO_2 laser-fabricated method [192, 193]. Similarly, by using the chemical mask etching method to fabricate an all-fiber CPS, the regular morphology generated on the surface successfully stripped 1.117 kW cladding power [194].

Fiber Isolator

Fiber isolator is a passive magneto-optical device based on the Faraday effect. To protect other components, this device only allows light to transmit in a specific direction and isolates the reflected light, which prevents the seed source from being adversely affected by back-reflection. Installing fiber isolators at both ends of active fiber can effectively improve the stability of fiber amplifier. The development of high-performance isolators on various technical indexes, miniaturization and practicability has been greatly accelerated in recent years, including both the polarization-dependent and polarization-independent types.

At present, the main pursuit of isolators is a wider working frequency band, a wider range of temperature operation and a deserved higher power handling capacity. Up to now, the progress of isolators is mainly attributed to the commercial products from Optizone Inc. [195, 196], Advanced Fiber Resources (AFR) Ltd. [191–199], CASTECH Inc. [200], Thorlabs [201], etc. For example, CASTECH Inc. utilizes high-quality crystals and optical components to fabricate free-space isolators with high power capacities of up to 200 W [200], high isolation ratios (33 dB for single-stage series and 50 dB for dual-stage series), low insertion losses, excellent environmental stability and low thermal lens effect. Besides, Optizone Inc. and AFR Ltd. have developed a series of fiber-free-space [195, 191–199] and collimating-output [196] isolators with a maximum power of 500 W, covering the wavelength range from 1030 to 1080 nm.

Fiber-Based Endcap

High-power fiber-based endcap (or quartz block head (QBH)), which attracts extensive attention with the gradual increase of laser output power, can effectively solve the problem of end facet damage by increasing the damage threshold of output fiber. The endcap usually employs a fused quartz block which is connected with the laser output fiber through fusion. To protect the output end of HPFL system, endcap expands the laser beam profile to reduce the power density in the output surface. By coating antireflection film on the emitting surface of the endcap, the transmittance of high-power laser beam can reach more than 99.9%, which effectively improves the output efficiency and reduces the backward light. Technologies incorporated in fiber-based endcap include cladding mode stripping, indirect water cooling, protective window and safety interlock. With the continuous development of HPFLs, the issue of fiber facet damage has gradually attracted greater attention, followed by the demand for fiber endcaps and related researches.

Historically, fiber endcaps were first utilized in practical applications of pulse fiber lasers with high peak power [202]. To fit the high-power capacity in CW applications, the sizes of fiber endcaps evolve to larger values gradually. In 2007, a fiber endcap that adopts a 2 cm glass plate was reported, whose handling capacity was limited to 700 watts due to the complexity of the glass bonding method [203]. To achieve a larger diameter design, an endcap structure employing the conical coreless fiber fusion method [204] and ring CO_2 laser method [205] was proposed. In 2014, Zhang et al. reported a fiber-based endcap fusion technology based on CO_2 laser method together with the inclined points annular heating technology. This endcap exhibited a high-power handling ability of 1002 W and a total coupling efficiency of 95.5% [206]. Adopting the glass cone rod endcap without water cooling, the transmission efficiency at several hundred watts was over 95% and the highest handling power reported earlier exceeds 1 kW [207]. In 2015, Nicholson et al. from OFS Laboratory applied the fiber endcap with a pyramidal structure for HOMs conversion, realizing an efficient mode conversion of $LP_{0,14}$ mode to a quasi-fundamental mode Gaussian output with a beam quality of $M^2 = 2.7$ [208].

According to the open-access reports, the power handling ability of high-power fiber-based endcap developed by Optoskand Inc. (acquired by Coherent Inc. later) has reached more than 20 kW [209]. Besides, the integration of endcap with other hardware has been realized, such as the sensor structure, online monitoring applications [210], etc. The Dragon products released by AFR Inc. can also provide high-power QBH-compatible connectors with power handling capacities of up to 20 kW [211].

Advances in the "Functionalization" of High-Power Laser Fibers

The unprecedented power scaling of HPFLs has made it an important enabling technology for advanced industrial manufacturing, but there are also fundamental obstacles that gradually emerge as the power continues to increase. The transmission of high-power density in the confined core area affects the spatial, spectral, and temporal characteristics of fiber laser simultaneously. Spatially, the desired single-mode feature at a high-power level becomes inaccessible due to the intrinsic few-mode operations in fiber with a large mode area and the lingering thermo-optic effect, which lead to TMI with kilohertz fluctuation in transverse mode contents and beam quality degradation. Now the TMI has almost become a common obstacle for power scaling of fiber lasers with various regimes including the conventional YDFLs, narrow linewidth YDFLs, Raman-gain fiber lasers, high-average-power pulsed fiber lasers, etc. Spectrally, the inelastic scattering that occurs in the fiber core limits the power scaling and conversion efficiency. As for the temporal mechanism

with more complexities, the complete manipulation depends on a long-term comprehensive analysis of HPFLs.

The function of optical fibers is generating and propagating high-power laser, so the performance of laser emission highly depends on the properties of fibers. Therefore, the key to further advance of practical high-power laser technology relies on the development of optical fibers with robust single-mode outputs at core sizes well beyond the limitations of conventional large-mode-area fibers, as well as the seamless compatibility with monolithic integration including the abilities of being spliced using standard splicing equipment and being coiled for packaging purposes.

The functionalization of optical fiber provides an intuitive and effective solution to address the existing problems. Functionalization means that specific functionalization features are given on the basis of retaining typical characteristics in conventional optical fibers. In other words, the functionalization of the fiber does not affect the amplification or high-efficiency transmission of high-power laser beams. For example, for active fibers, thermally induced refractive index variation under the high-power state affects the boundary conditions of core mode and thus alters the mode behavior. One possible option is developing fibers with special geometries in the cross-section to filter out the unexpected modes. Another possible idea is to maximize the gain extraction of fundamental mode by engineering the doping components distribution. Similar functionalization strategies are also applicable to passive optical fibers.

Functionalization of Active Optical Fibers

In this section, several representative functional fibers are discussed according to the structural or material modification strategies. Since the performance of optical fiber is determined by its waveguide structure and composite materials interactively, the two perspectives should be emphasized separately. Abundant achievements in advanced rare-earth doping technologies and step-by-step fabrication of fiber preforms endowed the functionalization of fibers with more diversities, and recent developments have shown significant benefits of addressing parasitic effects from the standpoint of waveguide propagation and the origins of light-matter interactions.

Geometric Structures Engineering

Generally speaking, a larger core diameter is required to increase the nonlinear threshold of a laser fiber, which, however, is accompanied by strict management on the support modes for preserving a good beam quality. Additionally, for high-power operation, effective suppression on the modal competition and TMI-related intermodal coupling presents

an opposite requirement, namely reducing the core diameter. As a result, there is an irreconcilable contradiction in achieving the simultaneous suppression of nonlinear effects and TMI based on conventional large-mode-area step-index fibers (SIFs). Recently, more and more attention refocused on the modification or functionalization of conventional SIFs. A variety of transverse or longitudinal improvements have been proposed to break down the barriers between increasing core diameter and effective single-mode operation, where the transverse mechanism refers to modifying the cross-section of SIFs, while the longitudinal mechanism tends to change the geometric structure along the fiber extension.

Conventional rare-earth doped fibers rely on a step-index profile to channel the light transmission. To distinguish the concept of functionalization from the traditional definition, the first type of functional fibers is generalized as a strategy of "beam shaping through constructing the cross-sectional structures" in this section. When the undesired mode contents become non-negligible in the core zone, the engineering of cross-sectional structure tends to make the fiber cross-section act as a beam shaper in favor of the fundamental mode output. By modifying the geometry of the cross-section appropriately, the fiber is functionalized in transverse mode selection. A representative principle of geometric engineering is designing fiber structures that induce the unexpected modes to experience significant leakage or bending loss by extracting HOMs energy from the core into the cladding region, while ensuring only negligible loss for the fundamental mode.

Typically, an important branch of geometric structure engineering is promoting the resonance between HOMs in the central core and the lateral structures, for example, the trench-assisted fibers [32, 34, 38–40, 42, 206–222], chirally coupled-core fibers (CCCF) [29, 43–45, 217–235], leakage channel fibers [30, 230–245], and large pitch fibers [31, 246, 247], etc. Compared with conventional SIFs, the cladding regions of these functional fibers are modified to non-uniform structures with lateral structures surrounding the central core, leading to a resonant coupling of the HOMs in the main core into the lateral structures. These structural designs greatly enhance the HOM suppression capability, enable a robust single-mode output even with a core size and improve the nonlinear threshold.

Jain et al. first proposed the single trench fiber (STF) in 2014 [34], which means a fiber design with a core surrounded by a low-index trench layer and a high-index ring layer, as schematically exhibited in Fig. 4a. This kind of fiber is easy to fabricate since it does not increase too much manufacturing difficulty on the basis of conventional modified chemical vapor deposition (MCVD) technology. To date, most of the related studies focus on the power scaling of active STFs. For the first demonstration, Jain et al.

fabricated a Yb-doped STF with a core diameter of 40 μm and a NA of 0.038. Simulated results show that the loss of LP_{11} mode can reach 5.4 dB/m, which is about 20 times larger than the SIF with the same core diameter and NA. A 10-W level single-mode fiber laser was constructed using this STF [34]. In 2015, they utilized a piece of STF with a 30-μm core diameter to build a picosecond MOPA and the average power of this MOPA was scaled to 52 W [38] with the single-mode property. Thicknesses or relative refractive index profiles (RIPs) of the trench layer and the ring layer are expected to be optimized comprehensively to increase the bending resistance and the mode discrimination on HOMs suppression, which has given rise to a robust single-mode output operating with a maximum power around 800 W [42]. Recently, An et al. achieved a recording output power of over 1.5 kW for Yb-doped STF [214]; the higher output power is expected by optimizing the fabrication technique and the design parameters.

As a novel functional fiber that is derived from the concept of chiro-waveguides [242–251], CCCF was proposed in 2007 to improve the limitation of single-mode output with a very large core size. Structurally, one or more side-cores are spirally wound outside the central core to form spiral cores. Through reasonable design, it is possible to achieve phase matching or quasi-phase matching between the fundamental mode of the side-cores and the HOMs of the central core, thus dissipating the energy of HOMs from the central core resonantly, as illustrated in Fig. 4b. The robust single-mode characteristic of CCCF was verified in a large-mode-area fiber with a large core diameter of 35 μm for the first time; this fiber shows an excellent beam quality of $M^2 = 1.03$ at 1550 nm [225]. Subsequently, an active CCCF with an equal core diameter was successfully tested through a MOPA architecture with a CW output of 250 W and a slope efficiency of 74% [229]. Compared with the conventional fiber with the same size, the output beam quality is greatly improved due to the high suppression ratio of CCCF. For a core diameter exceeding 50 μm, it is also realistic to achieve modal performance practically equivalent to a single-mode operation using a CCCF structure with multiple side-cores [29], as represented in Fig. 4b. In addition, owing to the existence of spiral cores, CCCF with a special structure design has a certain range of suppression band in the transmission spectrum. In this way, the SRS suppression is

Fig. 4 **a** and **b** Schematic diagram of functional fibers with modified cross-sectional structures: **a** The cross-sectional structure of a typical single trench fiber. **b** The cross-sectional structure and typical format of a chirally coupled-core fiber with one side-cores. **c** Schematic diagram of tapered fibers with different longitudinal structures. The upper row represents tapered fibers with a uniform core-cladding ratio and the nether row represents the non-uniform case. **d**–**f** Schematic diagram of rare-earth doped fibers with different doping profiles: **d** The fully doped fiber with a uniform doping profile. **e** Confined-doped fiber in the central core region. **f** Ring-doped fiber
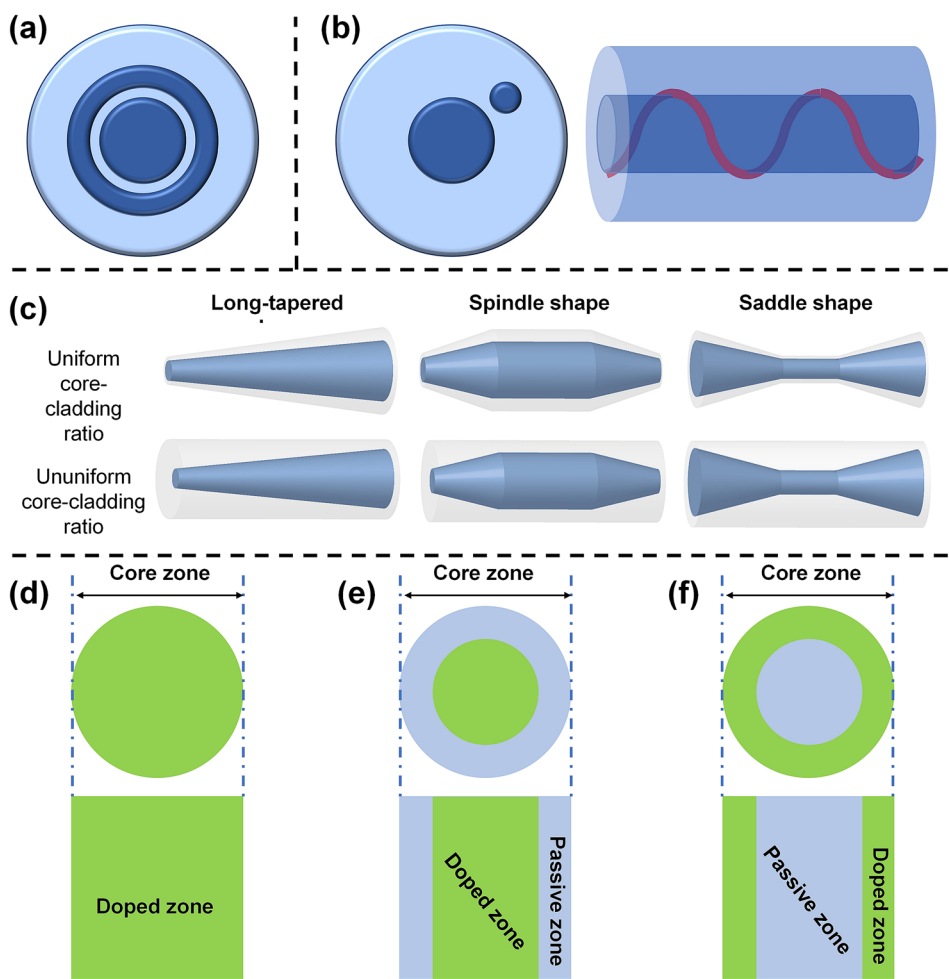
promising for CCCF if the suppression band coincides with the SRS region [230, 232].

Based on the robust single-mode output and the insensitivity to nonlinear effects, narrow linewidth amplification employing CCCF with better monochromaticity, better beam quality and the higher power has been reported [45, 231, 235]. Experimental observation indicates that CCCF has an excellent polarization-maintaining characteristic, and the extinction ratio reached 34 dB [225, 226]. Using a 2.7-m-length air-cladding CCCF as the gain fiber, a 511-W single-frequency and single-mode output has been realized with an extinction ratio of more than 15 dB [231].

As a new candidate to realize high peak power and high-energy fiber lasers [43, 44, 223, 233, 235], CCCF has made tremendous success in both commercial and scientific applications. Taking the CCCF released by nLight Corporation as an example, by exploiting a CCCF with a central core of 55 μm and eight side-cores, the generated sub-ns pulse laser has an average energy of over 8 mJ and a peak power of 600 kW, as well as a stable Gaussian-shaped output profile [233]. In 2018, a double-stage pulse amplification system based on CCCF was built for power scaling, eventually, an average power of 121.4 W, the pulse energy of 1.2 mJ and the beam quality of $M^2 = 1.2$ were obtained [44].

Through the adiabatic tapering technique [252, 253], tapered fiber has an asymptotic geometric size along the longitudinal direction, both the uniform and ununiform cases are schematically depicted in Fig. 4(c). Structurally, its small portion is beneficial to improve the launching beam quality and the TMI threshold. The large portion reduces the power density and boosts the threshold of nonlinear effects. Compared with conventional fibers with uniform size, tapered fiber has a larger core mode area, a stronger pump absorption and a better thermal management performance. Different from the mode control strategy through constructing the fiber cross-sectional structures, laser beam channeled in tapered fibers is shaped by inner-fiber manipulation along the longitudinal direction.

In the evolution history of tapered fiber for high-power applications, early researches mainly focused on the long-tapered type [248–269], covering different regimes from CW [254, 255, 270] to pulse operation [268, 269], or from broadband spectrum to narrow linewidth output [271, 272]. With the development of fiber preform preparation and mechanical polishing technology, the studies of tapered fibers has evolved to more degrees of freedom along the longitudinal dimension, which is driven by better pump absorption capacity and greater single-mode potential. A series of representative results at several-kilowatt-level have been reported with near single-mode outputs [76, 258–267, 267–280]. Table 2 summarizes the recent progress of tapered fibers for HPFLs applications.

Based on geometrical optics, the model of pump absorption in long-tapered fiber was analyzed by using the ray tracing theory [254]. Comprehensive analysis on the fiber geometric parameters shows that the paraxial pumping power is closely related to the taper shape, taper ratio, cladding filling factor and Yb^{3+} doping concentration [255]. Long-tapered fiber has the inherent advantage of restraining SRS because of the increasing core area along fiber extension, which is further enhanced by matching the delivery fiber with a larger core. In addition, the ability for SRS mitigation is more significant in backward pumping applications [257]. High-order Stokes threshold and the output laser power can also be improved greatly in long-tapered Raman fiber amplifiers [258].

Mode evolutions in long-tapered fiber originate from the mode coupling caused by core diameter variation and RIP fluctuation. Shi et al. have derived the coupled mode equation through considering the mode disturbance, in which fiber is differentiated as dz in the longitudinal gradient [256], showing that the beam quality maintenance is feasible for long-tapered fibers with different doping profiles. The cutting-back method was previously employed to study the mode evolution in a 7-m long-tapered fiber experimentally, although the fiber bending and local tension lead to deviation of field distribution, mode profiles in the far-field have a robust Gaussian distribution [259] for different fiber sections. The local bending or fiber coiling applied at the small end may excite a higher content of HOMs, which results in a significant reduction in the output power after the mode filtering of long-tapered fiber [260]. Since the first experimental observation based on a piece of 10.5-m long-tapered fiber in 2008, which generated a CW output of 80 W ($M^2 \sim 1.07$) by employing the Yb-doped fiber with two ends of 27/834 μm and 5.8/177 μm [261], many optimistic results have been obtained. For example, the 600 W and 750 W single-mode oscillators [254, 255], the 100 W polarization maintaining amplifier [262] and the ultra-large core birefringent fiber for high-power amplifiers [263]. To construct an all-fiberized format, a long-tapered fiber amplifier with a maximum output power of 1.47 kW was realized and the M^2 factor was 1.8 [264]. For better compatibility with commercial optical fiber devices, fiber with a small end of 20/400 μm and a large end of 30/600 μm was introduced for higher output power [265]. Similar applications in fiber amplifiers also increased the signal power to 2.17 kW [266]; most recently, the output power in long-tapered fiber was pulled to over 4 kW [76].

SBS frequency shift in tapered fiber changes with the variation of core diameter, which effectively broaden the SBS gain spectrum [287]. Thanks to the shorter fiber length and larger core diameter, the SBS threshold of single-frequency laser based on tapered fiber is supposed to exceed kilowatt

Table 2 Recent progress of tapered fibers for HPFLs applications

Fiber types	Year	Pump format	Fiber dimension	Power	Efficiency	BQ
Long-tapered	2008 [261]	bulk optics	27/834 µm–5.8/177 µm	80 W	92%	$M^2 \sim 1.07$
	2009 [254]	bulk optics	65/890 µm–11/null µm	600 W	63%	$M^2 \sim 1.08$
	2010 [255]	bulk optics	110/880 µm–20/158 µm	750 W	81.9%	$M^2 \sim 1.7$
	2017 [262]	bulk optics	35/250 µm–56/400 µm	100 W **PM**	84%	$M^2 \sim 1.2$
	2018 [263]	bulk optics	35/250 µm–96/792 µm	70 W **PM**	48%	$M^2 \sim 1.09$
	2018 [264]	All-fiber	21.2/417.3 µm–30.4/609.6 µm	1.47 kW	72.2%	$M^2 \sim 1.8$
	2019 [265]	All-fiber	20/400 µm–30/600 µm	1.72 kW	60%	$M^2 \sim 2.1$
	2019 [266]	All-fiber	20/400 µm–30/600 µm	2.17 kW	81.4%	$M^2 \sim 2.2$
	2022 [76]	All-fiber	20/400 µm–30/600 µm	4 kW	84.1%	$M^2 \sim 1.46$
	2012 [271]	All-fiber	7.5/120 µm–44/700 µm	110 W	**NL**/63%	$M^2 \sim 1.06$
	2018 [281]	All-fiber	20/237 µm–47/580 µm	260 W	**NL**/71.3%	$M^2 \sim 2.35$
	2013 [272]	All-fiber	7.5/120 µm–44/700 µm	160 W	**SF**/61.4%	$M^2 \sim 1.12$
	2016 [282]	All-fiber	20.4/237.1 µm–47/580 µm	53 W	**SF**/57.7%	$M^2 \sim 1.2$
	2021 [283]	All-fiber	30.3/245 µm–49.3/404 µm	>400 W	**SF**/81.7%	$M^2 < 1.3$
	2020 [284]	All-fiber	36/250 µm–58/397.3 µm	550 W	**SF**/80%	$M^2 \sim 1.47$
Spindle shape	2020 [285]	All-fiber	20/400 µm–30/600 µm–20/400 µm	1.8 kW	83.5%	$M^2 \sim 1.65$
	2020 [277]	All-fiber	27/410 µm–39.5/600 µm–27/410 µm	5 kW	66.6%	$M^2 \sim 1.9$
	2021 [276]	All-fiber	24/400 µm–31/400 µm–24/400 µm	3.42 kW	55.2%	$M^2 \sim 1.7$
Saddle shape	2020 [273]	All-fiber	30/400 µm–23/400 µm–30/400 µm	1.3 kW	46%	$M^2 \sim 2.0$
	2018 [286]	All-fiber	20/80 µm–12/49 µm–20/80 µm	10.6 W **@ 976 nm**	18.4%	$M^2 \sim 1.14$

BQ beam quality, *PM* polarization-maintaining, *NL* narrow-linewidth, *SF* single-frequency

level according the theoretical investigations. In 2020, a long-tapered polarization-maintaining fiber was exploited to realize a single-mode output of 300 W single-frequency linearly polarized laser [284]. Taking advantage of the stronger gain saturation and the higher single-frequency TMI threshold for 1030 nm lasers, results of 379 W and 550 W for single-frequency amplification based on long-tapered fiber were disclosed under polarization maintaining and non-polarization maintaining conditions, respectively [288].

As can be seen, for those reported long-tapered fiber lasers operating at kilowatt-level, the beam quality M^2 factor above 2 is estimated with a high content of HOMs. Although long-tapered fibers have obvious advantages over conventional fibers with similar sizes, poor beam quality is still a serious problem for fiber lasers. To realize further improvements, spindle-shaped fibers and saddle-shaped fibers were designed and fabricated.

The novel spindle-shaped fiber has two uniform small-core sections at both ends, a tapered region and a large core zone in the middle section [285], as shown in Fig. 4c. More practically, the small-core sections combined with appropriate fiber coiling help to suppress HOMs and to increase the TMI threshold. The large-core section in the middle section can effectively reduce the power density and suppress the SRS effect. By combining these advantages to balance SRS

and TMI synchronously, an experimental study based on a piece of homemade spindle-shaped fibers has been carried out in a fiber oscillator with the maximum power of 5 kW ($M^2 \sim 1.9$ and an efficiency of 66.6%) [277]. Due to the mismatching between the spindle-shaped fiber and other fiber components, the laser efficiency was limited to ~66.6%. Higher quality spindle-shaped fibers are expected to support more powerful and higher beam quality output if the tapering ratio/length, core-cladding ratio, and doping concentration are comprehensively optimized.

Unlike the spindle-shaped fiber, saddle-shaped fiber has a symmetrical shrink in the middle section [273, 286], as shown in Fig. 4c. This section acts as a mode filter in the cavity, which mitigates the oscillating of HOMs and guarantees the single-mode operation. At the same time, bilateral ends with larger core diameters reduce the power density and increase the nonlinear threshold. Experimentally, a saddle-shaped fiber has been utilized to generate a CW output of over 1.3 kW ($M^2 \sim 2.0$), the fiber has core diameters in bilateral ends and the middle section of 30 µm and 23 µm, respectively [273]. This is the first demonstration to verify the feasibility of saddle-shaped fiber for HPFLs, although serious misregistration of the core to cladding results in a relatively low optical-to-optical efficiency (~46%), this fiber has potential advantages in the power scaling by suppressing

SRS and TMI because mode filter works over a long distance in the middle section. In this situation, a challenging task is the mode field diameter matching between the large ends of the saddle-shaped fiber and the passive fibers inscribed with FBGs, which might be solved by producing passive fibers with a correspondingly larger core diameter.

Doping Components Engineering

Adopting the MCVD method combined with solution or vapor phase doping technique [283–294], the concentration of rare-earth material and co-dopants as well as the local RIP within optical fibers can be tailored in each soot layer. Tailoring the transverse doping profile of active fibers can lead to modal discrimination by providing a higher overlap of the gain with the fundamental mode, which is an effective way for fiber lasers to improve the beam quality. In addition, some customized doping profiles are considered to have a preferential advantage for specific wavelength emissions, such as lasers operating with a three-level regime or short-wavelength fiber lasers.

Ununiform doping profile i: confined-doped fiber A promising solution is the confined-doped fiber design, in which only the central part of core region is selectively doped. In a conventional active fiber, the core is fully doped with rare-earth ions (Fig. 4d), and all the supported modes propagating in the core could experience high gain. While in the confined-doped fiber, transverse mode discrimination, also known as the "gain filtering effect" [289–297], is established by separating the waveguiding function and the gain through selective doping, and only the modes that occupy the doped regions of the core could extract the gain [35], as illustrated in Fig. 4e. It has been proven both theoretically and experimentally that confining the doping area to the central part of the core can facilitate fundamental mode laser output [290–298]. After the TMI effect was observed experimentally and regarded as the main limiting factor for power scaling of HPFLs, researchers have predicted that the confined-doped fiber is an effective method to improve the TMI threshold of laser system [20] due to the gain tailoring effect among the guided modes. High-power fiber lasers/amplifiers employing confined-doped ytterbium-doped fiber have made continuous breakthroughs in power scaling and beam quality preservation [35, 48, 51, 52, 59, 71, 292–309] in recent years.

In 2016, Mashiko et al. demonstrated a 2-kW fiber oscillator operating at 1080 nm with the beam quality factor $M^2 = 1.2$ based on the confined-doped fiber [48], the output power was further scaled to 3 kW with $M^2 = 1.3$ in the following year by increasing the pump power [51]. The effective mode area of this confined-doped fiber is $\sim 400\ \mu m^2$, but the key parameters, for example, the relative doping ratio and profile of the core, were not mentioned. As for the more astonishing power records of 5 kW [52] and 8 kW [59], similar fiber design scheme, although not explicitly claimed, is inferred to be further applied, in which the fiber mode area was extended to 600 μm^2. Based on a confined-doped 20/30/400 μm fiber, a 2.42 kW output at 1080 nm was obtained with the beam quality factor of $M^2 = 1.32$ in a fiber amplifier [306]. A high-power narrow-linewidth amplifier, employing a confined-doped fiber with an 18-μm doping region in the 30-μm fiber core, achieved an output power up to 3.57 kW and the beam quality at the maximum power is $M^2 = 1.942/1.774$ [308]. This investigation demonstrates a TMI threshold improvement of up to 2.2 times over conventional fully-doped fiber.

As for the tandem pumping applications of confined-doped fibers, Seah et al. have reported a 4.1 kW output by employing the confined-doped fiber with core/inner-cladding of 42/250 μm and around $\sim 75\%$ doping ratio [303]. The beam quality factor M^2 was improved from 2.27 at the fully doped case to 1.59. To obtain a more appropriate doping ratio and a higher diffractive-limited output, the confined-doped fiber with a 75% doping ratio was designed and fabricated after a comprehensive evaluation of the gain filtering effect and the fiber length, a remarkable output of over 6 kW at 1080 nm was realized in a tandem pumping amplifier, and the beam quality was well maintained during the power scaling process [35]. The TMI threshold of the confined-doped fiber amplifier is estimated to ~ 4.74 kW, which is improved by $\sim 170\%$ compared with its fully-doped fiber amplifier counterpart. Most recently, based on an end coupling $(6 + 1) \times 1$ combiner, the output power of a confined-doped fiber amplifier was scaled to 8.14 kW. Due to the TMI effect, the beam quality factor at the highest power was degraded to $M^2 = 2.17$, the final power scaling is limited by pump power. Furthermore, the TMI effect is successfully suppressed by introducing higher-order mode contents into the seed laser, and the beam quality factor is maintained as $M^2 = 1.93$ at the output power of 7.08 kW [68].

In addition to the confined-doped fiber with a step-index profile, manipulation of gain dopant distribution has another novel type, in which the gain dopant concentration varies along the radial direction rather than being confined constantly in the central region [297, 309]. A representative case is the Gaussian-shaped distribution of Yb^{3+} ions, where the gain dopant profile is designed to generate maximum gain overlap with the fundamental mode while maintaining the step-index profile. Based on a bidirectional-pumping MOPA setup, the high modal discrimination of a Gaussian-shaped ytterbium-doped fiber, with the core/inner cladding diameters of 32 μm and 400 μm and a Gaussian width of 16.9 μm, was verified to radiate over 3 kW single-mode laser ($M^2 \sim 1.45$) [309].

Overall, the confined-doped fiber has a high laser efficiency that is close to conventional fiber and exhibits great potential to obtain extremely high-power output with an excellent beam quality. However, the fabrication process of confined-doped fibers, people should avoid significant RIP depression or saltation that may affect the core mode field. If the distribution of the core mode field changes, the overlap factor of each mode varies accordingly, which further alters the preferential gain of the fundamental mode. Furthermore, in a compact confined-doped fiber laser, the coil diameter of the fiber should be carefully optimized. If the gain fiber is coiled to a tight condition, the mode field distortion caused by fiber bending is likely to weaken the preferential gain effect on the fundamental mode. In this way, bending-resistant design is a conceivable pursuit for the future consideration of confined-doped fibers [304–313].

Ununiform doping profile ii: ring-doped fiber Although the preference gain on fundamental mode is a promising way for single-mode output of HPFLs, conventional central doped fibers do not make for efficient accumulation for several important three-level and two-level lasers operating with wavelengths at which the small-signal absorption is large [308–316]. Generally, higher particle population inversion and higher threshold of pumping power are required to obtain the laser output for the three-level and two-level regimes. A proper design of the dopant distribution profile across the fiber waveguide allows for increasing the output signal power with specific energy levels. For a given pump power, the ring-shaped doping profile, as presented in Fig. 4f, reduces the gain of ASE radiation, and tunes the effective gain peak to shorter wavelengths.

To achieve a high-power single-mode operation at 1018 nm with strong ASE suppression, a ring-doped Yb-doped fiber with a geometry of 32/260 µm was designed [317]. The core was fully doped with Yb^{3+} ions; however, the concentration was higher at the outer ring, producing an average NA of ~0.041. The ring-doped design is able to maintain sufficient pump absorption while reducing the overlap of the fundamental mode with the doped area and decreasing the gain at 1030 nm. Although the HOMs are intrinsically supported, differential bending loss between the fundamental mode and HOMs enables sufficient suppression on HOMs thanks to the ultra-low NA. A linearly polarized, narrow-bandwidth, high-power fiber amplifier at 1018 nm with an excellent beam quality ($M^2 < 1.1$) and an output power of 616 W was demonstrated finally. Another representative three-level thulium fiber laser operating at 1907 nm utilized a ring-doped profile to tailor the Tm^{3+} doping. With a high Tm concentration (> 3.5 wt%) in the Nested-ring doping region, a 10/125 µm fiber with the ring-shaped RIP was fabricated [318], which dramatically reduces the thermal load in per unit length without incurring the penalty of increased gain at parasitic wavelengths.

Owing to the efficient mitigation on parasitic lasing, the Tm-doped fiber laser with a high slope efficiency (> 65%) and a 62 W single-mode output at 1907 nm was realized.

In addition to customizing special doping profiles on the basis of conventional stepped SIFs, the ring-shaped doping profile is also portable for other advanced fibers. For example, a multicore Yb-doped fiber with a ring-shaped core array was designed to enable an efficient 976 nm laser generation [319] by introducing a severe bending loss at 1030 nm while maintaining a negligible bending loss at 976 nm.

Actually, the transmission property of laser fibers is intrinsically determined by both the cross-sectional structure and the doping materials. The parasitic effects within optical fibers are fundamentally resulted from the coupling between optical, thermal, and mechanical fields and their resultant influence on material properties [37]. In addition to addressing parasitic effects from the viewpoint of geometric engineering, people have advocated a more intrinsic approach by engineering the doping components, mainly focusing on the judicious selection of the core materials for mitigating nonlinearities [320]. To visualize this strategy, the effects of some material proportionalities on optical nonlinearities are provided in Fig. 5. As can be seen, different material components have inverse contribution to the optical properties of the fiber.

Fibers with lower thermo-optic coefficient One of the most intrinsic issues disrupting the power scaling of fiber lasers is thermo-optical effect, expressed by thermo-optic coefficient dn/dT mathematically. The reduction of thermo-optical effects in fibers is a straightforward strategy to mitigate TMI effect, which means reducing the thermo-optic coefficient (dn/dT) with the incorporation of special co-dopants in the fiber core. For example, both P_2O_5 and B_2O_3 compositions have negative thermo-optic coefficients dn/dT. The combination of glasses with both negative (e.g., P_2O_5 and B_2O_3) and positive (e.g., Al_2O_3 and SiO_2) contributions to thermo-optic coefficients can be an effective method to increase TMI threshold in silica fibers [323, 324]. To realize this functional target, two sample fibers, with highly doped P_2O_5 and B_2O_3 and the background loss of less than 50 dB/km, were fabricated to analyze the impact of lower thermo-optic core compositions [37]. One of them was specially designed as the commercial specification to generate an output power of over 1 kW with an efficiency exceeds > 70%, implying a more fascinating potential for thermal-free operation in laser fibers.

A lower thermo-optic coefficient means a slight modification towards standard glass materials to weaken the thermo-optical effect, requiring a non-zero dn/dT design in the core zone, which is not beyond the usual fabrication process and avoid additional cost [325]. The mode shrinking caused by thermo-optical effect can be reduced through lowering dn/dT in the active doped core and indicates an enhancement
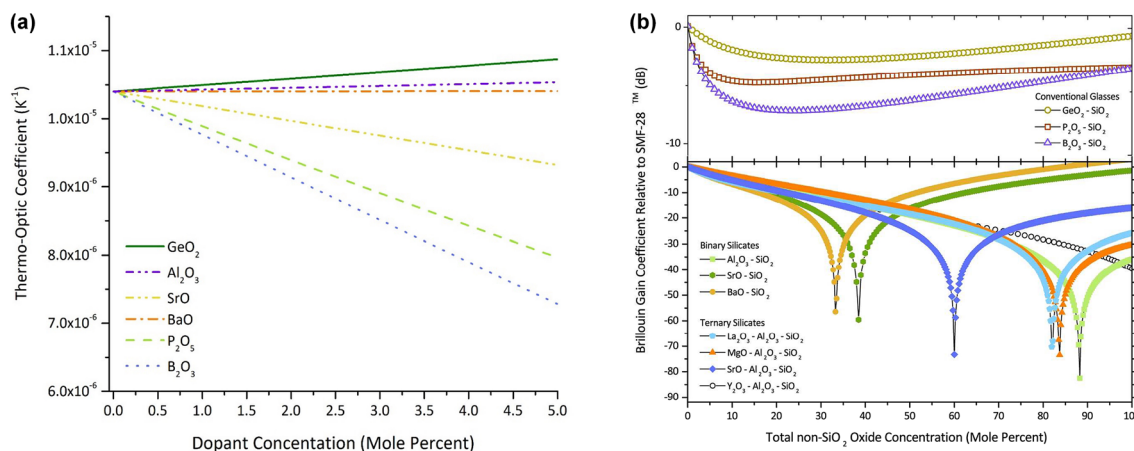
Fig. 5 Effects of material proportionalities on optical nonlinearities of laser fiber. **a** Relationships between the thermo-optic coefficient contribution and the dopant concentration of fiber doping materials. **b** Relationships between the nonlinear coefficient contribution and the dopant concentration of fiber doping materials; Reproduced with per-

mission from Ref. [321, 322], Copyright 2017, Wiley. (© 2017 The Authors. International Journal of Applied Glass Science published by American Ceramic Society and Wiley Periodicals, Inc., under the terms of the Creative Commons Attribution license, (http://creativecommons.org/licenses/by/4.0/))

of the mode field of the fundamental mode in a large pitch fiber [326]. However, to achieve a lower dn/dT fiber preform equivalent to a commercial product, the initial preform recipe has to be modified through numerous iterations. In addition, much higher power is anticipated to fully certify the suppression on TMI without affecting the high-power operation.

Fibers with lower Brillouin gain coefficient or Raman gain coefficient SBS and SRS are two forms of inelastic scattering effects in optical fibers that originate from an interaction of the incident light wave with acoustic phonons (related to SBS) or optical phonons (related to SRS) [25, 321]. As with all optical nonlinearities, fundamentally originated from the interaction of the incident light with the material through which they are propagating, a materials approach to their diminution may also be adopted.

SBS is well known to limit the intensity of light per unit bandwidth that can be transmitted through or generated in optical fiber systems, and typically has the lowest threshold among all the nonlinear processes in narrow linewidth or single frequency systems. The normal methods for SBS suppression include enhancing core mode size and acoustically engineered fiber designs that generally require complicated core doping profiles or cladding structures [321]. Another practical solution is controlling the Brillouin gain through fiber designing because fibers with different index profiles have different Brillouin gain spectra and therefore different SBS thresholds [321–329]. The acousto-optic effective area has been introduced to predict the SBS threshold in optical fibers with ununiform index profiles [330]. Alternatively, SBS suppression has been pursued by manipulating the optical and acoustic indices in the fiber core. The ramp-like

acoustic index profile in a large-mode-area Yb-doped fiber, constructed by varying the concentrations of Al and Ge in the fiber core demonstrated an SBS suppression of approximately 6 dB [331] and a further investigation demonstrated an SBS suppression level of 11.2 dB [332]. A passive case developed in 2021 considered that the multimode acoustic guiding regime carries a large potential for SBS gain suppression (8–10 dB) through complex doping of the core with different additives, such as P_2O_5 and F co-dopants. A double-cladding Yb-doped fiber exhibited a 9 dB suppression for SBS gain with respect to SiO_2 due to the heavily doped B_2O_3 and $AlPO_4$ [37].

In terms of suppressing SRS in silica-based specialty fibers through combining different glass compositions, actually, the silica material has an intrinsically low Raman gain coefficient. However, the additional doping compositions increase the emission section of pure silica SiO_2 [333]. Employing high concentrations of materials with low Raman gain coefficients [334] g_R or minimizing the overlap of Raman sections between multicomponent materials [320, 335] are possible approaches to realize an intrinsically low Raman gain material. It is a burgeoning topic nowadays but seems to be beyond the scope discussed in this context, please see the review articles in this topic if the readers are interested [321, 322, 336, 337].

Fibers working with thermally induced guidance Recently, a new type of large-mode-area fiber called thermally guided fiber has attracted much attention [332–345]. This kind of fiber is characterized by waveguide structures employing the thermal effect revolutionarily, in other words, creating an effective waveguide structure through the thermal lensing effect. Within a laser fiber, thermal

load is generated in the doped core due to the intrinsic heat sources, such as the quantum defect and the intrinsic absorption. Accordingly, the temperature in the core zone is much higher than that in the cladding, eventually forming a steady transverse heat distribution in the cross section of the fiber. This transverse thermal distribution makes the RIP increment in the core larger than that of the cladding (normally regarded as the thermal lensing effect), and a new waveguide structure called thermal waveguide structure is formed to confine laser transmission in the core region.

Interesting works have been conducted on thermally induced large-mode-area fibers [334–345], in which people assumed the core index is lower than cladding to circumvent the inconducive impacts of thermally induced transverse index gradient on the beam quality, such as the TMI fluctuation. A confirmatory study has been performed by using a 42-μm core air-cladding Yb-doped fiber to obtain the fundamental mode output with a mode field diameter of 68 μm [340]. This investigation verifies the feasibility of thermally induced large-mode-area fiber and further improvement on the mode field diameter. Numerical simulation indicated that, the evolution of fundamental mode in a thermally induced fiber can be divided into four stages corresponding to differential gain extraction abilities [342]. In 2021, An index-depressed, over 110 μm core large-pitch fiber was designed and fabricated together with a pre-compensation of thermally induced refractive index variations. At a certain thermal level related to pumping injection, the guidance of this fiber evolves from the anti-guiding state to the robust confinement on the core modes gradually. Power schedule of its amplifier format achieved a maximum power of 170 W with the M^2 value of below 1.3 [345].

Functionalization of Passive Optical Fibers

In this section, the concept of "Functionalization of Passive Optical Fibers" is introduced to distinguish functional fibers from traditional passive fibers. For instance, this type of fiber includes functional fibers with undesired gain suppression or mode maintenance, photonic crystal fibers (PCFs) and anti-resonant hollow-core fibers (AR-HCFs) with a completely new guidance mechanism. However, the most important point is that the slight modification on the fiber structure or the working mechanism enables them to fit the delivery applications that the conventional SIFs are tricky to deal with. Although most of them have not yet achieved industrial integration for high-power delivery applications, the emerging progress reported recently reminds us of considering them as the new outlet.

In recent decades, the breakthroughs of HPFLs in power scaling and brightness enhancement have further injected new impetus into the advanced applications requiring remote processing, lower beam divergence and higher

manufacturing precision. For example, the most classical application in laser cutting is likely to cover a working area usually larger than dozens of square meters. The field of rock drilling dictates a constant drive towards higher laser powers, more efficient transmission from further away and a good beam quality. Wobble-welding with higher precision has become an emerging market, as the prosperity of new-energy vehicle market in recent years. In summary, all of these applications derive a significant demand on the passive delivery of high-power laser towards further power scaling, longer transmission distance and requirement for beam quality maintenance. However, such an appeal may be impeded by the onset of either optical damage or nonlinear effects as the launched power gets higher, which limits the delivery length of a kilowatt-level single-mode beam to a few meters or even tens of centimeters.

A representative work accomplished by University of Stuttgart showed the high-power suitability of a 60 μm core multimode SIF by transmitting the 1 kW CW laser over 100 m length, without the onset of SRS while maintaining a nearly diffraction-limited output ($M^2 \approx 1.3$) [346]. Preservation of nearly diffraction-limited beam quality over hundred meters of length in this work relies on a careful design of fiber RIP and cascade modal matches to suppress the internal modal coupling [340–349]. However, the beam quality degrades as the fiber length increases to 380 m, which suggests that longer delivery length and better beam quality maintenance is a challenging task for conventional SIFs to meet higher demands on laser power.

Fulfillment of these special requirements entails novel fiber structures for robust single-mode output and nonlinear-free delivery. Fortunately, recent advent of modified filtering fibers opens a promising pathway toward powerful laser delivery by engineering the cross-sectional structure and confinement loss proactively. Although most of the delivery applications require high brightness or single-mode character, please note that the mode maintenance emphasized here is related to both the single-mode fidelity and the mode maintenance of high-order structured beams. Many approaches have been carried out to generate structured light patterns based on both the intracavity and the external elements, but the shape preservation of a structured beam is hard to achieve during long-distance delivery, which becomes more challenging with higher power levels [344–352].

Advanced Delivery Fiber for SRS-Free Propagation

Taking advantage of the wavelength manipulation technique called spectral filtering, researchers can design functional fibers with artificial RIPs to customize the transmission wavelength, especially for the long-distance delivery of signal laser. Transferring the concept of the selective filter

into delivery fibers is beneficial to mitigate the nonlinear or unwanted effects, which injects a new degree of spectrum freedom into fiber landscapes to dramatically boost long-distance delivery performance. To date, various fiber designs have been adopted for the mitigation of detrimental SRS, as described in the following.

Modified SIFs with resonant rings or absorbing inclusions A typical route for spectral filtering in functional fibers is the resonant coupling concept, as illustrated in Fig. 6a and b. For a general design with resonant rings in the cladding region, core mode at the matched wavelength couples to resonant rings resonantly while maintaining a tight confinement on the signal wavelength. At the wavelengths close to index-matching point, energy transduction occurs between the core mode and cladding mode, which results in mixed modes and high confinement loss, as shown in Fig. 6b. In 2005, Fini et al. designed and fabricated a novel type of distributed filter fiber based on the principle of resonant coupling between core and cladding [353], the fiber structure is depicted in Fig. 6c. This fiber was designed to have an index-matching point at a wavelength around 1100 nm for the core mode and the ring modes. Measured transmission spectra and imaging of output mode confirmed the expected

filtering of about 10 dB at 1100 nm, suggesting a preliminary SRS filtering potential for the delivery of high-power lasers around 1 μm. Recently, Aleshkina et al. proposed the anti-crossing approach for the suppression of undesirable wavelength in a few-mode step-index fiber by incorporating high-index absorbing inclusions into the fiber cladding [354, 355], which demonstrates the possibility of controlling spectral bandwidth through appropriate choice of fiber parameters and fiber bending. The developed technique can be very useful for the design of fiber-based spectral filters (i.e., active or active fibers with suppression of frequency shift to undesirable wavelengths, mitigation of SRS). Main advantage of this technique is the versatility in the RIP tolerances of high-index inclusions. It should be noted that the design philosophy of absorbing inclusions can be extensively duplicated to various kinds of fibers, for example, the hybrid multi-trench fiber [217] or hybrid PCF [356, 357] demonstrated previously.

Distributed filtering fiber with microstructure Through imbedding two high-index rings in the depressed cladding region of a W-type fiber, the performance of SRS suppression with such a modified fiber was presented [359]. This fiber has a concentric structure that is feasible to be

Fig. 6 Functional passive fibers for SRS-free propagation. **a** The principle of filter fiber with resonant rings in the cladding region, core mode at the matched wavelength couples to resonant rings resonantly while maintaining a tight confinement on the signal wavelength. **b** Schematic diagram of resonant coupling at the matched wavelength. **c** Structure of distributed filtering fiber with two resonant rings embedded in the cladding. **a–c**; Reproduced with permission from Ref. [353], Copyright 2005, Optical Society of America. (© 2005 Optical Society of America under the terms of the OSA Open Access Publishing Agreement). **d** Cross section of AS-PBGF for Raman gain suppression and the transmission spectra with different bending radii; Reproduced with permission from Ref. [358], Copyright 2007, IET
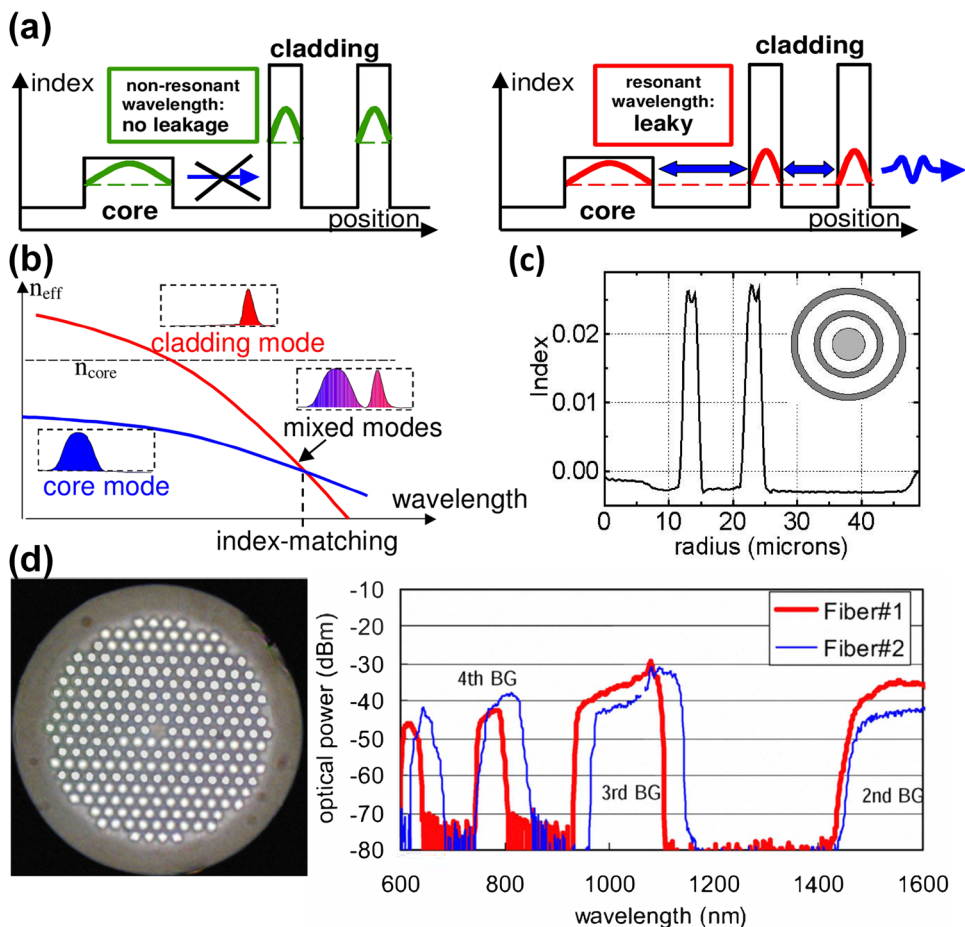
fabricated through the MCVD technique; however, the experimental characterization shows undesired couplings between core modes and high-order ring modes, indicating the fiber parameters are sensitive to manufacturing tolerances. As an improved scheme, Codemard et al. proposed a more advanced microstructure fiber by embedding a series of circularly arranged high-index rods in a leaky silica cladding [359, 360]. Enabled by the combination of the wavelength-dependent mode delocalization and the leakage mechanism, this microstructure fiber exhibited a loss extinction in the excess of 20 dB at the SRS waveband with negligible fundamental mode loss (< 0.01 dB/m) at the signal wavelength at the same time, even with a bending radius as small as ∼ 5 cm. This demonstration opens up the preliminary potential for SRS filtering delivery in HPFL applications. Specifically, over 9 m passive delivery with the peak power of up to 3 kW and a single-mode beam profile was experimentally executed.

All-solid photonic bandgap fiber (AS-PBGF) for spectral filtering AS-PBGF with all-solid substrate [361] is also attractive to increase the length of delivery fiber with enough suppression on SRS effect. Such an advanced fiber incorporates the advantages of all-solid fiber including bending-resistant operation and the feasibility for post-processing including tapering and splicing. Most importantly, its intrinsic potential superiority in spectral filtering which is evolved from the photonic bandgap guidance [356–365]. A mode is guided only when it falls within the photonic bandgap (PBG) of the cladding lattice, otherwise, a continuous waveband called photonic band suffers from high confinement loss because of the strong resonance leakage [365]. Controllable PBG distributions can be easily adjusted by drawing the fiber to various parameters with a certain RIP of the cladding lattice. A further development was the use of the high loss spectral regions between PBGs to selectively suppress undesired gain for some laser delivery. SRS gain was suppressed in a passive AS-PBGF by ensuring the 3rd PBG was spectrally positioned to provide high transmission at 1064 nm and high loss at the 1st Stokes wavelength of 1120 nm [358]. The index contrast of the germanium doped cladding rods was 3% and d/Λ was 0.6 giving an effective mode area of 50 μm². From a 50-m-length fiber, more than 40 dB of suppression was obtained, as illustrated in Fig. 6d. The relevant PBG edge was stable under bending down to a bending radius of 20 mm. Also, Blin et al. presented a large-mode-area AS-PBGF offering a 413 μm² core area for SRS-free propagation at 1064 μm [366]. The measured losses are 0.07 dB/m and 16 dB/m for signal and Stokes waves, respectively. Despite no experiments on the high-power CW delivery reported for AS-PBGF until now, this kind of fiber exhibits more powerful SRS suppression near 1 μm than any other published results. Three attempts for AS-PBGF to transcend are lower fiber loss, drawable uniformity along

with the longitudinal direction and single-mode designs with large core area, meanwhile the hetero-structured designs should be stressed [361–370].

Breakthrough of Microstructure Fibers for High-Power Delivery

In recent years, microstructure fiber technology has revolutionized the field of optical fibers [33, 363, 364, 365–374], enabling a wide range of novel optical properties to be realized. Air-hole-based PCFs are well-known to realize novel optical properties and are expected to suit various applications. The effective relative index difference between the core and the cladding area of air-hole layers can be flexibly controlled to 0.01–10% or higher. In particular, the PCF has great advantages in the "endlessly single-mode" operation, large core mode area and single material media, which can contribute to the large bandwidth and longer distance delivery. Laser transmission within the large-mode-area PCF is considered to directly improve the delivery distance of the high-quality and high-power single-mode beam.

10 kW-level delivery enabled by PCF It is the profound demand of laser processing that accelerates the potential of PCF to realize high-power transmission with good beam quality and a delivery length far away. Recently, researchers from Mitsubishi Heavy Industry Ltd. experimentally revealed the 300-kW m high-power delivery for the multi-kilowatt single-mode laser by utilizing the fabricated quasi-uniform PCF [375]. The first experiment was a 300-m-length transmission of the 1 kW single-mode laser beam. The second one was a 30-m-length transmission of the 10 kW single-mode laser beam. The 10 kW experiment successfully delivered over the 30-m-length fiber cable containing a fabricated PCF with a beam quality of $M^2 = 1.7$ [376], both the experimental results and the estimated data indicate a great potential of over 400 kW m for high-power delivery by employing this quasi-uniform PCF. This demonstration presents the charming potential of PCFs to support hundred meters delivery of the multi-kilowatt laser while maintaining the output beam quality.

AR-HCFs play the role of rising stars AR-HCFs have attracted significant attention in recent years as an ideal medium for ultra-high-power laser transmission with the advantages of lower nonlinearity, high damage threshold compared with the common solid-core fibers, much broader transmission windows and more flexible fiber designs. AR-HCF is one of the most popular microstructure fibers according to the emerging results reported recently. High-power pulse delivery employing AR-HCFs has been a well-known topic, it appears that researchers are turning more and more attention to its CW delivery applications [371–383].

Literally, Newkirk et al. tested a 5-m-length AR-HCF whose facet is possible to handle a testing power of up to 170 W input, 0.7 GW/cm^2 with no damage to the fiber [379]. The maximum 300 W power at 1080 nm was successfully delivered with nearly diffraction-limited output by using a 3-m-length uncooled AR-HCF [380], as shown in Fig. 7a. A recent study broke the debate over whether the AR-HCF could handle multi-kilowatt-level average power class (Fig. 7b). The tested 1.5-m-length negative-curvature AR-HCF shows a power handling up to 1.2 kW [377]. The experiment of kilowatt level delivery over kilometer-scale has been affirmed by Mulvad et al. more recently, and they realized the delivery of 1 kW of near-diffraction-limited CW laser over an unprecedented 1 km distance, with a total throughput efficiency of ~ 80% [381], the experimental setup and results can be found in Fig. 7c. It points out a potential route to achieving two or more orders of magnitude improvement in power or distance over what is possible with solid-core fibers.

All the above works were implemented with the launching condition of spatial coupling, but it is also crucial to systematically investigate low-loss splicing between an AR-HCF and a solid-core fiber to fully exploit the anticipated benefits of using the AR-HCF for beam delivery. When a high-power laser was coupled into a long AR-HCF, the energy resonance between HOMs and the cladding region results in thermal dissipation of laser power, leading to an increased temperature at the fiber facet and may cause possible damage. Consequently, researchers conducted an integrated demonstration for high-power delivery, by carefully splicing the AR-HCF with a widely used commercial large-mode-area SIF that is mode-matched to the AR-HCF [378,
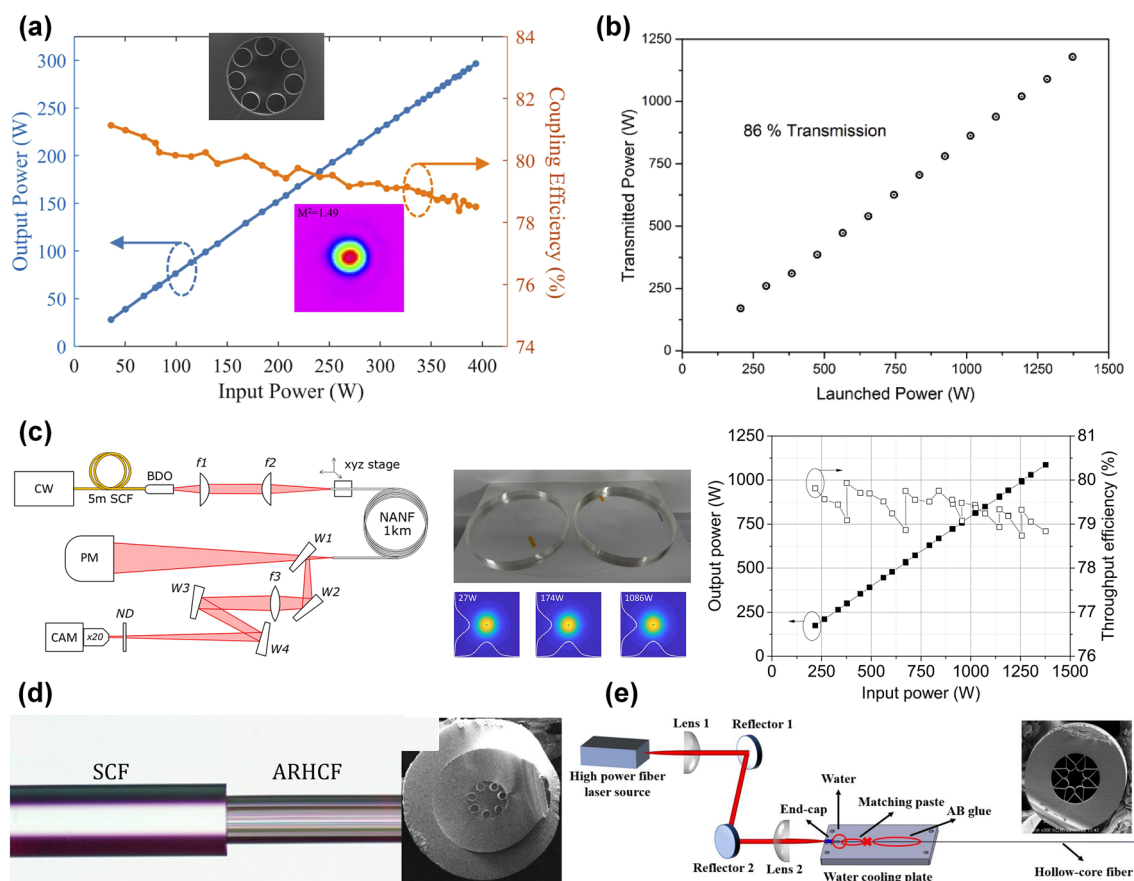
Fig. 7 Representative publications of AR-HCFs for high-power CW delivery. **a** Measured output power and coupling efficiency from an uncooled low-loss AR-HCF with the highest delivery power up to 300 W; Reproduced with permission from Ref. [380], Copyright 2021, Optical Society of America. (© 2021 Optical Society of America under the terms of the OSA Open Access Publishing Agreement). **b** Experimental results of a Kagome AR-HCF for high average power transmission, the maximum output power could be scaled to 1.2 kW with an overall efficiency of 86%; Reproduced with permission from Ref. [377], Copyright 2018, Optical Society of America. **c** Experimental demonstration of kilometer-scale, kilowatt average power, single-mode laser delivery through a nested AR-HCF; Reproduced with permission from Ref. [381], Copyright 2022, Springer Nature. **d** Longitudinal and transverse perspectives of AR-HCF fusion spliced with gain fiber for high-power delivery; Reproduced with permission from Ref. [383], Copyright 2022, Optica. (© 2022 Optica Publishing Group under the terms of the Optica Open Access Publishing Agreement). **e** Highly efficient coupling of kilowatt-level CW laser into AR-HCF through splicing the fiber with an end-cap; Reproduced with permission from Ref. [382], Copyright 2022, Chinese Laser Press

383], as shown in Fig. 7d. Their latest research demonstrated an efficiency of 90.4% and the CW delivery of 50 W with a stable and alignment-free all-fiber laser setup [378]. The newest result reported by Cui et al. obtained a highly efficient and stable launching into AR-HCF with the maximum transmission power reaching 1021 W through splicing the AR-HCF with a fiber endcap [382], the experimental setup can be found in Fig. 7e.

The Rising Power of Functional Fiber-Based Components

In this section, a series of common candidates for fiber-based components are reiterated. Although most of HPFLs employ them as major components, some novel functional advances are profoundly highlighted here, indicating the superiority for suppressing parasitic effects and higher power handling.

High-Power FBG: from Resonator to Spectral-Spatial Filtering

Since Hill et al. discovered the photosensitivity of germanium-doped fiber and wrote the first fiber-based grating by using the bi-directional propagation of argon ion laser in 1978 [384], FBG has achieved rapid development and become one of the most essential fiber-based components which are widely employed in fiber lasers, optical communication, fiber sensing and other fields. Up to now, conventional HPFLs exploiting dual-end FBGs, as discussed in Sect. 2.2.1, have experienced the power evolution from several hundred watts to several kilowatts and are deeply hampered by SRS effect. In 1990, Meltz et al. proposed the tilted FBG model for the first time [385]. The grating plane of a tilted FBG is not perpendicular to the axial direction, which strengthens the coupling of the fiber core mode transmitted forward to the cladding mode transmitted backward. Because of the special mode coupling characteristics, fiber filter has become the most basic application of tilted FBGs. It has been reported that a wideband bandpass filter with adjustable bandwidth can be fabricated by combining chirped modulation with a tilted FBG [386], which broadens the application scope of FBGs from high-power resonance to spectral filtering.

Few-mode FBG has reflection spectrum characteristics related to specific spatial modes, each mode corresponds to a different wavelength of reflection peak so that modes can be distinguished if the FBG is artificially designed. In this situation, FBG can be used as an all-fiber mode selector when combined with a wavelength selector (i.e., volume FBG or acousto-optical filter). Point-by-point fabrication of multimode FBG by femtosecond lasers offers an opportunity

to tailor the FBG transverse profile with high spatial resolution [62, 387].

Chirped and Tilted FBG (CT-FBG) and Long Period FBG (LP-FBG) for Raman Suppression

Typically, the function of both the CT-FBGs and LP-FBGs is to convert the core-guided light at unwanted Raman 1st-Stokes wavelength to the cladding-light and then strip it out to suppress the SRS effect. The CT-FBG evolves from the predecessor of tilted FBG under the chirp modulation [385, 386, 382–390], which is inscribed in large-mode-area fibers by using the side-writing technique with phase masks. Through the writing process, the phase mask rotates to generate a specific tilted angle, as shown in Fig. 8a. If a tilted FBG is chirped, the discrete resonances of core-cladding mode coupling are broadened to such an extent that they end up overlapping considerably [385, 386]. As for the transmission spectrum, instead of the multiple cladding resonances with clear sub-peaks at discrete wavelengths, a continuous spectral profile over a broadened band appears [386], see Fig. 8b. Consequently, CT-FBGs are considered to provide great potential for broadband fiber filters [391, 392].

The first experimental demonstration for SRS suppression by using CT-FBG after the seed showed a maximum suppression ratio of nearly 25 dB in a single-mode fiber amplifier [388]. Through developing the inscription technology in a piece of 20/400 photosensitive fiber, a CT-FBG was then applied in a 3.5 kW MOPA [390], achieving a maximum SRS suppression ratio of 10 dB. Subsequently, single-stage CT-FBG and two incorporated CT-FBGs were successfully exploited in a 5 kW tandem pumping fiber amplifier with a maximum SRS suppression ratio of above 15 dB [395]. Moreover, the SRS suppression by employing CT-FBG is also applicable for fiber lasers with other special features such as the narrow linewidth types [396] or the ability for ultra-long-distance delivery [397].

To further improve the power handling ability of CT-FBG, the method to reduce thermal slope is applied by lowering the working temperature together with variable-high-temperature annealing [389]. Suppression of SRS in a CW fiber laser near 1 kW was realized with a suppression ratio close to 23 dB. Note that it was a remarkable improvement for CT-FBG in terms of power handling capacity since it handles the full transmitted laser power rather than only modulates the seed laser. In addition, cascade CT-FBG is another solution to mitigate local thermal load. Multiplexed CT-FBG with five elements cascaded has been developed for SRS suppression in a fiber laser system with a 3 kW output [398]. Elements of the multiplexed CT-FBG extended along the longitudinal direction with a length of ~ 6 cm for each segment and are separated by ~ 4 cm, presenting a high thermal handling capacity of ~ 1.48 °C/kW.
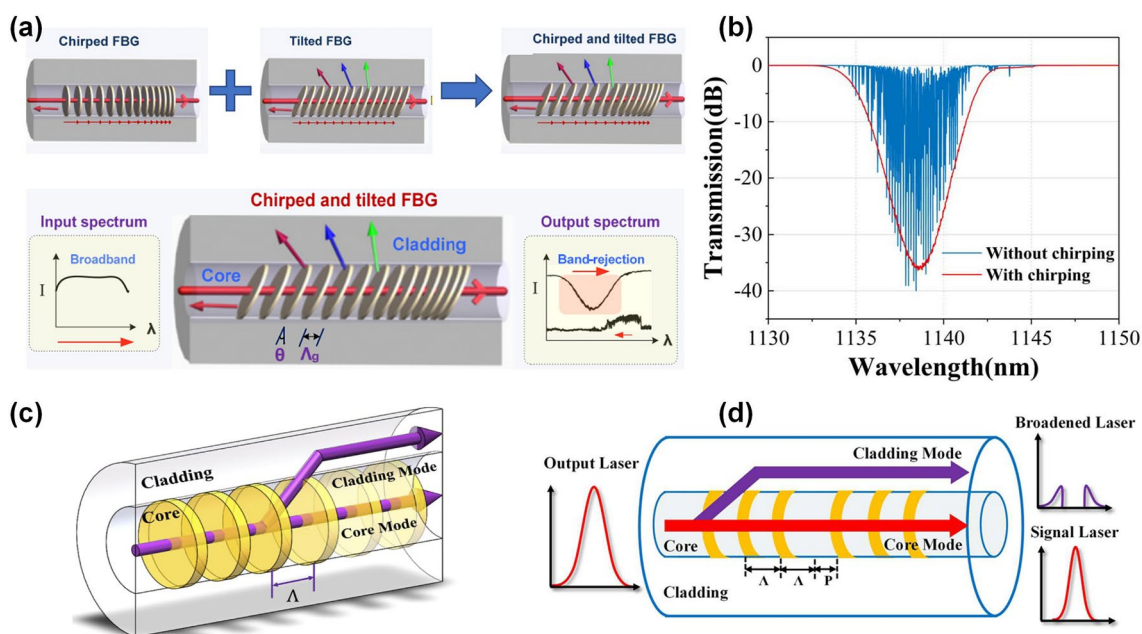
Fig. 8 Mechanisms of CT-FBG and LP-FBG for Raman suppression and spectrum compression. **a** The fabrication process of a CT-FBG and schematic diagram of bandpass filter based on CT-FBG for SRS mitigation; Reproduced with permission from Ref. [386], Copyright 2014, Optical Society of America. **b** Simulated transmission spectra of a tilted FBG and a CTFBG with a specific tilt angle; Reproduced with permission from Ref. [389]. Copyright 2019, Chinese Laser Press. **c** The structure of a LP-FBG; Reproduced with permission from Ref. [393]. **d** Suppression of spectrum broadening by using a LP-FBG in narrow linewidth fiber lasers [394], Copyright 2020, Optical Society of America.

Around the central wavelength ~ 13.2 THz downshift from pump wavelength corresponding to the peak Raman gain, the actual linewidth of Raman Stokes is relatively broad [333, 335, 399]. Thus, there is a problem that the rejection bandwidth of most of the CT-FBGs is not wide enough to cover the whole Raman spectral range at the high-power level, which results in ineradicable sidebands on both sides of the output spectrum [395, 397, 400]. To broaden the SRS suppression bandwidth of CT-FBGs, a simple tandem writing technique that inscribes two CT-FBGs with different inscription tilt angles has been reported, giving a 3 dB bandwidth of broader than 20 nm [400].

However, CT-FBGs have some drawbacks such as time-consuming pretreatment and back-propagating light caused by Bragg reflection, which may seriously affect the laser output power, efficiency and beam quality [401]. Hence, the transmission grating, i.e., LP-FBG [390, 393, 394, 396–405], may be a better alternative. LP-FBG can eliminate SRS band by coupling the Stokes light from the core mode to the forward cladding mode, through which the reflected light could be effectively avoided [404], as illustrated in Fig. 8(c). Based on this concept firstly proved by Nodop et al. [403], the feasibility of LP-FBG with strong attenuation of 16 dB at SRS band was demonstrated [402]. Recently, Jiao et al. reported that the LP-FBG fabricated by ultraviolet point-by-point scanning can also be effective for

suppressing SRS, the experimental results of which demonstrated SRS suppression ratios of over 15 dB and 24 dB in different fibers [393].

Except for the unwanted SRS effect, other nonlinear effects (such as self-phase modulation or four-wave mixing effect) related to spectral broadening require to be suppressed as well, especially in the case of narrow-linewidth fiber lasers. Bian et al. proposed to utilize a phase-shifted LP-FBG to filter the broadened spectrum in a high-power MOPA system, and the 3 dB linewidth of output spectrum was narrowed by approximately 37.97% [394], the basic principle can be found in Fig. 8d. However, the drawback of LP-FBG is high sensitivity to temperature, strain and bending, which might lead to a drift in the cladding-mode resonances and a reduction of the suppression ratio. Hence, the next major goal is to enhance the robustness with various environmental parameters.

FBGs for Transverse Modes Tailoring in Multimode Fibers

The reflection spectrum of mode resonance for an FBG inscribed in a large-mode-area fiber is closely related to the transverse RIP and spatial frequency. In the early days, a volume Bragg grating has been proposed for transverse mode selection in multimode fiber laser by tuning the incidence angle of the grating carefully [406]. This technique exploited

different spectral responses of feedback elements based on an FBG and a volume Bragg grating to achieve wavelength-dependent mode filtering. Fast switching between LP_{01} and LP_{11} mode at ~ 20 kHz repetition rates was realized [392]. In 2016, a more compact all-fiberized scheme with stable LP_{11} output was proposed based on a pair of few-mode FBGs, showing that the mode-related spectral response of few-mode FBGs can be used to design a mode-selective FBG pair [407]. The following power scaling pushed the maximum output power to 4.2 W, which suggests the potential of realizing higher power by using the FBG pair [408].

The possibility of FBG positioning in the fiber cross section makes it possible to change the grating coupling coefficient and select a desired group of transverse modes spectrally [387]. Wolf et al. have reported results for a multimode fiber where precise positioning of RIP modification in the transverse direction makes it possible to select different groups of modes in the spectral domain [409]. The fiber used in experiments for FBGs inscription was a 62.5/125 μm multimode optical fiber from Corning. Groups of modes having a field distribution beyond the central part of fiber core in a multimode fiber could be efficiently selected. Then, the spatial-spectral beam control was realized in a Kerr-cleaned Raman fiber laser, in which FBG acted as a spatial filter to generate dominant guidance for the fundamental mode [410].

An investigation on the LP-FBG reported in 2019 shows that, the selective mode control of tailored femtosecond-written LP-FBG could be realized with strong selectivity and high precision [411]. Near field measurements of modal profiles confirmed that the mode assignment and the intensity distributions are matches with simulated results. This developed tool paves the way for novel LP-FBGs together with several fiber-integrated devices, such as highly efficient transmission gratings or mode converters.

Tap Coupler (Tapper)

Fused fiber tap couplers are widely used in optical communications, sensing and fiber lasers for splitting optical signals between two fibers or combining optical signals from two fibers. For high-power fiber amplifiers, since the amplification of the signal laser occurs only in the optical domain, it is of paramount importance that these amplifiers exhibit excellent gain stability. Even very small changes in amplifier gain can have serious consequences in cascaded amplifier systems. The component labeled "tap" plays a key role in the stability of the amplifier, since it taps off a small amount (usually to 1–10%) of the amplified signal as a feedback signal to the monitor devices. Such tap components must exhibit extreme stability themselves if they are going to perform reliably in the high-power feedback loop. Any instability in this component can be misinterpreted by

monitors as instability in the amplifier gain. As is required for all passive fiber components, power capacity is the most daunting challenge faced by tap couplers when they are serving high-power laser systems.

For example, multiple tap couplers with a power capacity of ~ 50 W were exploited in an all-fiber structured laser array to achieve distributed active phase-locking [412]. Fiber couplers were inserted in the main laser chain to constitute a measuring loop that transmits the phases of main chains to the measurement loop for phase-locking information extraction. A similar application using two commercial 99.9/0.1 asymmetric fiber couplers was also reported with a power capacity of up to 100 W, and researchers claimed that per channel limit of laser power is expected to overcome 100 W by moving the tap couplers to fibers with larger mode area. In 2021, an improved fiber tap coupler based on large-mode-area fiber was fabricated. As a remarkable attempt, the coupling condition of this tap coupler was mechanically adjusted to increase the optical handling power to 740 W [413], with the insertion loss and coupling ratio of 0.20 dB and − 32 dB, respectively. Suitable tap couplers are available for kilowatt-level high-power fibers laser to monitor the output power if this technology is further customized.

Mode Convertor

The traditional applications of high-power fiber lasers mostly target single-mode signal operation with only fundamental mode maintaining. As the digital manufacturing revolution is forthcoming, the generation of dynamic spatial beam profiles is of particular interest, especially in material processing applications with high requirements on fine laser-material interaction control. Thus, not only the fundamental mode, but also multimode "donut" or flat-top beam profiles with certain modal contents are desirable. Nowadays, various routines to generate adjustable beam profiles, using a mechanical switch, external mode convertor or beam combination of laser cavity have been performed. However, the "smart" control on beam generation with high freedom at the power level of kilowatts level is emerging to respond to new challenges.

From 2019 to 2021, the SPI Lasers reported the variMODE-Pro technology [408–416], enabling adjustable output beam profile from diffraction-limited Gaussian profile to complex "quasi-ring" beam with higher-order azimuthal modes, namely as petal beam, as shown in Fig. 9. In contrast to other existing commercial solutions mentioned before, this unique approach is based on careful design on the refractive index change induced by the mode coupler, leading to the negligible measurable loss. Furthermore, the readily power can be scalable up to 2-kW

level [416], which is far beyond what other publications reported.

Fiber Combiners Based on Advanced Fibers

Although the advanced optical fibers with special structures are expected to bring the breakthrough in power scaling of fiber lasers and amplifiers mainly limited by nonlinear effects and TMI, the highly integrated signal and pump combiner is also a key component for the practical realization of a high-power fiber laser system based on the specialty fiber. However, the typical fused tapered fiber bundles are found to have the drawbacks of high requirement on optical mode matching and the fusion splice to the output fiber. Thus, the input signal beam quality is easily to be degraded significantly by a slight mismatch or misalignment in the TFB architecture, which is hard to be avoided in the case of fusion splice between the specialty fiber and standard fiber. By contrast, the side-pumping combiner can avoid the interruption on the signal fiber and thus benefit the maintaining of signal beam mostly, thanks to the pumping light coupling into the signal fiber via the outermost cladding surface. To achieve the pump coupling individual from the signal light, the coreless intermediate fiber is tapered and twisted around the signal fiber.

Recently, a novel side-pumping combiner based on CCCF is demonstrated [45, 234, 417], the schematic view is shown in Fig. 10a. Combining up to four fiber-coupled pump diodes, a pump-light limited power handling of 600 W was achieved with an efficiency of 78% [234]. Furthermore, the highly-integrated monolithic high-power fiber amplifier based on active Yb-doped CCCF and CCCF-based side-pumping combiner at 1064 nm is performed. The presented design allows a stable and robust amplifier with the least possible number of splices. Up to an output power level of 103 W, the measured fundamental mode content of the amplifier reaches as high as 98.9% [45]. Through further optimization on the CCCF combiner fabrication, single-frequency laser generation over 335 W released recently was measured with a fundamental mode content of 90.4% and no impact of TMI or other parasitic effects were observed [417]. Integration of optical components in specialty fibers as CCCF allows compact all-fiberized systems, which can be implemented in almost any high-power amplifier or laser architectures.

As the HPFLs exploiting microstructure PCFs become commercially and scientifically successful, fully fused and monolithic PCF-combiners are experiencing a time of peak demand. Compared with the commercial combiners based on conventional SIFs, integrated combiners designed for the air-cladding pump technology require a more serious treatment on the fabrication process, especially the efficient match between the bridging fiber and the air-glass interface of inner-cladding. In 2012, a $(6+1) \times 1$ polarization-maintaining PCF combiner with a maximum pump capacity of over 1.5 kW and a transmission efficiency of nearly 92% was experimentally demonstrated [418]. To achieve a high coupling efficiency, an etched taper that transforming the pump light from a low NA large diameter case into a high NA small diameter one was spliced as the bridging fiber [419], and the architecture is illustrated in Fig. 10b. With continuing improvements of the post-processing technique for microstructure fibers, the goal of fielding better beam quality, and highly efficient pump coupling operating at multi-kilowatt or higher level in ultra-compact PCF combiners should be realized. A monolithic tapered pump combiner for air-cladding PCF fibers fabricated by tapered fused buddle method was described with a maximum coupling
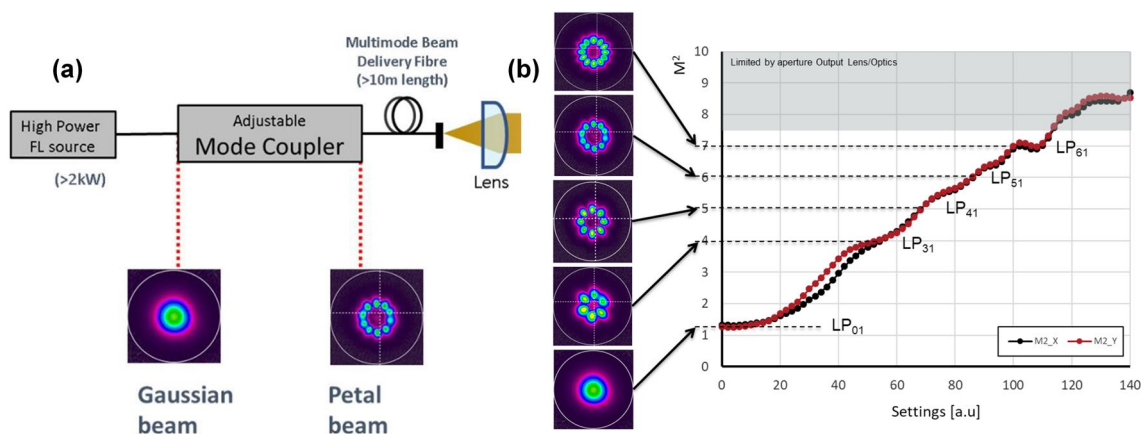
Fig. 9 Mode convertor with several-kilowatt-level power handling capacity for **a** generating fiber-delivered petal beams; Reproduced with permission from Ref. [416], Copyright 2020, Society of Photo-Optical Instrumentation Engineers (SPIE), and **b** the beam qual-

ity measurement of beam profiles for different orders; Reproduced with permission from Ref. [415], Copyright 2021, SPIE. (© The Author(s) 2021, distributed under the terms of the Creative Commons Attribution license (http://creativecommons.org/licenses/by/4.0/))
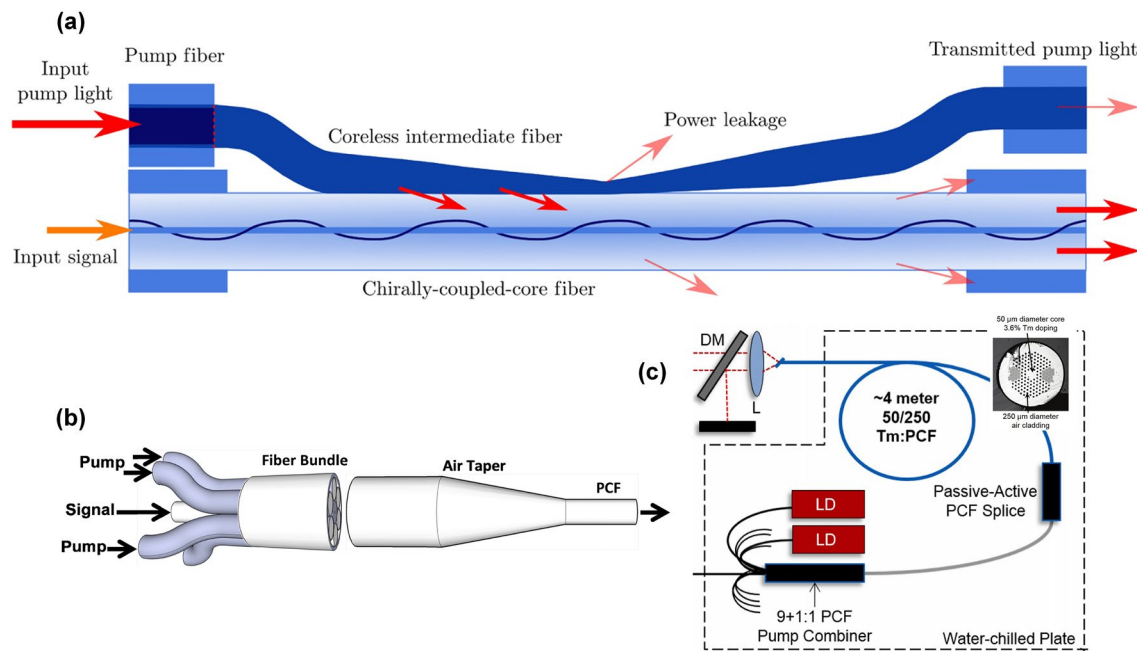
Fig. 10 Structures and applications of fiber combiners based on advanced fibers. **a** Schematic diagram of a side-pumped CCCF combiner; Reproduced with permission from Ref. [234], Copyright 2021, IEEE. (© The Author(s) 2021, distributed under the terms of the Creative Commons Attribution license (http://creativecommons.org/ licenses/by/4.0/)). **b** Monolithic signal-pump PCF combiner with over 1.5 kW pump power handling capacity; Reproduced with permission from Ref. [418], Copyright 2012, SPIE. **c** Tm-doped PCF pump combiner and its system integration for laser amplification; Reproduced with permission from Ref. [424], Copyright 2014, SPIE

capacity of 800 W at 915 nm [420], allowing for the production of 6×1 or 1×1 pump formats. The high-power test for the PCF combiner ends with a generation of a 350-W supercontinuum laser and a slope efficiency of 60%, indicating a strictly single-mode fidelity.

A side-coupling format for air-cladding PCF with a good coupling efficiency (> 90%) was also achieved [421, 422], in which the holes in the air-cladding region are collapsed and a multimode bridging fiber is fused with the side of the collapsed region. However, this concept was only demonstrated at a relatively low-average power. In addition to improving the pump coupling efficiency and further mode area scaling, fiber integration for high-peak power all-fiber Tm-doped laser application was performed. The reported $(9 + 1) \times 1$ PCF combiner was fabricated with a 25/250 µm, 0.06 NA polarization maintaining step-index signal input and a 50/250 µm, 0.06 NA PCF output port [423, 424], as schematically illustrated in Fig. 10c. Unfortunately, in this case, the all-fiberized integration further decreases the slope efficiency relative to the free-space coupling of pump light [424].

Adaptive Fiber Optics Collimator (AFOC)

In most cases, coherent combination of high-power laser arrays is considered as a promising technique to reach higher power when the laser amplification within a monolithic fiber was disturbed by parasitic effects. An efficient combination requires the coherent interaction of the multi-channel apertures under the phase-locked condition. However, due to the possible assembly error or the pointing error of collimating lens, mechanical vibration and atmospheric disturbance, etc., the optical axis of each unit beam deviates randomly from the ideal direction, which may result in the tilt aberration of wavefront degrading both the combination efficiency and the beam quality. Hence, it is an immense demand to develop adaptive elements with high working frequency and precise alignment on the tilt aberration correction.

AFOC is a kind of device that changes the position of fiber facet in the focal plane of collimation lens by controlling the strain medium, the basic principle is illustrated in Fig. 11(a) and b [425, 426]. Through changing the position of fiber tip adaptively, the tilt aberration of transmitting wavefront is compensated precisely at a high speed. Investigations on power capacity and working frequency enhancement of AFOC have been extensively implemented in recent years, as described in the following.

The first AFOC developed for free-space communication was reported in 2005, and the tilt range of the collimated beam is 3 mrad [427]. The initial type based on bimorph piezoelectric fiber actuators was then applied in a seven sub-aperture system to compensate wavefront distortions

induced by atmospheric turbulence [428]. Further optimization on the AFOC fabrication showed an increment of fiber tip displacement to ± 35 μm, and the resonance frequency was improved to ~ 4 kHz [429]. At this point, the first adaptive experiment of AFOC for dynamic phase distortion compensation was demonstrated. Over 7 km transmission from a 0.5-kW MOPA coherent array, which electronically controlled the piston phases of outgoing beamlet with a fiber-array laser head, consists of 21-channel AFOCs, and the power capacity of the monolithic AFOC was near 20 W [430].

Remarkably, the annular SPIE Prism Awards in 2015 revealed a commercial product of Optonicus Ltd. with the single channel capacity exceeding 1.5 kW, however, no detailed results were published in the report [431]. To further enhance the power capacity and working ability of AFOC, Geng et al. have devoted themselves to improve the controllable displacement of single-channel AFOC, which increases the tunable displacement from to hundreds of microns, enabling a more flexible compensation to the tilt offset [432,

433]. Then, the AFOC with a 500-W power capacity was successfully developed to support the 1.5-kW incoherent Combination system [433]. At present, they are actively exploring the aberration correction ability of AFOCs. The wavefront sensor based on AFOC array can effectively correct the Root Mean Square of the beam combining system and has great application potential in anti-atmospheric turbulence transmission and target tracking [425, 426].

The main reason obstructing the power scaling of monolithic AFOC is the limited capacity of piezoelectric driver to drive the output fiber endcap with large volume and weight. To solve this problem, Zhi et al. have designed a novel structure of flexible hinge AFOC, as shown in Fig. 11c, which directly controls the fiber endcap instead of the bare fiber and preliminarily validates its performance in a beam combination system with an output power of near 5 W [434]. Compared with the scheme using piezoelectric ceramics, the driving force of AFOC with flexible hinges can be increased from newton to kilo-newton level. By improving the structure of key components, an AFOC with the maximal
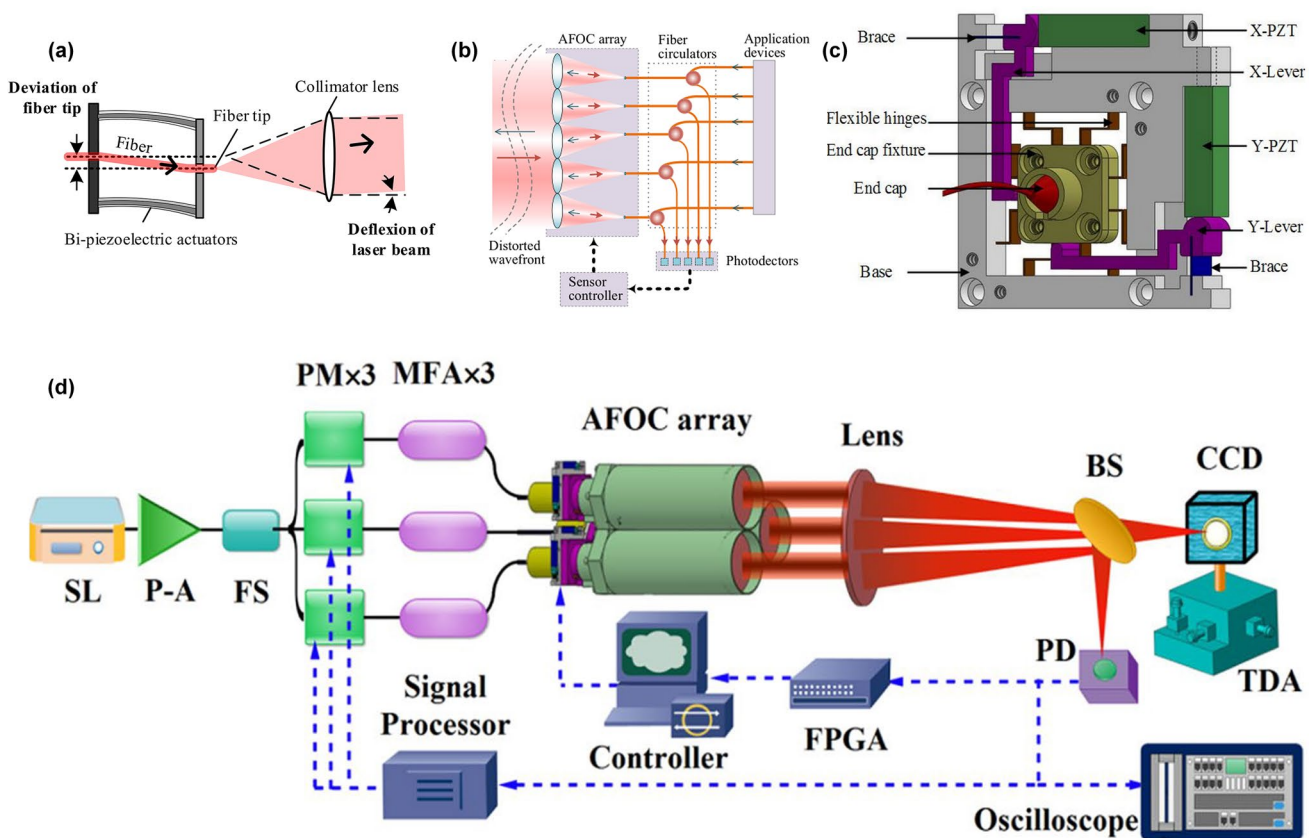
Fig. 11 Basic principle, modified designs, further power capacity scaling and applications of AFOC. **a** and **b** Working principle of an AFOC device and **b** Application of AFOC for inherent wavefront sensing; Reproduced with permission from Ref. [426], Copyright 2019, Optical Society of America. **c** Structural diagram of the modified AFOC with a large deflection angle and a preserved near-

diffraction-limited beam quality; Reproduced with permission from Ref. [435], Copyright 2014, Optical Society of America. **d** Application of AFOC for highly efficient coherent conformal projection system; Reproduced with permission from Ref. [436], Copyright 2019, Springer Nature

output power of 300 W was experimentally demonstrated, showing a larger deflection angle and a preserved near-diffraction-limited beam quality [435]. In 2019, a coherent beam combination experiment was carried out with a three-channel transmitting system based on the AFOC with flexible hinges [436], as shown in Fig. 11d. The effects of beam tilt, beam defocus and beam truncation on the combination efficiency were systematically analyzed. Most recently, a modified AOFC based on piezoelectric bimorph actuators, which adopts the cantilevered structure with a diameter of only 6 mm, was well developed to handle more than 2 kW laser power [437]. This novel AFOC can generate deflection angles of more than 1 mrad at a 20-V driving voltage. Displacements in the X and Y directions of up to 330 μm and 770 μm are supported, respectively.

As a modular approach for the development of laser transmitter systems, AFOC is an effective and suitable optical fiber device for engineering applications in multi-channel laser systems, especially in the field of long-distance laser transmission, such as the application of target in loop. With the continuous increase of single-channel laser power, it is still an urgent demand to develop AFOC with higher resonant frequency and higher power capacity that can be used in practical systems.

The Emerging Functional Fiber-Based Components for High-Power Lasers

Recent progress in functional fiber-based components has enabled positive control of light amplification and inter-modal interactions inside fiber laser system. In this section, several typical devices that facilitate customization of fiber laser output are discussed in detail.

Tunable Fiber Filter

Tunable fiber laser sources operating at ~ 1 μm have extensive applications in optical fiber sensing, laser cooling, photochemical, spectroscopy and medical fields. Generally, to generate sources with wavelength tunability, four types of fiber lasers including the traditional Yb-doped fiber lasers, cascade Raman fiber lasers, random fiber lasers and narrowband filter of super-fluorescence sources (SFSs) can be employed with the wavelength tunable device integrated into laser system. Although the output power of wavelength tunable source developed to kilowatt level at present, it should be noted that another dimension of judging the output spectrum, "the linewidth", was rarely studied. The linewidth of a laser is closely related to its temporal coherence, if this parameter is controllable, it creates a new approach for the fields of sensing or speckle imaging.

In recent years, tunable optical filters (TOFs) operating in low-power regimes (typical power capabilities of several milliwatts or watts) have been proposed to enable high-power laser output [432–441]. Commercial TOFs with different central wavelengths and filtering bandwidths are adopted to modulate the intracavity feedback or the front stage of fiber amplifier (namely, the seed laser). A distinctive feature is that, although the spectral manipulation of TOFs is carried out at a relatively low-power scale, the high-power output characteristics after multi-stage amplification are manipulated with great flexibility. Several kilowatts level fiber lasers with both the tunable center wavelength and the tunable linewidth have been built based on this device.

By employing a TOF and a half-open cavity structure, a linearly polarized random fiber laser with tunable wavelength and linewidth was reported firstly with a maximum output power of about 23 W [438], the experimental setup and representative results are shown in Fig. 12a. The wavelength tuning range is close to 20 nm (from 1095 to 1115 nm) and the linewidth tuning range exceeds 2.5 nm. Further, an improved point feedback scheme breaks through the hundred-watt-level controllable output [439], of which the central wavelength can be tuned from 1095 nm to 1115 nm continuously, the 3-dB linewidth has a tunable range of 2.1–5.5 nm, and the maximum output power exceeds 110 W.

SFSs based on amplified spontaneous emission are considered as laser sources with better temporal stability and ideal pump sources for the power scaling of fiber lasers working with special regimes, such as random fiber lasers. In the architecture of tunable SFS, the seed laser is first regulated by a TOF and then enters the main amplifier. A 120-W SFS amplifier was constructed successfully, whose operating wavelength could be tuned from 1050 to 1075 nm continuously with a linewidth tunability from 0.4 to 15.2 nm [440]. Recently, the maximum output power was further increased to 2010 W, in which the tunable linewidth range covers 2.5–9.7 nm [441], as schematically shown in Fig. 12b. As a next-generation light source serving more complex environments, fiber lasers with more flexible output and greater manipulation freedom in frequency manipulation are highly desirable. In this case, the strategy of regulating at the low power scale to obtain high-power flexible output provides an alternative approach.

Photonic Lantern

A photonic lantern consists of a collection of single-mode waveguides that are interfaced to a multimode waveguide through an adiabatic physical transition [442, 443]. A compelling feature of photonic lanterns, based on mode multiplexers, is that their mode selectivity is adjustable by
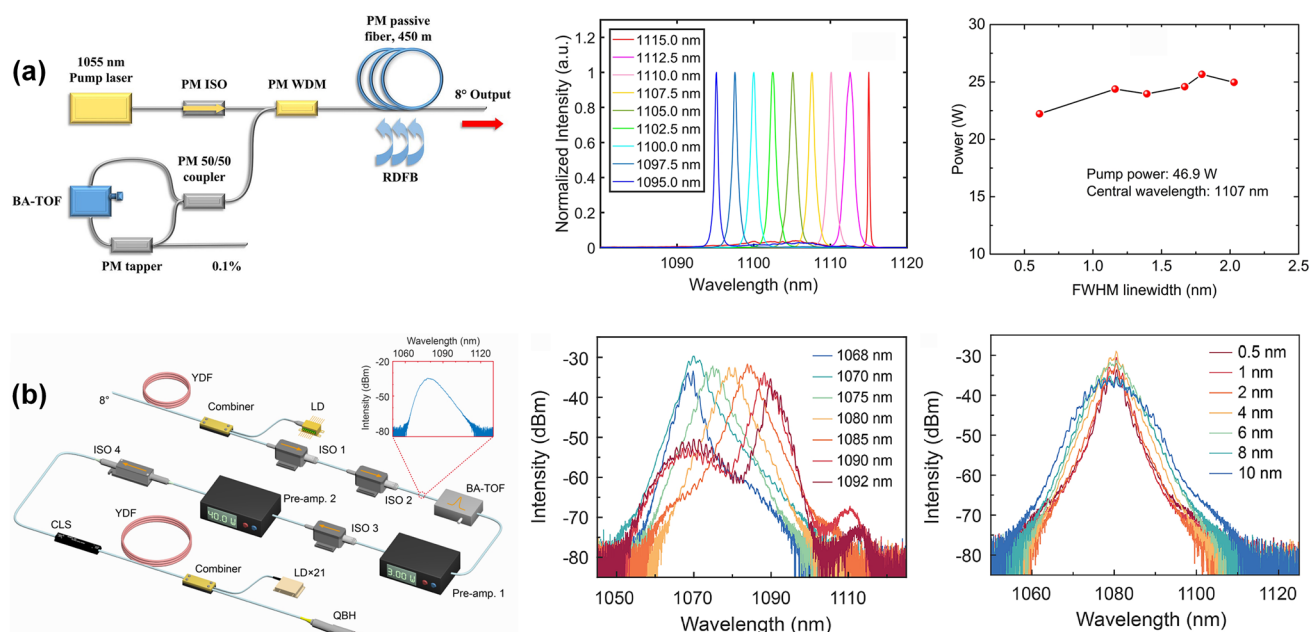
Fig. 12 Experimental demonstrations of high-power laser sources with linewidth- and wavelength-tunable outputs. **a** Investigation of flexible spectral manipulation property in a high-power linearly polarized random fiber laser; Reproduced with permission from Ref. [438],

Copyright 2018, Springer Nature. **b** Experimental setup and results of 2 kW SFS with flexible wavelength and linewidth tunable characteristics; Reproduced with permission from Ref. [441], Copyright 2021, Chinese Laser Press

selecting the arrangement of single-mode fibers judiciously. Fiber-based photonic lanterns got their name because of the similar structure to handmade lantern, as shown in Fig. 13a. If a handmade lantern is split from the middle section, the basic architecture of a photonic lantern illustrated in Fig. 13b is formed, in which each branch represents a single-mode input fiber. Ideally, if the single-mode fibers are launched with controllable amplitude and phase separately, a mode-selective device is prepared in which the output mode shows a synthetic aperture combination of all eigen modes.

Photonic lanterns were initially employed as non-mode selective scenes such as astronomical applications [444] or mode multiplexers [445, 446]. Until 2016, related studies began to develop the ability of active feedback to stabilize the fundamental mode output from a multimode fiber by appropriately launching the correct superposition of input modes in both phase and amplitude [443, 441–450]. At first, mode controllable output from a two-mode fiber amplifier that reaches several watts was realized based on the selective mode amplification in a photonic lantern [447]. Subsequent efforts were successfully made to introduce this device into the spatial mode control in higher power fiber amplifiers. More specifically, with a beam quality M^2 of 1.17 and a 97% combining efficiency, a stable fundamental mode output was emitted when the phases of multiple single-mode channels were precisely locked [443], the laser system is exhibited in Fig. 13(c). Dynamic manipulation of photonic

lanterns on the unit field refers to its multi-dimensional parameters involving the amplitude, phase and polarization. It was shown that the TMI threshold in a narrow linewidth amplifier can be profoundly boosted from 800 W to 1.27 kW through the controllable launching of seed mode generated by a 3×1 photonic lantern, revealing a prospective strategy for mitigating the TMI issue [448].

By exploiting the fabrication method based on a capillary template, the number of modes, the number of cores and the core arrangement can be customized in a photonic lantern. For HPFLs pursuing higher output power and more freedom for spatial mode manipulation, an efficient mode control in photonic lantern adopting the signal fiber with a larger core diameter requires an increasing number of single-mode input channels, which imposes more pressure on the fabrication process and overall coupling efficiency [442, 450]. Recently, a modified photonic lantern based on 30/125 μm output fiber integrated with five input single-mode ports was reported, and the output beam divergence corresponding to a beam quality of $M^2 \sim 1.2$ was obtained with the assistance of active phase control algorithm [450]. Although the operation power level is relatively low, it provides a possible technical solution to increase the tunable freedom and efficiency of spatial modes. More focus ought to be wagered on photonic lanterns, as this new class of all-fiberized spatial modulator could be a critical component for the evolution of higher power, higher flexibility, more
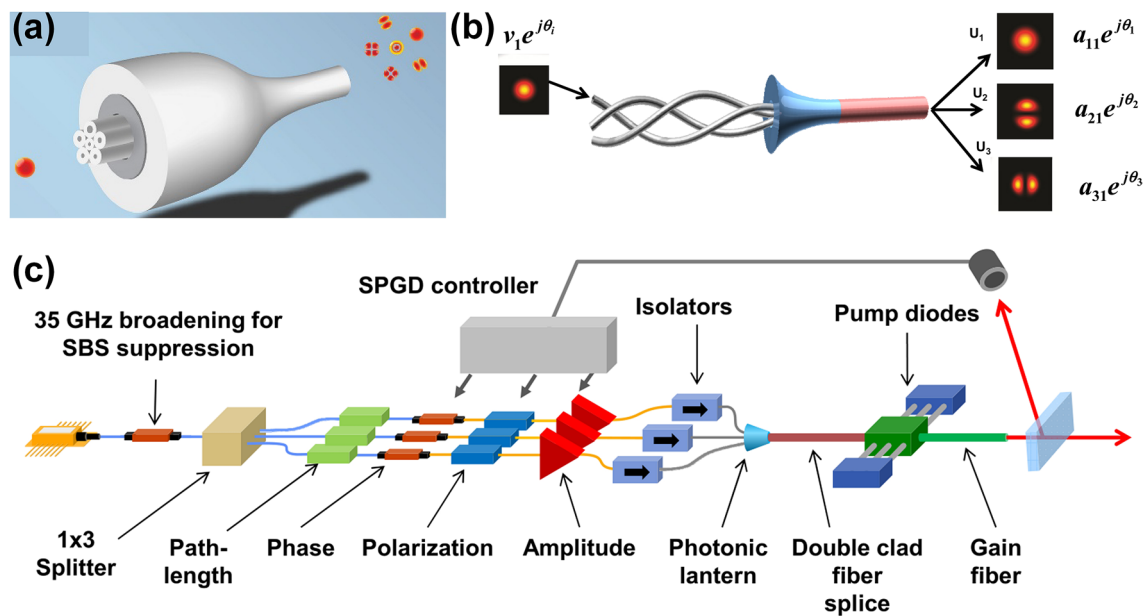
Fig. 13 Design principle, basic structure of photonic lantern and its application in mode control experiment. **a** Structure of a 6×1 photonic lantern; Reproduced with permission from Ref. [454], Copyright 2018, Optical Society of America. **b** Instructional schematic of the photonic lantern when launching a single input on one of the input channels in a three-mode lantern, which results in a superposition of the three modes supported by the output fiber; Reproduced with permission from Ref. [443], Copyright 2016, Optical Society of America. **c** Schematical diagram of photonic lantern fiber amplifier operating at kilowatt level; Reproduced with permission from Ref. [448], Copyright 2017, Optical Society of America

compactable and mode switchable fiber lasers. Also, it suggests a selective scheme for high-power coherent beam combination wherein inner phase locking can be accomplished within a monolithic integrated fiber device and hence a large amount of free-space collimators [451, 452] or micro-lens arrays [453] can be removed.

Acoustically Induced Fiber Grating (AIFG)

In addition to single-mode operation, fiber lasers with dynamic spatial mode profiles have attracted much attention due to their significance for both fundamental research and practical applications [414, 455, 456]. Taking advantage of the mode switchable output, higher processing efficiency and quality are expected for laser drilling. As described in Sect. 4.1.2, the electronically controllable system developed by Daniel et al. adopts a few-mode FBG together with an acoustic-optic tunable filter operating as an extra-cavity element [392], of which the bulk filter plays a key role in switching the output mode. However, such a fiber laser architecture seems to deviate from the original pursuit of an all-fiber format. In recent years, the invention of AIFG which facilitates the inscription in large-mode-area fibers has become an alternative solution [451–464].

Figure 14a shows the basic architecture and working mechanism of an AIFG, which is composed of a Piezo-electric Transducer, a radio frequency source and a piece of few-mode fiber [459]. Partial coating of the unjacketed fiber is stripped to form the acoustic-optic coupling region. The acoustic wave produced by radio frequency source propagates along the unjacketed fiber and makes a periodical micro-bend on the fiber and creates a dynamic LP-FBG [457, 460], the period of LP-FBG is modulated by radio frequency applied onto the Piezo-electric Transducer and obeys the phase matching condition. In this way, mode conversion among different modes is realized if different radio frequencies are applied. AIFGs contain a variety of flexible working formats: (i) intracavity operation for oscillation mode selection [459]; (ii) tailoring the mode for gain extraction in the amplifier stage through modulating the seed laser mode [464].

Mode switchable AIFG was firstly reported to generate switching LP_{11} modes and ±1-order vortex beams at a switching speed up to 4.3 kHz [457]. For this attempt, the laser operates in CW regime with narrow response bandwidth, and the switchable mode is limited to the first-order modes. To extend the transverse modes and the laser output states, a broadband AIFG-based laser working in femtosecond pulse regime was developed with the capacity for mode
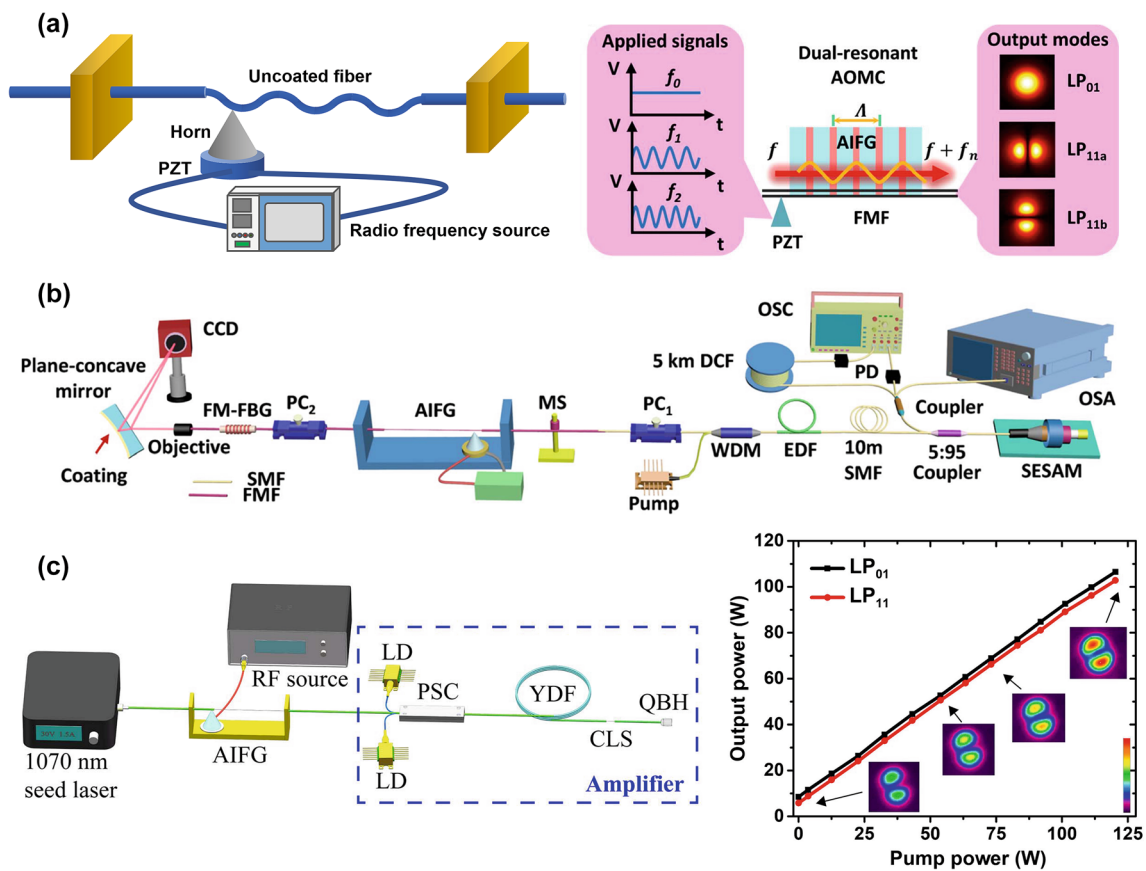
Fig. 14 Working mechanism and applications of AIFGs for mode switchable output. **a** Basic architecture of an AIFG. **b** Experimental setup of spatial mode switching in a mode-locked fiber laser based on the AIFG; Reproduced with permission from Ref. [460], Copyright 2020, Chinese Laser Press. **c** Experimental setup of the mode switch- able fiber laser based on the MOPA scheme, in which the AIFG was inserted between the seed laser and the amplifier stage; Reproduced with permission from Ref. [464], Copyright 2022, Chinese Laser Press

conversion of the second-order mode, which provides a new way to study the formation process of mode-locked pulses under the view of spatial domain [459, 460], and the experimental setup is depicted in Fig. 14b. As for the high-power CW AIFG-based fiber laser, Wu et al. have demonstrated a ~ 6 W intracavity mode conversion and agile mode switching with a switching speed between LP_{01} and LP_{11} of 250 Hz [459] and further boosted its potential in hundred-watt-level mode conversion [464], as shown in Fig. 14c. Future work could be expected to realize mode switching between more transverse modes by adopting fibers with higher NA or larger core diameter and reach higher output power for more practical applications, or facilitate agile mode switching in Raman fiber lasers [465].

All-Fiberized Isolator

The optical isolator with unidirectional light propagation is highly desirable to protect the high-power fiber lasers, optical amplifiers, and high-speed fiber optic communication systems from unwanted back reflections and propagation of light. The commercial isolator based on magneto-optic Faraday effect is commonly designed based on the bulk optics made by the magneto-optical materials, leading to the difficulty on integration and power scaling. Therefore, thanks to the advantages of low insertion loss, high return loss, and high isolation together with no need for bulky optical parts and precise alignment, the all-fiber isolator is greatly attractive for all-optical device applications [466, 467]. Until now, the all-fiberized isolators made by paramagnetic glasses with highly concentrated certain rare-earth dopants, such as Terbium (Tb), Pr, Cerium (Ce), and Dy, have been utilized to realize effective Faraday effect.

In 2010, Sun et al. from University of Rochester reported the fiber isolators based on the terbium-doped-core fiber [468, 469]. The optical isolation of 17 dB has been achieved by improving the Verdet constant to -24.5 ± 1.0 rad/(Tm) at 1053 nm, with 56 wt% and 55 wt% terbium (Tb)-doped concentration in core and cladding of silicate fiber, respectively. Later on, the terbium–doped concentration increases to

65 wt% and the fiber length reduces to 4 cm, with the Verdet constant of 32 rad/(Tm) and optical isolation of 19 dB [470]. At present, by employing this proprietary fiber technology, commercial products with 50 W power handling capacity are available from AdValue Photonics, which are claimed as the world's first all-fiber isolator with bidirectional isolation of more than 20 dB [471, 472]. The design is inherently reliable and ideal for HPFLs applications. Similarly, the all-fiber isolator based on CdSe quantum dots reaches 14 dB isolation at 660 nm [473, 474]. Recently, a new glass composition of SiO_2–Al_2O_3–B_2O_3–Pr_6O_{11} with high Pr^{3+} concentration has been reported, with a Verdet constant of 17.28 rad/(Tm) at 650 nm [475].

Summary and Prospects

Looking back to history, significant progress has been made in the power scaling of rare-earth doped HPFLs [13, 14, 16–18]. As with other advanced technologies, the continuous evolution of fiber lasers is accompanied by tremendous challenges, of which the TMI and SRS have become major bottlenecks for ensuring a near-diffraction-limited operation and for achieving further power scaling [20, 21, 23, 24, 476]. To date, employing fibers with extended core diameters is the most effective way to mitigate nonlinear effects [29–32, 34, 35, 471–484]. It is of primary importance to overcome the tendency of large-mode-area fibers to support multiple modes. In addition to concentrating on the creation of more advanced cross-sectional structures, inner-fiber light manipulation along with the longitudinal direction shows great vitality [76, 270, 273, 275]. Compared with a conventional fiber with uniform size, tapered gain fiber has a larger mode field area and stronger pump absorption, which can suppress nonlinear effects while maintaining good beam quality. If more reasonable structures are proposed, tapered fiber is expected to achieve effective-single-mode and higher power outputs than the uniform size fiber by promoting the thresholds of nonlinear effects and TMI simultaneously.

Regarding the behavior of fibers employed in laser architectures, restrictions occurring in the current fiber may be addressed from an intrinsic perspective considering the fundamental characteristics [314–322, 329–337, 485]. For instance, new glass compositions or resultant fibers should exhibit greater control over the parasitic effects. An increased understanding of how manufacturing method influences the properties of these materials benefits new fibers generated from new compositions. Moreover, it has been reported that the quantum defect induced high thermal load in HPFLs can be effectively eliminated in phosphorus-doped fiber [480–488] and over the hundred-watt level fiber laser with less than 1% quantum defect [486] has been demonstrated. From a more intrinsic view of light-matter interactions, the increment of both P_2O_5 and B_2O_3 continues to reduce heat generation and decreases the value of dn/dT [36, 37], which suppresses the induction to parasitic effects such as SBS and TMI as well. This research yields new understandings into the materials science and engineering of advanced multi-component glass systems, pointing out a critical direction for next-generation fiber lasers operating at extreme power levels.

To match the application of long-distance delivery of high-power laser beams, the design principles of future delivery fibers need to comprehensively consider the following points: (a) larger core mode area and lower bending sensitivity, (b) efficient control on the inter-modal coupling, and efficient suppression on HOMs and (c) stable transmission at the signal wavelength and effective mitigation on the SRS band. The extremely low overlap between the light and fiber structure, besides giving low non-linearity, indicates a very high damage threshold. In this way, hollow-core fibers can be exploited for the delivery of high-power lasers. In this field, the possibility of delivering a diffraction-limited beam is particularly interesting. At present, kilometer-scale kilowatt transmission has been successfully demonstrated [381], and the future pursuit is compact integration of laser source and delivery system.

Passive fiber-based components were endowed with functional characteristics since their inception; however, the limited power handling capacity confines their applications in high-power operations. Benefiting from the diversity and stability of laser fiber and fiber post-processing processes, developments in recent years have pulled them from the dilemma of low-power levels to high-power platforms. For example, mode converters and tap couplers have been adopted to facilitate the operation of kilowatt-scale systems [414, 415], which provides a new perspective for online monitoring or switching of fiber lasers.

In view of the parasitic effects in high-power states, future development of laser fibers should be discussed from a multi-dimensional perspective. Taking full advantage of the potential of transverse and longitudinal structures enables the application of optical fibers to transition from traditional transmission to functional scenes. While most reports do not maturely apply them to systems integration, continued advances in manufacturing processes is supposed to drive their further development. In pursuit of higher power levels, typical single-mode outputs tend to evolve to flexible manipulation on spatial modes, which have been extensively validated in laboratory and commercial products. In the frequency domain, tunability of output spectrum under different linewidth regimes is an ongoing requirement for applications of coherent or incoherent applications. At the same time, the power handling capabilities of fiber-based components used for online modulation are greatly enhanced, indicating an additional dimension to customize the operation of HPFL

systems. With proper design and combination of functional laser fibers and fiber-based components, the development of next-generation fiber lasers is sparked by multi-domain controllability while guaranteeing high-power output characteristics. While the power scaling in few-mode laser fibers has been thoroughly investigated, only a few studies have addressed the customized output and quantitative analysis of HPFLs, leaving this field largely unexplored with opportunities to exploit the multi-modal degrees of freedom for controlling and diagnosing multi-dimensional spectral-spatial–temporal interactions.

In addition to developing fiber lasers with higher output power and multi-dimensional controllability, there is an urgent demand for real-time analysis of laser beam characteristics, i.e., the mode decomposition (MD) [483–491]. Beam characterization represented by MD technology and beam quality measurement is an important tool for further study of fiber lasers. The mode information carried by laser beam is the key to understand intrinsic properties and transmission characteristics of HPFLs, which are challenging to be completely analyzed even with complicated measurement methods [489, 492, 493]. However, it should be noted that the emerging machine learning technology is expected to provide an effective and accurate technical scheme for on-line analysis [488–496].

Declarations

Conflict of interest The authors declare that there are no known competing financial interests or personal relationships that could have appeared to influence the work reported in this manuscript.

References

1. Kao KC, Hockham GA. Dielectric fibre surface waveguide for optical frequencies. In: Brown J, editor. Electromagnetic wave theory. Oxford: Pergamon; **1967**. p. 441.

2. Hecht J. The remarkable fiber optic vision of Charles Kao. *Opt Photonics News* **2019**;*30*:26.

3. Macchesney JB, O'connor DB, Dimarcello FV, Simpson JB, Lazay PD. Preparation of low loss optical fiber using simultaneous vapor phase deposition and fusion. **1974**.

4. Izawa T, Inagaki N. Materials and processes for fiber preform fabrication—vapor-phase axial deposition. *Proc IEEE* **1980**;*68*:1184.

5. Blankenship M, Deneka C. The outside vapor deposition method of fabricating optical waveguide fibers. *IEEE J Quantum Electron* **1982**;*18*:1418.

6. Macchesney JB, Digiovanni DJ. Materials development of optical fiber. *J Am Ceram Soc* **1990**;*73*:3537.

7. Izawa T. Early days of VAD process. *IEEE J Sel Top Quantum Electron* **2000**;*6*:1220.

8. Kapron FP, Keck DB, Maurer RD. Radiation losses in glass optical waveguides. *Appl Phys Lett* **1970**;*17*:423.

9. BWT Inc. Fiber-coupled laser diodes. https://www.bwt-bj.com/product/details64_4725.html.

10. EverBright Photonics. High-power laser chips. http://www.everbrightphotonics.com/product/54/.

11. COHERENT Inc. Diode laser components. https://www.coherent.com/components-accessories/diode-lasers.

12. Snitzer E, Po H, Hakimi F, Tumminelli R, Mccollum BC, editors. Double clad, offset core Nd fiber laser. Optical fiber sensors. New Orleans: Optica Publishing Group; **1988**.

13. O'connor M, Gapontsev V, Fomin V, Abramov M, Ferin A, editors. Power scaling of SM fiber lasers toward 10 kW. In: Conference on lasers and electro-optics/international quantum electronics conference, Optical Society of America, Baltimore, **2009**.

14. Shiner B, editor. The impact of fiber laser technology on the world wide material processing market. In: CLEO: 2013. San Jose, California: Optica Publishing Group; **2013**.

15. High Power CW Fiber Lasers. https://www.ipgphotonics.com/en/products/lasers/high-power-cw-fiber-lasers.

16. Jauregui C, Limpert J, Tünnermann A. High-power fibre lasers. *Nat Photonics* **2013**;*7*:861.

17. Shi W, Fang Q, Zhu XS, Norwood RA, Peyghambarian N. Fiber lasers and their applications [invited]. *Appl Opt* **2014**;*53*:6554.

18. Zervas MN, Codemard CA. High power fiber lasers: a review. *IEEE J Sel Top Quantum Electron* **2014**;*20*:219.

19. Zuo JX, Lin XC. High-power laser systems. *Laser Photonics Rev*. **2022**; 2100741.

20. Eidam T, Wirth C, Jauregui C, Stutzki F, Jansen F, Otto H-J, Schmidt O, Schreiber T, Limpert J, Tünnermann A. Experimental observations of the threshold-like onset of mode instabilities in high power fiber amplifiers. *Opt Express* **2011**;*19*:13218.

21. Smith AV, Smith JJ. Mode instability in high power fiber amplifiers. *Opt Express* **2011**;*19*:10180.

22. Ward B, Robin C, Dajani I. Origin of thermal modal instabilities in large mode area fiber amplifiers. *Opt Express* **2012**;*20*:11407.

23. Tao RM, Wang XL, Zhou P. Comprehensive theoretical study of mode instability in high-power fiber lasers by employing a universal model and its implications. *IEEE J Sel Top Quantum Electron* **2018**;*24*:1.

24. Jauregui C, Stihler C, Limpert J. Transverse mode instability. *Adv Opt Photonics* **2020**;*12*:429.

25. Kobyakov A, Sauer M, Chowdhury D. Stimulated Brillouin scattering in optical fibers. *Adv Opt Photonics* **2010**;*2*:1.

26. Li RX, Wu HS, Xiao H, Leng JY, Zhou P. More than 5 kW counter tandem pumped fiber amplifier with near single-mode beam quality. *Opt Laser Technol* **2022**;*153*:108204.

27. Smith AV, Smith JJ. Influence of pump and seed modulation on the mode instability thresholds of fiber amplifiers. *Opt Express* **2012**;*20*:24545.

28. Stihler C, Jauregui C, Kholaif SE, Limpert J. Intensity noise as a driver for transverse mode instability in fiber amplifiers. *PhotoniX* 2020, 1.

29. Ma XQ, Zhu C, Hu IN, Kaplan A, Galvanauskas A. Single-mode chirally-coupled-core fibers with larger than 50 μm diameter cores. *Opt Express* 2014;22:9206.

30. Liang D, Mckay HA, Marcinkevicius A, Libin F, Jun L, Thomas BK, Fermann ME. Extending effective area of fundamental mode in optical fibers. *J Lightwave Technol* 2009;27:1565.

31. Stutzki F, Jansen F, Otto H-J, Jauregui C, Limpert J, Tünnermann A. Designing advanced very-large-mode-area fibers for power scaling of fiber-laser systems. *Optica* 2014;1:233.

32. Jain D, Baskiotis C, May-Smith TC, Jaesun K, Sahu JK. Large mode area multi-trench fiber with delocalization of higher order modes. *IEEE J Sel Top Quantum Electron* 2014;20:242.

33. Russell PSJ. Photonic-crystal fibers. *J Lightwave Technol* 2006;24:4729.

34. Jain D, Jung Y, Nunez-Velazquez M, Sahu JK. Extending single mode performance of all-solid large-mode-area single trench fiber. *Opt Express* 2014;22:31078.

35. Wu HS, Li RX, Xiao H, Huang LJ, Yang H, Pan ZY, Leng JY, Zhou P. High-power tandem-pumped fiber amplifier with beam quality maintenance enabled by the confined-doped fiber. *Opt Express* 2021;29:31337.

36. Ballato J, Hawkins T, Yu NJ, Dragic P. Materials for TMI mitigation. In: SPIE LASE. SPIE, 2021.

37. Hawkins TW, Dragic PD, Yu NJ, Flores A, Engholm M, Ballato J. Kilowatt power scaling of an intrinsically low Brillouin and thermo-optic Yb-doped silica fiber. *J Opt Soc Am B* 2021;38:F38.

38. Jain D, Alam S, Codemard C, Jung Y, Zervas MN, Sahu JK. High power, compact, picosecond MOPA based on single trench fiber with single polarized diffraction-limited output. *Opt Lett* 2015;40:4150.

39. Jain D, Alam S, Jung Y, Barua P, Velazquez MN, Sahu JK. Highly efficient Yb-free Er-La-Al doped ultra-low NA large mode area single-trench fiber laser. *Opt Express* 2015;23:28282–7.

40. Jain D, Sahu JK. Large mode area single trench fiber for 2 μm operation. *J Lightwave Technol* 2016;34:3412.

41. Kong LC, Huang LJ, Gu SY, Leng JY, Guo SF, Zhou P, Xu XJ, Jiang ZF. Experimental investigation of thermally induced core laser leakage in large mode area single trench fiber. High-Power Lasers and Applications VIII, 2016. p. 100161M.

42. Huang LJ, Yao TF, Yang BH, Leng JY, Zhou P, Pan ZY, Gu SY, Cheng XA. Modified single trench fiber with effective single-mode operation for high-power application. *IEEE J Sel Top Quantum Electron* 2018;24:1.

43. Želudevičius J, Danilevičius R, Viskontas K, Rusteika N, Regelskis K. Femtosecond fiber CPA system based on picosecond master oscillator and power amplifier with CCC fiber. *Opt Express* 2013;21:5338.

44. Bai JX, Zhang J, Koponen J, Kanskar M, Towe E. A unified approach to achieving high power and high energy in chirally coupled-core ytterbium-doped fiber amplifier systems. *IEEE Photonics J* 2018;10:1.

45. Hochheim S, Steinke M, Wessels P, De Varona O, Koponen J, Lowder T, Novotny S, Neumann J, Kracht D. Single-frequency chirally coupled-core all-fiber amplifier with 100 W in a linearly polarized TEM00 mode. *Opt Lett* 2020;45:939.

46. Xiao Y, Brunet F, Kanskar M, Faucher M, Wetter A, Holehouse N. 1-kilowatt CW all-fiber laser oscillator pumped with wavelength-beam-combined diode stacks. *Opt Express* 2012;20:3296.

47. Yu HL, Wang XL, Tao RM, Zhou P, Chen JB. 1.5 kW, near-diffraction-limited, high-efficiency, single-end-pumped all-fiber-integrated laser oscillator. *Appl Opt* 2014;53:8055.

48. Mashiko Y, Nguyen HK, Kashiwagi M, Kitabayashi T, Shima K, Tanaka D, editors. 2 kW single-mode fiber laser with 20-m long delivery fiber and high SRS suppression. In: Proc. SPIE, 2015.

49. Shi W, Fang Q, Xu Y, Qin YG, Fan JL, Meng XJ, Zhang QH. 1.63 kW monolithic continuous-wave single-mode fiber laser oscillator. *J Optoelectron Laser*. 2015;26:662.

50. Yang BL, Zhang HW, Shi C, Wang XL, Zhou P, Xu XJ, Chen JB, Liu ZJ, Lu QS. Mitigating transverse mode instability in all-fiber laser oscillator and scaling power up to 2.5 kW employing bidirectional-pump scheme. *Opt Express* 2016;24:27828.

51. Ikoma S, Nguyen HK, Kashiwagi M, Uchiyama K, Shima K, Tanaka D. 3 kW single stage all-fiber Yb-doped single-mode fiber laser for highly reflective and highly thermal conductive materials processing. In: SPIE LASE, SPIE. 2017.

52. Kensuke S, Shinya I, Keisuke U, Yuya T, Masahiro K, Daiichiro T, editors. 5-kW single stage all-fiber Yb-doped single-mode fiber laser for materials processing. In: Proc. SPIE. 2018.

53. Yang BL, Zhang HW, Shi C, Tao RM, Su RT, Ma PF, Wang XL, Zhou P, Xu XJ, Lu QS. 3.05 kW monolithic fiber laser oscillator with simultaneous optimizations of stimulated Raman scattering and transverse mode instability. *J Opt* 2018;20:025802.

54. Yang BL, Shi C, Zhang HW, Ye Q, Pi HY, Tao RM, Wang XL, Ma PF, Leng JY, Chen ZL, Zhou P, Xu XJ, Chen JB, Liu ZJ. Monolithic fiber laser oscillator with record high power. *Laser Phys Lett* 2018;15:075106.

55. Yang BL, Zhang HW, Ye Q, Pi HY, Shi C, Tao RM, Wang XL, Xu XJ. 4.05 kW monolithic fiber laser oscillator based on home-made large mode area fiber Bragg gratings. *Chin Opt Lett* 2018;16:031407.

56. Zhang F, Zheng WY, Shi PY, Zhang XH, editors. 2-kW single-mode fiber laser employing bidirectional-pump scheme. In: Proc SPIE, 2018.

57. Klein S, Giesberts M, Baer P, Raguse M, Fitzau O, Traub M, Hoffmann HD, Krause V, Rehmann G, editors. Fiber Bragg gratings in active multimode XLMA fibers for high-power kW-class fiber lasers. In: Proc. SPIE, 2020.

58. Krämer RG, Möller F, Matzdorf C, Goebel TA, Strecker M, Heck M, Richter D, Plötner M, Schreiber T, Tünnermann A, Nolte S. Extremely robust femtosecond written fiber Bragg gratings for an ytterbium-doped fiber oscillator with 5 kW output power. *Opt Lett* 2020;45:1447.

59. Wang Y, Kitahara R, Kiyoyama W, Shirakura Y, Kurihara T, Nakanish Y, Yamamoto T, Nakayama M, Ikoma S, Shima K. 8-kW single-stage all-fiber Yb-doped fiber laser with a BPP of 0.50 mm-mrad. In: SPIE LASE. SPIE, 2020.

60. Xi XM, Wang P, Yang BL, Wang XL, Zhang HW, Ning Y, Han K, Wang ZF, Zhou P, Xu XJ, Chen JB. The output power of the all-fiber laser oscillator exceeds 7 kW. *Chin J Lasers* 2021;48:0116001.

61. Li HY, Tian X, Wang M, Zhao XF, Wu B, Gao CH, Li H, Rao B, Xi XM, Wang ZF. Fabrication of fiber Bragg gratings by visible femtosecond laser for multi-kW fiber oscillator. *IEEE Photonics J* 2022;14:1.

62. Wolf A, Dostovalov A, Bronnikov K, Skvortsov M, Wabnitz S, Babin S. Advances in femtosecond laser direct writing of fiber Bragg gratings in multicore fibers: technology, sensor and laser applications. *Opto-Electronic Advances* 2022;5:210055.

63. Yang BL, Wang P, Zhang HW, Xi XM, Shi C, Wang XL, Xu XJ. 6 kW single mode monolithic fiber laser enabled by effective mitigation of the transverse mode instability. *Opt Express* 2021;29:26366.

64. Zhou P, Xiao H, Leng JY, Xu JM, Chen ZL, Zhang HW, Liu ZJ. High-power fiber lasers based on tandem pumping. *J Opt Soc Am B* 2017;34:A29.

65. Lin HH, Xu LX, Li CY, Shu Q, Chu QH, Xie LH, Guo C, Zhao PF, Li ZB, Wang JJ, Jing F, Tang X. 10.6 kW high-brightness

cascade-end-pumped monolithic fiber lasers directly pumped by laser diodes in step-index large mode area double cladding fiber. *Results Phys.* **2019**;*14*:102479.

66. Chen XL, Yu H, Xu ZW, Guo XC, Ye R, Liu K, Yang YF, Shen H, Zhang HB, Yu CL, He B, Hu L, Zhou J. Theoretical and experimental investigation of a 10-kw high-efficiency 1070-nm fiber amplifier. *Chin J Lasers* **2020**;*47*:1006001.

67. Fang Q, Li JH, Shi W, Qin YG, Xu Y, Meng XJ, Norwood RA, Peyghambarian N. 5 kW near-diffraction-limited and 8 kW high-brightness monolithic continuous wave fiber lasers directly pumped by laser diodes. *IEEE Photonics J* **2017**;*9*:1506107.

68. Wu HS, Li RX, Xiao H, Huang LJ, Yang H, Leng JY, Pan ZY, Zhou P. First demonstration of a bidirectional tandem-pumped high-brightness 8 kW level confined-doped fiber amplifier. *J Lightwave Technol* **2022**;*40*:5673.

69. Wirth C, Schmidt O, Kliner A, Schreiber T, Eberhardt R, Tünnermann A. High-power tandem pumped fiber amplifier with an output power of 2.9 kW. *Opt Lett* **2011**;*36*:3061.

70. Popp A, Voss A, Graf T, Unger S, Kirchhof J, Bartelt H. Thin-disk laser-pumping of ytterbium-doped fiber laser. *Laser Phys Lett* **2011**;*8*:887.

71. Zhang FF, Wang YB, Lin XF, Cheng YS, Zhang ZL, Liu YH, Liao L, Xing YB, Yang LY, Dai NL, Li HQ, Li JY. Gain-tailored Yb/Ce codoped aluminosilicate fiber for laser stability improvement at high output power. *Opt Express* **2019**;*27*:20824.

72. Ma PF, Xiao H, Meng DR, Liu W, Tao RM, Leng JY, Ma YX, Su RT, Zhou P, Liu ZJ. High power all-fiberized and narrow-bandwidth MOPA system by tandem pumping strategy for thermally induced mode instability suppression. *High Power Laser Sci Eng* **2018**;*6*:04000e57.

73. Yu HL, Zhang HW, Lv HB, Wang XL, Leng JY, Xiao H, Guo SF, Zhou P, Xu XJ, Chen JB. 3.15 kW direct diode-pumped near diffraction-limited all-fiber-integrated fiber laser. *Appl Opt* **2015**;*54*:4556.

74. Jiao WX, Rong XQ, Ping Y, Xiao C, Dan L, Cheng D, Qi M, Qing YY, Rong P, Li GM. 3000 W direct-pumping all-fiber laser based on domestically produced fiber. *Acta Phys Sin* **2015**;*64*:164204.

75. Xiao H, Leng JY, Zhang HW, Huang LJ, Xu JM, Zhou P. High-power 1018 nm ytterbium-doped fiber laser and its application in tandem pump. *Appl Opt* **2015**;*54*:8166.

76. Ye Y, Lin XF, Yang BL, Xi XM, Shi C, Zhang HW, Wang XL, Li JY, Xu XJ. Tapered Yb-doped fiber enabled a 4 kW near-single-mode monolithic fiber amplifier. *Opt Lett* **2022**;*47*:2162.

77. Zhan H, Peng K, Liu S, Wang YY, Li Y, Wang XL, Ni L, Sun SH, Jiang JL, Yu J, Jiang L, Wang JJ, Jing F, Lin AX. Pump-gain integrated functional laser fiber towards 10 kW-level high-power applications. *Laser Phys Lett* **2018**;*15*:095107.

78. Wang P, Xi XM, Zhang HW, Lai YB, Chen S, Hu X, Lun CZ, Yong PZ, Lin WX, Feng WZ, Pu Z, Jun XX, Bao CJ. Laser-diode-pumped fiber laser amplifier for 13 kW high-beam-quality output. *High Power Laser Part Beams* **2022**. https://doi.org/10.11884/HPLPB202234.220247.

79. Huang LJ, Wu HS, Li RX, Xiao H, Yang H, Yan ZP, Leng JY, Pan ZY, Zhou P. Homemade confined-doped fiber for 10 kW level fiber laser output with good beam quality. *High Power Laser Part Beams* **2022**;*34*:111002.

80. Xiao H, Pan ZY, Chen ZL, Xi XM, Huang LJ, Wang M, Yang H, Yan ZP, Leng JY, Wang XL, Wang ZF, Zhou P, Xu XJ, Chen JB. 20 kW high beam quality laser stable output based on self-developed fiber and device. *Chin J Lasers* **2022**;*49*:216.

81. Li RX, Wu HS, Xiao H, Leng JY, Zhou P. More than 8 kW fiber laser amplifier with high beam quality enabled by counter tandem pumping scheme. *Acta Optica Sinica* **2022**;*42*:1436001.

82. Yang BL, Yang H, Ye Y, Xi XM, Zhang HW, Huang LJ, Wang P, Shi C, Wang XL, Yan ZP, Pan ZY, Wang ZF, Zhou P, Xu XJ,

Chen JB. 6 kW broadband fiber laser based on home-made ytterbium-doped fiber with gradually varying spindle-shape structure. *High Power Laser Part Beams* **2022**;*34*:081001.

83. Li FY, Dai JY, Liu N, Gao C, Shen CL, He HL, Li F, Jiang L, Zhang LH, Lu JK, Chen Y, Zhang HY, Liu Y, Chu QH, Shi Y, Lin HH, Wang JJ, Jing F. *Chin J Lasers* **2022**;*49*:2016004.

84. Shen DY, Sahu JK, Clarkson WA. Highly efficient Er, Yb-doped fiber laser with 188 W free-running and >100W tunable output power. *Opt Express* **2005**;*13*:4916.

85. Jeong Y, Yoo S, Codemard CA, Nilsson J, Sahu JK, Payne DN, Horley R, Turner PW, Hickey L, Harker A, Lovelady M, Piper A. Erbium: ytterbium codoped large-core fiber laser with 297-W continuous-wave output power. *IEEE J Sel Top Quantum Electron* **2007**;*13*:573.

86. Zhang J, Fromzel V, Dubinskii M. Resonantly cladding-pumped Yb-free Er-doped LMA fiber laser with record high power and efficiency. *Opt Express* **2011**;*19*:5574.

87. Kotov LV, Likhachev ME, Bubnov MM, Medvedkov OI, Yashkov MV, Guryanov AN, Lhermite J, Février S, Cormier E. 75 W 40% efficiency single-mode all-fiber erbium-doped laser cladding pumped at 976 nm. *Opt Lett* **2013**;*38*:2230.

88. Jebali MA, Maran JN, Larochelle S. 264 W output power at 1585 nm in Er-Yb codoped fiber laser using in-band pumping. *Opt Lett* **2014**;*39*:3974.

89. Leonid VK, Mikhail EL, Mikhail MB, Oleg IM, Mikhail VY, Alexei NG, Sébastien F, Jérôme L, Eric C, editors. Yb-free Er-doped all-fiber amplifier cladding-pumped at 976 nm with output power in excess of 100 W. In: Proc. SPIE, **2014**.

90. Han Q, Yao YZ, Chen YF, Liu FC, Liu TG, Xiao H. Highly efficient Er/Yb-codoped fiber amplifier with an Yb-band fiber Bragg grating. *Opt Lett* **2015**;*40*:2634.

91. Daniel C, Herman P, Julia L, Scott DS, editors. Single frequency 1560 nm Er:Yb amplifier with 207 W output power and 50.5% slope efficiency. In: Proc. SPIE, **2016**.

92. De Varona O, Fittkau W, Booker P, Theeg T, Steinke M, Kracht D, Neumann J, Wessels P. Single-frequency fiber amplifier at 1.5 μm with 100 W in the linearly-polarized TEM00 mode for next-generation gravitational wave detectors. *Opt Express* **2017**;*25*:24880.

93. Han Q, Yao YZ, Tang XY, Chen YF, Yan WC, Liu TG, Song HL. Highly efficient Er–Yb codoped double-clad fiber amplifier with an Yb-band resonant cavity. *Laser Phys Lett* **2017**;*14*:025105.

94. Kotov LV, Aleshkina SS, Khudyakov MM, Bubnov MM, Medvedkov OI, Lipatov DS, Guryanov AN, Likhachev MM. High-brightness multimode fiber lasers for resonant pumping. *J Lightwave Technol* **2017**;*35*:4540.

95. Lin HQ, Feng YJ, Feng YT, Barua P, Sahu JK, Nilsson J. 656 W Er-doped, Yb-free large-core fiber laser. *Opt Lett* **2018**;*43*:3080.

96. Matniyaz T, Kong F, Kalichevsky-Dong MT, Dong L. 302 W single-mode power from an Er/Yb fiber MOPA. *Opt Lett* **2020**;*45*:2910.

97. Michaud L-C, Veilleux C, Bilodeau G, Gilbert-Paquet O, Lebel-Cormier M-A, Lemieux-Tanguay M, Pelletier-Ouellet S, Paradis P, Bellec M, Grégoire N, Morency S, Messaddeq Y, Bernier M. 100-W-level single-mode ytterbium-free erbium fiber laser. *Opt Lett* **2021**;*46*:2553.

98. Yu WL, Xiao QR, Wang LL, Zhao Y, Qi TC, Yan P, Gong ML. 219.6 W large-mode-area Er: Yb codoped fiber amplifier operating at 1600 nm pumped by 1018 nm fiber lasers. *Opt Lett* **2021**;*46*:2192.

99. Yu WL, Yan P, Qi TC, Wu YL, Li D, Xiao QR, Gong ML. High-power and high-brightness Er: Yb codoped fiber MOPA operating at 1535 nm. *Opt Express* **2022**;*30*:16837.

100. Goodno GD, Book LD, Rothenberg JE. Low-phase-noise, single-frequency, single-mode 608 W thulium fiber amplifier. *Opt Lett* **2009**;*34*:1204.

101. Moulton PF, Rines GA, Slobodtchikov EV, Wall KF, Frith G, Samson B, Carter ALG. Tm-doped fiber lasers: fundamentals and power scaling. *IEEE J Sel Top Quantum Electron* **2009**;*15*:85.

102. Ehrenreich T, Leveille R, Majid I, Tankala K, Rines G, Moulton P. 1-kW, all-glass Tm:fiber laser. Fiber lasers VII; San Jose, Calif, **2010**. pp. xxxvii.

103. Stutzki F, Gaida C, Gebhardt M, Jansen F, Wienke A, Zeitner U, Fuchs F, Jauregui C, Wandt D, Kracht D, Limpert J, Tünnermann A. 152 W average power Tm-doped fiber CPA system. *Opt Lett* **2014**;*39*:4671.

104. Gaida C, Gebhardt M, Stutzki F, Jauregui C, Limpert J, Tünnermann A. Thulium-doped fiber chirped-pulse amplification system with 2 GW of peak power. *Opt Lett* **2016**;*41*:4130.

105. Walbaum T, Heinzig M, Schreiber T, Eberhardt R, Tünnermann A. Monolithic thulium fiber laser with 567 W output power at 1970 nm. *Opt Lett* **2016**;*41*:2632.

106. Yin K, Zhu RZ, Zhang B, Liu GC, Zhou P, Hou J. 300 W-level, wavelength-widely-tunable, all-fiber integrated thulium-doped fiber laser. *Opt Express* **2016**;*24*:11085.

107. Jiang L, Chen L, Xing SH, Pu W. 342 W narrow-linewidth continuous-wave thulium-doped all-fiber laser. *Acta Phys Sin* **2016**;*65*:194209.

108. Gaida C, Gebhardt M, Heuermann T, Stutzki F, Jauregui C, Limpert J. Ultrafast thulium fiber laser system emitting more than 1 kW of average power. *Opt Lett* **2018**;*43*:5853.

109. Yao WC, Shen CF, Shao ZH, Wang JL, Wang F, Zhao YG, Shen DY. 790 W incoherent beam combination of a Tm-doped fiber laser at 1941 nm using a 3x1 signal combiner. *Appl Opt* **2018**;*57*:5574.

110. Liu YZ, Cao C, Xing YB, Liao L, Cao RT, Zhang FF, Chen YS, Wang YB, Peng JG, Li HQ, Yang LY, Dai NL, Li JY. 406 W narrow-linewidth all-fiber amplifier with Tm-doped fiber fabricated by MCVD. *IEEE Photonics Technol Lett* **2019**;*31*:1779.

111. Zi LY, Bing XY, Lei L, Bo WY, Gang PJ, Qing LH, Li DN, Yan LJ. 530 W all-fiber continuous-wave Tm-doped fiber laser. *Acta Phys Sin* **2020**;*69*:184209.

112. Motard A, Louot C, Robin T, Cadier B, Manek-Hönninger I, Dalloz N, Hildenbrand-Dhollande A. Diffraction limited 195-W continuous wave laser emission at 2.09 μm from a Tm^{3+}, Ho^{3+}-codoped single-oscillator monolithic fiber laser. *Opt Express* **2021**;*29*:6599.

113. Shin Jae S, Cha Y-H, Chun Byung J, Jeong D-Y, Park H. 200-W continuous-wave thulium-doped all-fiber laser at 2050 nm. *Curr Opt Photonics* **2021**;*5*:306.

114. Woodward RI, Majewski MR, Bharathan G, Hudson DD, Fuerbach A, Jackson SD. Watt-level dysprosium fiber laser at 3.15 μm with 73% slope efficiency. *Opt Lett* **2018**;*43*:1471.

115. Maes F, Fortin V, Poulain S, Poulain M, Carrée J-Y, Bernier M, Vallée R. Room-temperature fiber laser at 3.92 μm. *Optica* **2018**;*5*:761.

116. Snitzer E. Optical maser action of Nd^{3+} in a barium crown glass. *Phys Rev Lett* **1961**;*7*:444.

117. Maiman TH. Stimulated optical radiation in ruby. *Nature* **1960**;*187*:493.

118. Koester CJ, Snitzer E. Amplification in a fiber laser. *Appl Opt* **1964**;*3*:1182.

119. Shcherbakov EA, Fomin VV, Abramov AA, Ferin AA, Mochalov DV, Gapontsev VP, editors. Industrial grade 100 kW power CW fiber laser. In: Advanced solid-state lasers congress. Paris: Optica Publishing Group; **2013**.

120. Nikolai P, Oleg S, Valentin F, Daniil M, Roman Y, Anton F, Alexey D, Ivan U, Valentin G, editors. High-efficient kW-level single-mode ytterbium fiber lasers in all-fiber format with diffraction-limited beam at wavelengths in 1000–1030 nm spectral range. In: Proc. SPIE, **2020**.

121. Li WO, Matniyaz T, Gafsi S, Kalichevsky-Dong MT, Hawkins TW, Parsons J, Gu GC, Dong L. 151W monolithic diffraction-limited Yb-doped photonic bandgap fiber laser at ~978nm. *Opt Express* **2019**;*27*:24972.

122. Todorov F, Aubrecht J, Peterka P, Schreiber O, Jasim AA, Mrázek J, Podrazký O, Kamrádek M, Kanagaraj N, Grábner M, Baravets Y, Cajzl J, Koška P, Fišar A, Kašík I, Honzátko P. Active optical fibers and components for fiber lasers emitting in the 2-μm spectral range. *Materials* **2020**. https://doi.org/10.3390/ma13225177 .

123. Hemming A, Simakov N, Haub J, Carter A. A review of recent progress in holmium-doped silica fibre sources. *Opt Fiber Technol* **2014**;*20*:621.

124. Kim JW, Boyland A, Sahu JK, Clarkson WA, editors. Ho-doped silica fibre laser in-band pumped by a Tm-doped fibre laser. In: CLEO/Europe-EQEC 2009-European conference on lasers and electro-optics and the European quantum electronics conference. 14–19 June 2009. **2009.**

125. Hemming A, Simakov N, Davidson A, Bennetts S, Hughes M, Carmody N, Davies P, Corena L, Stepanov D, Haub J, Swain R, Carter A, editors. A monolithic cladding pumped holmium-doped fibre laser. In: CLEO: 2013. San Jose, California: Optica Publishing Group; **2013**.

126. Alexander H, Nikita S, John H, Adrian C, editors. High power resonantly pumped holmium-doped fibre sources. In: Proc. SPIE, **2014**.

127. Almeida RM, Mackenzie JD. Vibrational spectra and structure of chloro-fluorozirconate glasses. *J Non Cryst Solids* **1982**;*51*:187.

128. Tokita S, Hirokane M, Murakami M, Shimizu S, Hashida M, Sakabe S. Stable 10 W Er:ZBLAN fiber laser operating at 2.71–2.88 μm. *Opt Lett* **2010**;*35*:3943.

129. Faucher D, Bernier M, Androz G, Caron N, Vallée R. 20 W passively cooled single-mode all-fiber laser at 2.8 μm. *Opt Lett* **2011**;*36*:1104.

130. Fortin V, Bernier M, Bah ST, Vallée R. 30W fluoride glass all-fiber laser at 2.94 μm. *Opt Lett* **2015**;*40*:2882.

131. Aydın YO, Fortin V, Maes F, Vallée R, Bernier M, editors. Long-term operation of high-power 3 μm fiber lasers. In: Laser congress 2019 (ASSL, LAC, LS&C), 2019/09/29. Vienna: Optica Publishing Group; **2019**.

132. He HY, Jia ZX, Jia SJ, Hu Q, Ohishi Y, Qin WP, Qin GS. Ho^{3+}/Pr^{3+} co-doped AlF3 based glass fibers for efficient ~2.9 μm lasers. *IEEE Photonics Technol Lett* **2020**;*32*:1489.

133. Aydın YO, Fortin V, Vallée R, Bernier M. Towards power scaling of 2.8 μm fiber lasers. *Opt Lett* **2018**;*43*:4542.

134. Golding PS, Jackson SD, King TA, Pollnau M. Energy transfer processes in Er^{3+}-doped and Er^{3+}, Pr^{3+}-codoped ZBLAN glasses. *Phys Rev B* **2000**;*62*:856.

135. Aydın YO, Fortin V, Maes F, Jobin F, Jackson SD, Vallée R, Bernier M. Diode-pumped mid-infrared fiber laser with 50% slope efficiency. *Optica* **2017**;*4*:235.

136. Crawford S, Hudson DD, Jackson SD. High-power broadly tunable 3 μm fiber laser for the measurement of optical fiber loss. *IEEE Photonics J* **2015**;*7*:1.

137. He HY, Jia ZX, Ohishi Y, Qin WP, Qin GS. Efficient ~4 μm emission from Pr^{3+}/Yb^{3+} co-doped fluoroindate glass. *Opt Lett* **2021**;*46*:5607.

138. He H, Jia Z, Wang T, Ohishi Y, Qin W, Qin G. Intense emission at ~3.3 μm from Er^{3+}-doped fluoroindate glass fiber. *Opt Lett* **2021**;*46*:1057.

139. Kränkel C, Marzahl D-T, Moglia F, Huber G, Metz PW. Out of the blue: semiconductor laser pumped visible rare-earth doped lasers. *Laser Photonics Rev* **2016**;*10*:548.

140. Sandrock T, Scheife H, Heumann E, Huber G. High-power continuous-wave upconversion fiber laser at room temperature. *Opt Lett* **1997**;*22*:808.

141. Zellmer H, Riedel P, Kempe M, Tunnermann A. High-power diode pumped upconversion fibre laser in red and green spectral range. *Electron Lett* **2002**;*38*:1250.

142. 2014. TNPIP. Blue LEDs—filling the world with new light. 2014. https://www.nobelprize.org/uploads/2018/06/popular-physicsprize2014-1.pdf.

143. Fujimoto Y, Ishii O, Yamazaki M. Multi-colour laser oscillation in Pr^{3+}-doped fluoro-aluminate glass fibre pumped by 442.6 nm GaN-semiconductor laser. *Electron Lett* **2010**;*45*:1301.

144. Nakanishi J, Yamada T, Fujitomo Y, Ishii O, Yamazaki M, editors. Sub-watt output power at 638 nm in wavelength by direct oscillation with Pr-doped waterproof fluoro-aluminate glass fiber laser. In: 2011 Conference on lasers and electro-optics Europe and 12th European quantum electronics conference (CLEO EUROPE/EQEC), 22–26 May 2011; **2011**.

145. Nakanishi J, Horiuchi Y, Yamada T, Ishii O, Yamazaki M, Yoshida M, Fujimoto Y. High-power direct green laser oscillation of 598 mW in Pr^{3+}-doped waterproof fluoroaluminate glass fiber excited by two-polarization-combined GaN laser diodes. *Opt Lett* **1836**;*2011*:36.

146. Fujimoto Y, Nakahara M, Binun P, Motokoshi S, Ishii O, Watanabe M, Yamazaki M, Shinozaki T, Sato T, Yanomori Y, editors. 2 W single-mode visible laser oscillation in Pr-doped double-clad structured waterproof fluoro-aluminate glass fiber. In: 2019 Conference on lasers and electro-optics Europe and European quantum electronics conference, 2019/06/23. Munich: Optica Publishing Group, **2019**.

147. Lord M-P, Maes F, Fortin V, Bernier M, Vallée R, editors. Watt-level visible laser emission in a double-clad praseodymium-doped fluoride fiber. In: Laser congress 2020 (ASSL, LAC), 2020/10/13. Washington, D.C.: Optica Publishing Group; **2020**.

148. Kifle E, Starecki F, Loiko P, Cozic S, Joulain F, Berthelot T, Georges T, Stojcevski D, Deubel D, Camy P. Watt-level visible laser in double-clad Pr^{3+}-doped fluoride fiber pumped by a GaN diode. *Opt Lett* **2021**;*46*:74.

149. Lord M-P, Fortin V, Maes F, Talbot L, Bernier M, Vallée R. 2.3 W monolithic fiber laser operating in the visible. *Opt Lett* **2021**;*46*:2392.

150. Zou JH, Li TR, Dou YB, Li J, Chen N, Bu YK, Luo ZQ. Direct generation of watt-level yellow Dy^{3+}-doped fiber laser. *Photonics Res* **2021**;*9*:446.

151. Yin L, Yan M, Han Z, Wang H, Shen H, Zhu R. High power cladding light stripper using segmented corrosion method: theoretical and experimental studies. *Opt Express* **2017**;*25*:8760.

152. Stachowiak D. High-power passive fiber components for all-fiber lasers and amplifiers application—design and fabrication. *Photonics* **2018**;*5*:38.

153. Lei CM, Li ZX, Zhang H, Chen ZU, Hou J. Taper-fused side pump combiner for all-fiber lasers and amplifiers: a review. *Opt Laser Technol* **2020**;*130*:106353.

154. Xiao QR, Ren HC, Chen X, Yan P, Gong ML. Tapered fiber bundle 7×1 end-pumping coupler capable of high power CW operation. *IEEE Photonics Technol Lett* **2013**;*25*:2442.

155. Zhou H, Chen ZL, Zhou XF, Hou J, Chen JB. All-fiber 7×1 pump combiner for high power fiber laser. *Opt Commun* **2015**;*347*:137.

156. Xiao QR, Huang YS, Sun JY, Wang XJ, Li D, Gong ML, Yan P. Research on multi-kilowatts level tapered fiber bundle N×1 pumping combiner for high power fiber laser. *Front Optoelectron* **2016**;*9*:301.

157. Han LX, Hao MM, Tao LL, Li JB. Fiber combiner terminated with quartz block head for direct beam combining of fiber coupled laser diodes. *Optik* **2019**;*184*:35.

158. Han LX, Hao MM. Direct combining output of fiber coupled laser diodes via fiber combiner with high efficiency and multiple input ports. *Optik* **2020**;*218*:165268.

159. ITF Technologies, 3x1, 4x1, 7x1,19x1 and 31 x 1 high power pump combiners. http://www.itftechnologies.com/files/13/ITF_DataSheet_D_3x1_4x1_7x1_19x1_v7_2020-10-26-15-34.pdf. Accessed 15 May 2022.

160. Lin HH, Guo C, Zhao PF, Li CY, Qi L, Wang BP, Huang ZH, Chu QH, Xuan T. Design and experiment of 10 kW class monolithic fiber pump coupling device. *Infrared Laser Eng* **2016**;*45*:11.

161. Jin Kun Z, Wei Z, Bao Yin Z, Zhe L, Chang C, Gang L, Qi G, Pei J, Wei G, Sheng Fei S, Peng W, Chao Qi H, Wei NL. High pumping-power fiber combiner for double-cladding fiber lasers and amplifiers. *Opt Eng* **2018**;*57*:1.

162. Gu Y, Lei C, Yang H, Xiao H, Leng J, Chen Z. High-beam-quality signal and pump combiner with large-mode-area fiber for high-power fiber laser and amplifier. *Appl Opt* **2019**;*58*:1336.

163. Liu Y, Wu WJ, Huang S, Li M, Feng X, Shen BJ, Song HQ, Zhang C, Xie LH, Li HK, Tao RM, Lin HH, Wang JJ, Jing F, editors. Backward pump and signal combiner with negligible beam quality degradation for 5KW-level fiber lasers. In: Conference on lasers and electro-optics, 2021/05/09. San Jose, California: Optica Publishing Group; **2021**.

164. Liu Y, Huang S, Wu W, Xie L, Zhang C, Li H, Li Y, Li Y, Tao R, Lin H, Wang J. 5-kW-level bi-directional high-efficiency pump and signal combiner with negligible beam quality degradation. *IEEE Photonics J* **2022**;*14*:1.

165. Laser Components. Pump combiners and other optical components for high power fiber lasers. https://www.lasercomponents.com/de/?embedded=1&file=fileadmin/user_upload/home/Datasheets/lightel/pump-combiners.pdf&no_cache=1. Accessed 15 May 2022.

166. ITF Technologies, (6+1)x1, (18+1)x1 and (24+1)x1 high power pump and signal combiner. http://www.itftechnologies.com/files/13/JR_ITF_DataSheet_C_6_1x1_18_1x1_v6_2021-03-05-16-45.pdf. Accessed 15 May 2022

167. Martinez-Rios A, Torres I, Hernandez D, Garcia O, Manuel V. Reduction of splice loss between dissimilar fibers by tapering and fattening. *Revista Mexicana de Física*. **2010**;56.

168. Theeg T, Sayinc H, Neumann J, Overmeyer L, Kracht D. Pump and signal combiner for bi-directional pumping of all-fiber lasers and amplifiers. *Opt Express* **2012**;*20*:28125.

169. Li ZX, Tian X, Lei CM, Zhang H, Chen ZL, Yang BL, Xi XM, Wang XL, Wang ZF, Chen JB. Fabrication of a side pump combiner and realization of a 2 kW single mode all-fiber laser oscillator. *OSA Contin* **2020**;*3*:1240.

170. Li Z, Min F, Xin T, Zhao X, Li H, Chen Z, Wang Z, Chen J. Investigation of the pump coupling efficiency of a side-pumping combiner based on tapered-fused method. *Opt Express* **2021**;*29*:17784.

171. Li ZX, Fu M, Zhao XF, Li HY, Chen ZL, Wang ZF, Chen JB. Fabrication of side pump combiners when pumping with a laser diode and a fiber laser. *Chin Opt Lett* **2022**;*20*:021401.

172. Wang Z, Yu W, Tian X, Qi T, Li D, Xiao Q, Yan P, Gong M. 5.1 kW tandem-pumped fiber amplifier seeded by random fiber laser with high suppression of stimulated Raman scattering. *IEEE J Quantum Electron* **2021**;*57*:1.

173. Gu YR, Lei CM, Liu J, Li RX, Liu L, Xiao H, Chen ZL. Side-pumping combiner for high-power fiber laser based on tandem pumping. *Opt Eng* **2017**;*56*:1.

174. Dong FL, Zhang XH, Song F. Side coupler applied in a multi-pumped Yb-doped triple-clad fiber laser. *Laser Phys* **2018**;*28*:125106.

175. Injeyan H, Goodno G, Palese S. High power laser handbook. New York: McGraw Hill Professional; **2011**.

176. Ferin A, Gapontsev V, Fomin V, Abramov A, Abramov M, Mochalov D, editors. 17 kW CW laser with 50 µm delivery. In: 6th Int. symp. on high-power fiber lasers and their applications. IPG Photonics Corporation; **2012**.

177. Ferin A, Gapontsev V, Fomin V, Abramov A, Abramov M, Mochalov D. 31.5 kW CW fiber laser with 100 um delivery. In: 6th International symposium on high-power fiber lasers and their applications. IPG Photonics Corporation; **2012**.

178. IPG Photonics successfully tests world's first 10 kilowatt single-mode production laser. http://www.ipgphotonics.com/Collateral/Documents/English-US/PR_FinaI_10kW_SM_laser.pdf.

179. Raycus laser's "key technology research and industrialization of 10,000-watt fiber laser" was selected as the leading technology list of "Sci-Innovation China" in 2021 https://www.raycuslaser.com/view/3065.html.

180. The project "Core Technology and Industrialization of 100 kW Fiber Laser with High Beam Quality" passed the achievement evaluation successfully. https://www.raycuslaser.com/view/3105.html.

181. Poozesh R, Norouzy A, Golshan AH, Roohforouz A, Babazadeh A, Nasirabad RR, Jafari NT, Heidariazar A, Hejaz K, Alavian A, Amidian A. A novel method for stripping cladding lights in high power fiber lasers and amplifiers. *J Lightwave Technol* **2012**;*30*:3199.

182. Guo W, Chen ZL, Zhou H, Li J, Hou J. Cascaded cladding light extracting strippers for high power fiber lasers and amplifiers. *IEEE Photonics J* **2014**;*6*:1.

183. Yan MJ, Wang Z, Meng LQ, Yin L, Han ZG, Shen H, Wang HL, Zhu RH. Heat suppression of the fiber coating on a cladding light stripper in high-power fiber laser. *Appl Opt* **2018**;*57*:485.

184. Yapar Yıldırım E, Karatutlu A, Teslime Balk E, Midilli Y, Ortaç B. Combined method for the fabrication of high-power cladding light stripper using a buffered oxide etchant. *Appl Opt* **2019**;*58*:6926.

185. Yan P, Sun J, Huang YS, Li D, Wang XJ, Xiao QR, Gong ML. Kilowatt-level cladding light stripper for high-power fiber laser. *Appl Opt* **1935**;*2017*:56.

186. Zou SZ, Chen H, Zhang JY, Yu HJ, Zhang ZY, Sun J, Lin XC. Cladding light stripper of high average stripped power density with high attenuation of 39 dB and low temperature rise. *IEEE Photonics J* **2018**;*10*:1.

187. Liu Y, Huang S, Tang X, Wu WJ, Feng X, Li M, Shen BJ, Tao RM, Wang JJ, Jing F, editors. > 2 KW cladding mode stripping device for high power fiber lasers. In: 14th Pacific Rim conference on lasers and electro-optics (CLEO PR 2020), 2020/08/03. Sydney: Optica Publishing Group; **2020**.

188. Liu Y, Huang S, Tang X, Wu WJ, Feng X, Li M, Shen BJ, Tao RM, Wang JJ, Jing F. > 2 kW high stability robust fiber cladding mode stripper with moderate package temperature rising. *IEEE Photonics Technol Lett* **2020**;*32*:1151.

189. Babazadeh A, Nasirabad RR, Norouzey A, Hejaz K, Poozesh R, Heidariazar A, Golshan AH, Roohforouz A, Jafari SNT, Lafouti M. Robust cladding light stripper for high-power fiber lasers using soft metals. *Appl Opt* **2014**;*53*:2611.

190. Kliner A, Kai-Chung H, Plötner M, Ch H, Th S, Schreiber T, Eberhardt R, Tünnermann A, editors. Fabrication and evaluation of a 500 W cladding-light stripper. In: Proc. SPIE, **2013**.

191. Wysmolek M, Ottenhues C, Pulzer T, Theeg T, Sayinc H, Steinke M, Morgner U, Neumann J, Kracht D. Microstructured fiber cladding light stripper for kilowatt-class laser systems. *Appl Opt* **2018**;*57*:6640.

192. Boyd K, Simakov N, Hemming A, Daniel J, Swain R, Mies E, Rees S, Andrew Clarkson W, Haub J. CO_2 laser-fabricated cladding light strippers for high-power fiber lasers and amplifiers. *Appl Opt* **2016**;*55*:2915.

193. Steinke M, Theeg T, Wysmolek M, Ottenhues C, Pulzer T, Neumann J, Kracht D, editors. CO_2 laser radiation as a versatile tool for the fabrication of fiber-based components. Advanced photonics 2018 (BGPP, IPR, NP, NOMA, Sensors, Networks, SPPCom, SOF), 2018/07/02. Zurich: Optica Publishing Group; **2018**.

194. Zou SZ, Yu HJ, Zhang JY, Zuo JX, Dong ZY, Xu S, Chang L, Zhao PF, Lin XC. Highly efficient fiber cladding light stripper fabricated by chemical mask etching method. *J Lightwave Technol* **2020**;*38*:5136.

195. Optizone Inc. Free-space isolator. https://www.optizonetech.com/Product/434601.html.

196. Optizone Inc. HPICI 1064 nm 500W. High-power collimating spot output isolator. https://www.optizonetech.com/ProductDetail/6476836.html.

197. Advanced Fiber Resources (HK), Ltd. 500 W fiber to free space isolator. http://www.afrlaser.com/UpFiles/File/2021-06/ff5cd77b3d1adb78a1440bca29c26b3a.pdf.

198. Advanced Fiber Resources (HK), Ltd. High power polarization insensitive isolator. http://www.afrlaser.com/UpFiles/File/2021-07/1064%20nm%20200%20W%20In-Line%20Isolator(1).pdf.

199. Advanced Fiber Resources (HK), Ltd. SteadiBeam®200 W 1064 nm Isolator. http://www.afrlaser.com/UpFiles/File/2021-06/912e4395235a4cbec59c3d423db2b71e.pdf.

200. CASTECH Inc. Fiber—free space isolators. https://www.castech.com/product/Fiber---Free-Space-Isolators-30.html.

201. Thorlabs, Fiber isolator. https://www.thorlabschina.cn/search/thorsearch.cfm?search=isolator.

202. Limpert J, Höfer S, Liem A, Zellmer H, Tünnermann A, Knoke S, Voelckel H. 100-W average-power, high-energy nanosecond fiber amplifier. *Appl Phys B* **2002**;*75*:477.

203. Sinha S, Urbanek KE, Krzywicki A, Byer RL. Investigation of the suitability of silicate bonding for facet termination in active fiber devices. *Opt Express* **2007**;*15*:13003.

204. Alexandre W, Mathieu F, Benoit S, Nelson V, editors. High core and cladding isolation termination for high-power lasers and amplifiers. In: Proc. SPIE, **2009**.

205. Boehme S, Beckert E, Eberhardt R, Tuennermann A, editors. Laser splicing of end caps: process requirements in high power laser applications. In: Proc. SPIE, **2009**.

206. Zhang ZY, Niu B, Gao WY, Hou W, Lin XC. Splicing technology of fiber large diameter end-cap based on CO_2 laser. *Chin J Lasers* **2014**;*41*:0703001.

207. Zhou XF, Chen ZL, Wang ZF, Hou J. Monolithic fiber end cap collimator for high-power free-space fiber-fiber coupling. *Appl Opt* **2016**;*55*:4001.

208. Nicholson JW, Desantolo A, Westbrook PS, Windeler RS, Kremp T, Headley C, Digiovanni DJ. Axicons for mode conversion in high peak power, higher-order mode, fiber amplifiers. *Opt Express* **2015**;*23*:33849.

209. Coherent Inc. High-power laser beam light delivery. https://www.coherent.com/components-accessories/beam-delivery.

210. Ola B, Mats B, Hans B, Magnus P, editors. High-power fiber optic cable with integrated active sensors for live process monitoring. In: Proc. SPIE, **2012**.

211. Advanced Fiber Resources (HK), Ltd. Dragon 20 kW high power laser cable. http://www.afrlaser.com/UpFiles/File/2022-03/Dragon%2020kW%20High%20Power%20Laser%20Cable%20with%2013mm%20cable%EF%BC%8CRev11A.pdf.

212. Shaw LB, Jain D, Gorman P, Codemard C, Jung Y, Zervas MN, Sahu JK. Picosecond Yb-doped single-trench fiber amplifier with diffraction limited output. In: Fiber lasers XII: technology, systems, and applications, **2015**.

213. Han J, Lou S, Xing Z, Wang X. Design and analysis of a multi-layer core, hole-assisted bend-resistant large mode area fiber for 2 µm operation. *Opt Fiber Technol* **2021**;*66*:102682.

251. Cao YS, Li JQ, Su QY. Guided modes in chiral fibers. *J Opt Soc Am B* **2011**;*28*:319.

252. Li L, Ma X. Adiabaticity analysis of multimode optical fiber tapers in phase space. *J Opt Soc Am B* **2021**;*38*:3632.

253. Rukhlenko ID, Noskov RE, Fleming S, Jain D. Engineering profiles of thermally drawn optical fiber tapers. *J Lightwave Technol* **2021**;*39*:3237.

254. Filippov V, Chamorovskii Y, Kerttula J, Kholodkov A, Okhotnikov OG. 600 W power scalable single transverse mode tapered double-clad fiber laser. *Opt Express* **2009**;*17*:1203.

255. Filippov V, Kerttula J, Chamorovskii Y, Golant K, Okhotnikov OG. Highly efficient 750 W tapered double-clad ytterbium fiber laser. *Opt Express* **2010**;*18*:12499.

256. Shi C, Wang XL, Zhou P, Xu XJ, Lu QS. Theoretical study of mode evolution in active long tapered multimode fiber. *Opt Express* **2016**;*24*:19473.

257. Shi C, Wang X, Zhou P, Xu X. Theoretical study of stimulated Raman scattering in long tapered fiber amplifier. *Chin Opt Lett* **2017**;*15*:110605.

258. Tian Y, Chen YZ, Leng JY, Yao TF, Zhou P, Chen JB. Numerical modeling and optimization of cladding-pumped tapered fiber Raman amplifiers. *Opt Commun* **2018**;*423*:6.

259. Kerttula J, Filippov V, Ustimchik V, Chamorovskiy Y, Okhotnikov OG. Mode evolution in long tapered fibers with high tapering ratio. *Opt Express* **2012**;*20*:25461.

260. Kerttula J, Filippov V, Chamorovskii Y, Ustimchik V, Golant K, Okhotnikov OG. Principles and performance of tapered fiber lasers: from uniform to flared geometry. *Appl Opt* **2012**;*51*:7025.

261. Filippov V, Chamorovskii Y, Kerttula J, Golant K, Pessa M, Okhotnikov OG. Double clad tapered fiber for high power applications. *Opt Express* **1929**;*2008*:16.

262. Roy V, Paré C, Labranche B, Laperle P, Desbiens L, Boivin M, Taillon Y, editors. Yb-doped large mode area tapered fiber with depressed cladding and dopant confinement. In: Proc. SPIE, **2017**.

263. Fedotov A, Noronen T, Gumenyuk R, Ustimchik V, Chamorovskii Y, Golant K, Odnoblyudov M, Rissanen J, Niemi T, Filippov V. Ultra-large core birefringent Yb-doped tapered double clad fiber for high power amplifiers. *Opt Express* **2018**;*26*:6581.

264. Shi C, Zhang HW, Wang XL, Zhou P, Xu XJ. kW-class high power fiber laser enabled by active long tapered fiber. *High Power Laser Sci Eng* **2018**;*6*:02000e16.

265. Yang BL, Zhang HW, Shi C, Wang XL, Pan ZY, Wang ZF, Zhou P, Xu XJ. High power monolithic tapered ytterbium-doped fiber laser oscillator. *Opt Express* **2019**;*27*:7585.

266. Ye Y, Xi XM, Shi C, Yang BL, Wang XL, Zhang HW, Zhou P, Xu XJ. Comparative study on transverse mode instability of fiber amplifiers based on long tapered fiber and conventional uniform fiber. *Laser Phys Lett* **2019**;*16*:085109.

267. Zhang HW, Du XY, Zhou P, Wang XL, Xu XJ. Tapered fiber based high power random laser. *Opt Express* **2016**;*24*:9112.

268. Kerttula J, Filippov V, Chamorovskii Y, Golant K, Okhotnikov OG. Actively Q-switched 1.6-mJ tapered double-clad ytterbium-doped fiber laser. *Opt Express* **2010**;*18*:18543.

269. Kerttula J, Filippov V, Chamorovskii Y, Golant K, Okhotnikov OG. 250 μJ broadband supercontinuum generated using a q-switched tapered fiber laser. *IEEE Photonics Technol Lett* **2011**;*23*:380.

270. Filippov V, Chamorovskii Y, Kerttula J, Kholodkov A, Okhotnikov OG. Single-mode 212 W tapered fiber laser pumped by a low-brightness source. *Opt Lett* **2008**;*33*:1416.

271. Kerttula J, Filippov V, Chamorovskii Y, Ustimchik V, Golant K, Okhotnikov OG. Tapered fiber amplifier with high gain and output power. *Laser Phys* **2012**;*22*:1734.

272. Trikshev AI, Kurkov AS, Tsvetkov VB, Filatova SA, Kertulla J, Filippov V, Chamorovskiy YK, Okhotnikov OG. A 160 W single-frequency laser based on an active tapered double-clad fiber amplifier. *Laser Phys Lett* **2013**;*10*:065101.

273. Zeng LF, Xi XM, Ye Y, Lin XF, Wang XL, Li JY, Shi C, Yang BL, Zhang HW, Wang P, Zhou P, Xu XJ. A novel fiber laser oscillator employing saddle-shaped core ytterbium-doped fiber. *Appl Phys B* **2020**;*126*:185.

274. Fedotov A, Ustimchik V, Rissanen J, Noronen T, Gumenyuk R, Kolosovskii A, Voloshin V, Vorob'ev I, Chamorovskii Y, Filippov V. Large mode area double-clad ytterbium-doped spun tapered fiber. *J Opt Soc Am B* **2021**;*38*:F161.

275. Lin XN, Zhang ZL, Chu YB, Wang YB, Xing YB, Chen G, Peng JG, Li HQ, Dai NL, Li JY. Fabrication and laser performance of cladding uniform core tapered fiber. *Opt Fiber Technol* **2021**;*64*:102561.

276. Ye Y, Lin XF, Xi XM, Shi C, Yang BL, Zhang HN, Wang XL, Li JY, Xu XJ. Novel constant-cladding tapered-core ytterbium-doped fiber for high-power fiber laser oscillator. *High Power Laser Sci Eng* **2021**;*9*:02000e21.

277. Zeng LF, Pan ZY, Xi XM, Yang H, Ye Y, Huang LJ, Zhang HW, Wang XL, Wang ZF, Zhou P, Xu XJ, Chen JB. 5 kW monolithic fiber amplifier employing homemade spindle-shaped ytterbium-doped fiber. *Opt Lett* **2021**;*46*:1393.

278. Zeng LF, Wang XL, Yang BL, Zhang HW, Xu XJ. A 3.5-kW near-single-mode oscillating–amplifying integrated fiber laser. *High Power Laser Sci Eng* **2021**;*9*:03000e41.

279. Zeng LF, Xi XM, Zhang HW, Yang BL, Wang P, Wang XL, Xu XJ. Demonstration of the reliability of a 5-kW-level oscillating–amplifying integrated fiber laser. *Opt Lett* **2021**;*46*:5778.

280. Lin XF, Ye Y, Zhang ZL, Wang XL, Xing YB, Chen G, Peng JG, Li HQ, Dai NL, Li JY. 2.7 kW co-pumped fiber amplifier based on constant-cladding tapered-core fiber. *Opt Fiber Technol* **2022**;*68*:102773.

281. Huang L, Zhou ZC, Shi C, Tao RM, Ma PF, Wang XL, Zhou P. Towards tapered-fiber-based all-fiberized high power narrow linewidth fiber laser. *Sci China Technol Sci* **2018**;*61*:971.

282. Zhou ZC, Zhang HW, Wang XL, Pan ZY, Su RT, Yang BL, Zhou P, Xu XJ. All-fiber-integrated single frequency tapered fiber amplifier with near diffraction limited output. *J Opt* **2016**;*18*:065504.

283. An Y, Pan ZY, Yang H, Huang LJ, Ma PF, Yan ZP, Jiang ZF, Zhou P. 400-W single-mode single-frequency laser output from homemade tapered fiber. *Acta Phys Sin* **2021**;*70*:204204.

284. Huang L, Lai W, Ma P, Wang J, Su R, Ma Y, Li C, Zhi D, Zhou P. Tapered Yb-doped fiber enabled monolithic high-power linearly polarized single-frequency laser. *Opt Lett* **2020**;*45*:4001.

285. Zeng LF, Xi XM, Ye Y, Wang XL, Yang BL, Pan ZY, Shi C, Zhang HW, Wang P, Wang ZF, Zhou P, Xu XJ, Chen JB. A 18 kW fiber laser oscillator employing a section of spindle-shaped core ytterbium-doped fiber. *Laser Phys Lett* **2020**;*17*:095104.

286. Aleshkina SS, Levchenko AE, Medvedkov OI, Bobkov KK, Bubnov MM, Lipatov DS, Guryanov AN, Likhachev ME. Photodarkening-free Yb-doped saddle-shaped fiber for high power single-mode 976-nm laser. *IEEE Photonics Technol Lett* **2018**;*30*:127.

287. Shiraki K, Ohashi M, Tateda M. Suppression of stimulated Brillouin scattering in a fibre by changing the core radius. *Electron Lett* **1995**;*31*:668.

288. Lai WC, Ma PF, Liu W, Huang L, Li C, Ma YX, Zhou P. 550 W single frequency fiber amplifiers emitting at 1030 nm based on a tapered Yb-doped fiber. *Opt Express* **2020**;*28*:20908.

289. Matějec V, Kaík I, Berková D, Hayer M, Langrová A. Properties of optical fiber preforms prepared by inner coating of substrate tubes. *Ceram Silik* **2001**;*45*:62.

290. Boyland AJ, Webb AS, Kalita MP, Yoo S, Codemard CA, Standish RJ, Nilsson J, Sahu JK, editors. Rare-earth doped optical fiber fabrication using novel gas phase deposition technique. In: Conference on lasers and electro-optics, 2010/05/16; San Jose, California: Optical Society of America; **2010**.

291. Webb AS, Boyland AJ, Standish RJ, Yoo S, Sahu JK, Payne DN. MCVD in-situ solution doping process for the fabrication of complex design large core rare-earth doped fibers. *J Non Cryst Solids* 2010;*356*:848.

292. Boyland AJ, Webb AS, Yoo S, Mountfort FH, Kalita MP, Standish RJ, Sahu JK, Richardson DJ, Payne DN. Optical fiber fabrication using novel gas-phase deposition technique. *J Lightwave Technol* **2011**;*29*:912.

293. Lindner F, Aichele C, Schwuchow A, Leich M, Scheffel A, Unger S, editors. Optical properties of Yb-doped fibers prepared by gas phase doping. In: Proc. SPIE, **2014**.

294. Saha M, Pal A, Sen R. Vapor phase doping of rare-earth in optical fibers for high power laser. *IEEE Photonics Technol Lett* **2014**;*26*:58.

295. Offerhaus HL, Broderick NG, Richardson DJ, Sammut R, Caplen J, Dong L. High-energy single-transverse-mode Q-switched fiber laser based on a multimode large-mode-area erbium-doped fiber. *Opt Lett* **1998**;*23*:1683.

296. Gong ML, Yuan YY, Li C, Yan P, Zhang HT, Liao SY. Numerical modeling of transverse mode competition in strongly pumped multimode fiber lasers and amplifiers. *Opt Express* **2007**;*15*:11.

297. Marciante JR. Gain filtering for single-spatial-mode operation of large-mode-area fiber amplifiers. *Select Top Quantum Electron IEEE J* **2009**;*15*:30.

298. Leidner JP, Marciante JR. Three fiber designs for mitigating thermal mode instability in high-power fiber amplifiers. *Opt Express* **2020**;*28*:28502.

299. Marciante JR, Roides RG, Shkunov VV, Rockwell DA. Near-diffraction-limited operation of step-index large-mode-area fiber lasers via gain filtering. *Opt Lett* **1828**;*2010*:35.

300. Ye C, Koponen J, Kokki T, Ponsoda JMI, Tervonen A, Honkanen S. Near-diffraction-limited output from confined-doped ytterbium fibre with 41 μm core diameter. *Electron Lett* **2011**;*47*:819–21.

301. Ye C, Koponen J, Kokki T, Montiel I, Ponsoda J, Tervonen A, Honkanen S, editors. Confined-doped ytterbium fibers for beam quality improvement: fabrication and performance. San Francisco: SPIE; **2012**.

302. Liao L, Zhang FF, He XL, Chen YS, Wang YB, Li HQ, Peng JG, Yang LY, Dai NL, Li JY. Confined-doped fiber for effective mode control fabricated by MCVD process. *Appl Opt* **2018**;*57*:3244.

303. Seah CP, Lim WYW, Chua SL, editors. A 4kW fiber amplifier with good beam quality employing confined-doped gain fiber. In: Laser congress 2018 (ASSL), 2018/11/04. Boston, Massachusetts: Optical Society of America; **2018**.

304. Gausmann S, Lopez JEA, Anderson J, Wittek S, Correa RA, Schülzgen A, editors. Gain dependent mode analysis of large mode area fiber with confined ytterbium doping. In: Conference on lasers and electro-optics, 2019/05/05; San Jose, California: Optical Society of America; **2019**.

305. Gausmann S, Antonio-Lopez JE, Anderson J, Wittek S, Eznaveh ZS, Jang H, Habib MS, Cook J, Richardson M, Correa RA, Schulzgen A. S^2 measurements showing suppression of higher order modes in confined rare earth doped large core fibers. *J Lightwave Technol* **2020**;*1*:1953–8.

306. Wang B, Pang L, Liu J. Single mode 2.4kW part-doped ytterbium fiber fabricated by modified chemical vapor deposition technique. In: Second target recognition and artificial intelligence summit forum. SPIE; **2020**.

307. Choudhury N, Chowdhury S, Das Chowdhury S, Kumar Shekhar N, Jain D, Sen R, Dhar A. Novel dopant tailored fibers using vapor phase chelate delivery technique. *Phys Status solidi (A)* **2022**;*219*:2100484.

308. Huang ZM, Shu Q, Luo Y, Tao RM, Feng X, Liu Y, Lin HH, Wang JJ, Jing F. 35 kW narrow-linewidth monolithic fiber amplifier at 1064 nm by employing a confined doping fiber. *J Opt Soc Am B* **2021**;*38*:2945.

309. Zhang Z, Lin X, Chen G, Liao L, Xing Y, Li H, Peng J, Dai N, Li J. Gaussian-shaped gain-dopant distributed fiber for high output power fiber amplifier. *IEEE Photonics J* **2021**;*13*:1.

310. Fini JM. Large mode area fibers with asymmetric bend compensation. *Opt Express* **2011**;*19*:21866.

311. Fini JM, Nicholson JW. Bend compensated large-mode-area fibers: achieving robust single-modedness with transformation optics. *Opt Express* **2013**;*21*:19173.

312. Ramachandran S, Fini JM, Nicholson JW. Fibers design with a bend-compensated cladding for distributed wavelength filtering. In: Fiber lasers XI: technology, systems, and applications. **2014**.

313. Fini JM. Design of large-mode-area amplifier fibers resistant to bend-induced distortion. *J Opt Soc Am B* **2007**;*24*:1669.

314. Petrov MP, Kiyan RV, Kuzin EA, Rogacheva EA, Spirin VV. Gain saturation in three- and four-level fiber amplifiers. *Opt Commun* **1994**;*109*:499.

315. Nilsson J, Paschotta R, Caplen JE, Hanna DC. Yb^{3+}-ring-doped fiber for high-energy pulse amplification. *Opt Lett* **1997**;*22*:1092.

316. Nilsson J, Minelly JD, Paschotta R, Tropper AC, Hanna DC. Ring-doped cladding-pumped single-mode three-level fiber laser. *Opt Lett* **1998**;*23*:355.

317. Palma-Vega G, Walbaum T, Heinzig M, Kuhn S, Hupel C, Hein S, Feldkamp G, Sattler B, Nold J, Haarlammert N, Schreiber T, Eberhardt R, Tünnermann A. Ring-up-doped fiber for the generation of more than 600 W single-mode narrow-band output at 1018 nm. *Opt Lett* **2019**;*44*:2502.

318. Barber MJ, Shardlow PC, Barua P, Sahu JK, Clarkson WA. Nested-ring doping for highly efficient 1907 nm short-wavelength cladding-pumped thulium fiber lasers. *Opt Lett* **2020**;*45*:5542.

319. Li HZ, Zang JC, Raghuraman S, Chen SX, Goel C, Xia N, Ishaaya A, Yoo S. Large-mode-area multicore Yb-doped fiber for an efficient high power 976 nm laser. *Opt Express* **2021**;*29*:21992.

320. Ballato J, Hawkins T, Cavillon M, Dragic P. The materials science and engineering of optical nonlinearities and their mitigation in high power lasers. In: SPIE Security + Defence. SPIE; **2019**

321. Ballato J, Cavillon M, Dragic P. A unified materials approach to mitigating optical nonlinearities in optical fiber. I. Thermodynamics of optical scattering. *Int J Appl Glass Sci* **2018**;*9*:263.

322. Cavillon M, Kucera C, Hawkins T, Dawson J, Dragic PD, Ballato J. A unified materials approach to mitigating optical nonlinearities in optical fiber. III. Canonical examples and materials road map. *Int J Appl Glass Sci.* **2018**;*9*:447.

323. Baker CC, Dragic PD, Burdett A, Yu N, Vargas AL, Friebele EJ, Rhonehouse DL, Sanghera J, editors. Design solutions for increased thresholds of non-linear processes in silica fiber. In: Laser congress 2019 (ASSL, LAC, LS&C), 2019/09/29. Vienna: Optica Publishing Group; **2019**.

324. Pan G, Yu N, Meehan B, Hawkins TW, Ballato J, Dragic PD. Thermo-optic coefficient of B$_2$O$_3$ and GeO$_2$ co-doped silica fibers. *Opt Mater Express* **2020**;*10*:1509.

325. Palma-Vega G, Kuhn S, Walbaum T, Haarlammert N, Schreiber T, editors. Simplified, athermal fiber designs for high power laser applications. In: 2021 Conference on lasers and electro-optics Europe and European quantum electronics conference, 2021/06/21. Munich: Optical Society of America; **2021**.

326. Gonzalo P-V, Stefan K, Johannes N, Till W, Nicoletta H, Thomas S, editors. Investigations towards easy-to-fabricate effective

athermal fibers for high average power lasers. In: Proc. SPIE, **2022**.

327. Lee CC, Chi S. Measurement of stimulated-Brillouin-scattering threshold for various types of fibers using Brillouin optical-time-domain reflectometer. *IEEE Photonics Technol Lett* **2000**;*12*:672.

328. Jaewang Y, Il-Bum K, Kyunghwan O. Analysis of Brillouin frequency shift and longitudinal acoustic wave in a silica optical fiber with a triple-layered structure. *J Lightwave Technol* **2003**;*21*:1779.

329. Koyamada Y, Sato S, Nakamura S, Sotobayashi H, Chujo W. Simulating and designing Brillouin gain spectrum in single-mode fibers. *J Lightwave Technol* **2004**;*22*:631.

330. Kobyakov A, Kumar S, Chowdhury DQ, Ruffin AB, Sauer M, Bickham SR, Mishra R. Design concept for optical fibers with enhanced SBS threshold. *Opt Express* **2005**;*13*:5338.

331. Li MJ, Chen X, Wang J, Gray S, Liu A, Demeritt JA, Ruffin AB, Crowley AM, Walton DT, Zenteno LA. Al/Ge co-doped large mode area fiber with high SBS threshold. *Opt Express* **2007**;*15*:8290.

332. Mermelstein MD, Andrejco MJ, Fini J, Yablon A, C. Headley I, Digiovanni DJ, Mccurdy AH, editors. 11.2 dB SBS gain suppression in a large mode area Yb-doped optical fiber. In: Proc. SPIE, **2008**.

333. Galeener FL, Mikkelsen JC, Geils RH, Mosby WJ. The relative Raman cross sections of vitreous SiO_2, GeO_2, B_2O_3, and P_2O_5. *Appl Phys Lett* **1978**;*32*:34.

334. Dragic P, Hawkins T, Foy P, Morris S, Ballato J. Sapphire-derived all-glass optical fibres. *Nat Photonics* **2012**;*6*:627.

335. Dragic PD, Cavillon M, Ballato J. Materials for optical fiber lasers: a review. *Appl Phys Rev* **2018**;*5*:041301.

336. Dragic PD, Cavillon M, Ballato A, Ballato J. A unified materials approach to mitigating optical nonlinearities in optical fiber. II. B. The optical fiber, material additivity and the nonlinear coefficients. *Int J Appl Glass Sci.* **2018**;*9*:307.

337. Dragic PD, Cavillon M, Ballato A, Ballato J. A unified materials approach to mitigating optical nonlinearities in optical fiber. II. A. Material additivity models and basic glass properties. *Int J Appl Glass Sci* **2018**;*9*:278.

338. Siegman AE. Gain-guided, index-antiguided fiber lasers. *J Opt Soc Am B* **2007**;*24*:1677.

339. Casperson LW, Her T-H. Thermal refraction focusing in very-large-core step-index antiguided fiber lasers. *J Opt Soc Am B* **2013**;*30*:3095.

340. Jansen F, Stutzki F, Otto H-J, Jauregui C, Limpert J, Tünnermann A. High-power thermally guiding index-antiguiding-core fibers. *Opt Lett* **2013**;*38*:510.

341. Darwich D, Dauliat R, Jamier R, Benoit A, Schuster K, Roy P. Precompensation of the thermal-induced refractive index changes into a fully aperiodic LPF for heat load resilience. *Appl Opt* **2016**;*55*:8213.

342. Kong LC, Cao JQ, Guo SF, Jiang ZF, Lu QS. Thermal-induced transverse-mode evolution in thermally guiding index-antiguided-core fiber. *Appl Opt* **2016**;*55*:1183.

343. Cao JQ, Liu WB, Chen JB, Lu QS. Modeling the single-mode thermally guiding very-large-mode-area Yb-doped fiber amplifier. *Acta Phys Sin* **2017**;*66*:064201.

344. Smith CR, Simakov N, Hemming A, Clarkson WA. Thermally guided Yb-doped fiber-rod amplifier and laser. *Appl Phys B* **2019**;*125*:32.

345. Malleville M-A, Leconte B, Dauliat R, Jamier R, Schwuchow A, Wondraczek K, Roy P. Pre-compensation of thermally induced refractive index changes in a depressed core fully aperiodic large-pitch fiber for high average power operation. *Opt Lett* **2021**;*46*:2956.

346. Rohrer C, Codemard CA, Kleem G, Graf T, Ahmed MA. Preserving nearly diffraction-limited beam quality over several hundred meters of transmission through highly multimode fibers. *J Lightwave Technol* **2019**;*37*:4260.

347. Austerschulte A, Vogel MM, Rataj T, Negel J-P, Voss A, Abdou Ahmed M, Graf T. 800 W cw nearly diffraction-limited beam delivery through a 100 m long multi-mode fiber. In: Fiber lasers IX: technology, systems, and applications; **2012**.

348. Negel J-P, Austerschulte A, Vogel MM, Rataj T, Voss A, Abdou Ahmed M, Graf T. Delivery of 800 W of nearly diffraction-limited laser power through a 100 m long multi-mode fiber. *Laser Phys Lett* **2014**;*11*:055104.

349. Rohrer C, Kleem G, Ahmed MA, Graf T. Analysis of fundamental-mode beam transport in highly multimode fibers. *J Lightwave Technol* **2017**;*35*:3637.

350. Ramachandran S, Nicholson JW, Ghalmi S, Yan MF, Wisk P, Monberg E, Dimarcello FV, editors. Robust light propagation in ultra-large mode-area fibers. In: 2006 European conference on optical communications, 24–28 Sept. 2006; **2006.**

351. Ramachandran S, Fini JM, Mermelstein M, Nicholson JW, Ghalmi S, Yan MF. Ultra-large effective-area, higher-order mode fibers: a new strategy for high-power lasers. *Laser Photonics Rev* **2008**;*2*:429.

352. Vukovic N, Almeida P, Chan J, Codemard C, Zervas MN. Fast and controllable beam switching in a pulsed fiber laser. *IEEE Photonics Technol Lett* **2019**;*31*:927.

353. Fini J, Bise R, Yan M, Yablon A, Wisk P. Distributed fiber filter based on index-matched coupling between core and cladding. *Opt Express* **2006**;*13*:10022.

354. Aleshkina S, Kashaykina T, Yashkov M, Salganskii M, Velmiskin V, Bubnov M, Likhachev M. Spectral filtering in single-mode fibers using resonant coupling with absorbing rods. *Opt Lett* **2021**;*46*:1458.

355. Aleshkina S, Yashkov MV, Salganskiy MY, Velmiskin VV, Guryanov AN, Bubnov MM, Likhachev ME. Spectrally selective optical loss in fibers with high-index rods embedded into silica cladding. *J Lightwave Technol* **2022**;*1*:4848–54.

356. Alkeskjold TT. Large-mode-area ytterbium-doped fiber amplifier with distributed narrow spectral filtering and reduced bend sensitivity. *Opt Express* **2009**;*17*:16394.

357. Tankala K, Alkeskjold TT. Single-mode large-mode area fiber amplifier with higher-order mode suppression and distributed passband filtering of ASE and SRS. In: Fiber lasers VII: technology, systems, and applications; **2010**.

358. Taru T, Hou J, Knight J. Raman gain suppression in all-solid photonic bandgap fiber. In: European conference and exhibition of optical communication. Berlin, **2007**. p 1.

359. Codemard CA, Vukovic NT, Chan JS, Almeida PJ, Hayes JR, Petrovich MN, Baskiotis C, Malinowski A, Zervas MN. Resonant SRS filtering fiber for high power fiber laser applications. *IEEE J Sel Top Quantum Electron* **2018**;*24*:1.

360. Chan J, Vukovic NT, Codemard CA, Zervas MN, Dong L, Zervas MN. All-fiber bandwidth tunable filter for high power fiber lasers. In: Fiber lasers XVII: technology and systems; **2020**.

361. Luan F, George AK, Hedley TD, Pearce GJ, Bird DM, Knight JC, Russell PSJ. All-solid photonic bandgap fiber. *Opt Lett* **2004**;*29*:2369.

362. Duguay MA, Kokubun Y, Koch TL, Pfeiffer L. Antiresonant reflecting optical waveguides in SiO_2-Si multilayer structures. *Appl Phys Lett* **1986**;*49*:13.

363. Litchinitser NM, Abeeluck AK, Headley C, Eggleton BJ. Antiresonant reflecting photonic crystal optical waveguides. *Opt Lett* **2002**;*27*:1592.

364. White TP, Mcphedran RC, De Sterke CM, Litchinitser NM, Eggleton BJ. Resonance and scattering in microstructured optical fibers. *Opt Lett* **1977**;*2002*:27.

365. Litchinitser NM, Dunn SC, Usner B, Eggleton BJ, White TP, Mcphedran RC, De Sterke CM. Resonances in microstructured optical waveguides. *Opt Express* **2003**;*11*:1243.

366. Blin S, Provino L, Traynor N, Mugnier A, Pureur D, Chartier T. Design of all-solid photonic-bandgap fibers for Raman-free propagation. In: CLEOE-EQEC.5194720; 06/01; **2009**.

367. Baz A, Bigot L, Bouwmans G, Quiquempois Y. Single-mode, large mode area, solid-core photonic bandgap fiber with hetero-structured cladding. *J Lightwave Technol* **2013**;*31*:830.

368. Gu G, Kong F, Hawkins TW, Jones M, Dong L. Extending mode areas of single-mode all-solid photonic bandgap fibers. *Opt Express* **2015**;*23*:9147.

369. Chen X, Huang LJ, Xi XM, Yang H, An Y, Yan ZP, Pan ZY, Zhou P. Leakage channels enabled multi-resonant all-solid photonic bandgap fiber for effective single-mode propagation. *Opt Express* **2021**;*29*:22455.

370. Chen X, Huang LJ, An Y, Yang H, Yan ZP, Chen YS, Xi XM, Pan ZY, Zhou P. Spectrally U-shaped profile of beam propagation factor in all-solid photonic bandgap fiber. *Chin Opt Lett* **2022**;*20*:010602.

371. Knight JC, Broeng J, Birks TA, Russell PSJ. Photonic band gap guidance in optical fibers. *Science* **1998**;*282*:1476.

372. Abeeluck AK, Litchinitser NM, Headley C, Eggleton BJ. Analysis of spectral characteristics of photonic bandgap waveguides. *Opt Express* **2002**;*10*:1320.

373. Argyros A, Birks TA, Leon-Saval SG, Cordeiro CMB, Russell PSJ. Guidance properties of low-contrast photonic bandgap fibres. *Opt Express* **2005**;*13*:2503.

374. Renversez G, Boyer P, Sagrini A. Antiresonant reflecting optical waveguide microstructured fibers revisited: a new analysis based on leaky mode coupling. *Opt Express* **2006**;*14*:5682.

375. Corporation NTaT, Mitsubishi Heavy Industries L. Completely Rewrite Industry's Understanding of Transmitting High Quality Laser Processing Light over Long Distances. **2018**. https://www.mhi.com/news/18042503.html?style=preview.

376. Matsui T, Tsujikawa K, Okuda T, Hanzawa N, Sagae Y, Nakajima K, Fujiya Y, Shiraki K. Effective area enlarged photonic crystal fiber with quasi-uniform air-hole structure for high power transmission. *IEICE Trans Commun* **2020**;*E103.B*:415.

377. Palma-Vega G, Beier F, Stutzki F, Fabian S, Schreiber T, Eberhardt R, Tünnermann A, editors. High average power transmission through hollow-core fibers. InL Laser congress 2018 (ASSL), 2018/11/04. Boston, Massachusetts: Optical Society of America; **2018**.

378. Goel C, Li HZ, Abu Hassan MR, Chang WK, Yoo S. Anti-resonant hollow-core fiber fusion spliced to laser gain fiber for high-power beam delivery. *Opt Lett* **2021**;*46*:4374.

379. Van Newkirk A, Martinez Mercado J, Antonio Lopez E, Amezcua Correa R, Schulzgen A. High power laser delivery using anti-resonant hollow core fiber. In: SPIE Optical Engineering + Applications. SPIE; **2021**.

380. Zhu XY, Wu DK, Wang YZ, Yu F, Li QR, Qi YF, Knight J, Chen SF, Hu LL. Delivery of CW laser power up to 300 watts at 1080 nm by an uncooled low-loss anti-resonant hollow-core fiber. *Opt Express* **2021**;*29*:1492.

381. Mulvad HCH, Abokhamis Mousavi S, Zuba V, Xu L, Sakr H, Bradley TD, Hayes JR, Jasion GT, Numkam Fokoua E, Taranta A, Alam SU, Richardson DJ, Poletti F. Kilowatt-average-power single-mode laser light transmission over kilometre-scale hollow-core fibre. *Nat Photonics* **2022**;*16*:448.

382. Cui Y, Huang W, Zhou Z, Li H, Wang M, Chen Z, Wang Z. Highly efficient and stable coupling of kilowatt-level continuous wave laser into hollow-core fibers. *Chin Opt Lett* **2022**;*20*:040602.

383. Li HZ, Goel C, Zang JC, Raghuraman S, Chen SX, Abu Hassan MR, Chang W, Yoo S. Integration of an anti-resonant

hollow-core fiber with a multimode Yb-doped fiber for high power near-diffraction-limited laser operation. *Opt Express* **2022**;*30*:7928.

384. Hill KO, Fujii Y, Johnson DC, Kawasaki BS. Photosensitivity in optical fiber waveguides: application to reflection filter fabrication. *Appl Phys Lett* **1978**;*32*:647.

385. Meltz G, Morey WW, Glenn WH, editors. In-fiber Bragg grating tap. In: Optical fiber communication, 1990/01/22. San Francisco, California: Optica Publishing Group; **1990**.

386. Liu F, Guo T, Wu C, Guan BO, Lu C, Tam HY, Albert J. Wideband-adjustable reflection-suppressed rejection filters using chirped and tilted fiber gratings. *Opt Express* **2014**;*22*:24430.

387. Dostovalov AV, Wolf AA, Skvortsov MI, Abdullina SR, Kuznetsov AG, Kablukov SI, Babin SA. Femtosecond-pulse inscribed FBGs for mode selection in multimode fiber lasers. *Opt Fiber Technol* **2019**;*52*:101988.

388. Wang M, Zhang YJ, Wang ZF, Sun JJ, Cao JQ, Leng JY, Gu XJ, Xu XJ. Fabrication of chirped and tilted fiber Bragg gratings and suppression of stimulated Raman scattering in fiber amplifiers. *Opt Express* **2017**;*25*:1529.

389. Jiao KR, Shu J, Shen H, Guan ZW, Yang FY, Zhu RH. Fabrication of kW-level chirped and tilted fiber Bragg gratings and filtering of stimulated Raman scattering in high-power CW oscillators. *High Power Laser Sci Eng* **2019**;*7*:02000e31.

390. Wang M, Liu L, Wang ZF, Xi XM, Xu XJ. Mitigation of stimulated Raman scattering in kilowatt-level diode-pumped fiber amplifiers with chirped and tilted fiber Bragg gratings. *High Power Laser Sci Eng* **2019**;*7*:01000e18.

391. Jansen F, Nodop D, Jauregui C, Limpert J, Tünnermann A. Modeling the inhibition of stimulated Raman scattering in passive and active fibers by lumped spectral filters in high power fiber laser systems. *Opt Express* **2009**;*17*:16255.

392. Daniel JM, Clarkson WA. Rapid, electronically controllable transverse mode selection in a multimode fiber laser. *Opt Express* **2013**;*21*:29442.

393. Jiao KR, Shen H, Guan ZW, Yang FY, Zhu RH. Suppressing stimulated Raman scattering in kW-level continuous-wave MOPA fiber laser based on long-period fiber gratings. *Opt Express* **2020**;*28*:6048.

394. Bian YX, Jiao KR, Wu XC, Shen H, Yang FY, Zhu RH. Utilizing phase-shifted long-period fiber grating to suppress spectral broadening of a high-power fiber MOPA laser system. *High Power Laser Sci Eng* **2021**;*9*:03000e39.

395. Wang M, Wang ZF, Liu L, Hu QH, Xiao H, Xu XJ. Effective suppression of stimulated Raman scattering in half 10 kW tandem pumping fiber lasers using chirped and tilted fiber Bragg gratings. *Photonics Res* **2019**;*7*:167.

396. Tian X, Gao CH, Wang CW, Zhao XF, Wang M, Xi XM, Wang ZF. 2.58 kW narrow linewidth fiber laser based on a compact structure with a chirped and tilted fiber Bragg grating for Raman suppression. *Photonics* **2021**;*8*:532.

397. Zhao XF, Tian X, Hu QH, Rao BY, Wang M, Wang ZF. Raman suppression in a high-power single-mode fiber oscillator using a chirped and tilted fiber Bragg grating. *Laser Phys Lett* **2021**;*18*:035103.

398. Song HQ, Yan DL, Wu WJ, Shen BJ, Feng X, Liu Y, Li L, Chu QH, Li M, Wang JJ, Tao RM. SRS suppression in multi-kW fiber lasers with a multiplexed CTFBG. *Opt Express* **2021**;*29*:20535.

399. Ballato J, Dragic P. Glass: the carrier of light—a brief history of optical fiber. *Int J Appl Glas Sci* **2016**;*7*:413.

400. Zhao XF, Tian X, Wang M, Li HY, Rao BY, Wang ZF. Design and fabrication of wideband chirped tilted fiber Bragg gratings. *Opt Laser Technol* **2022**;*148*:107790.

401. Tian X, Zhao XF, Wang M, Hu QH, Li HY, Rao BY, Xiao H, Wang ZF. Influence of Bragg reflection of chirped tilted fiber

Bragg grating on Raman suppression in high-power tandem pumping fiber amplifiers. *Opt Express* **2020**;*28*:19508.

402. Hu QH, Zhao XF, Tian X, Wang M, Wang ZF, Xu XJ. Raman suppression in high-power fiber laser oscillator by long period fiber grating. *Results in Physics* **2021**;*26*:104460.

403. Nodop D, Jauregui C, Jansen F, Limpert J, Tünnermann A. Suppression of stimulated Raman scattering employing long period gratings in double-clad fiber amplifiers. *Opt Lett* **2010**;*35*:2982.

404. Maximilian H, Victor B, Ria GK, Daniel R, Thorsten AG, Christian M, Andreas L, Thomas S, Andreas T, Stefan N, editors. Mitigation of stimulated Raman scattering in high power fiber lasers using transmission gratings. In: Proc. SPIE, **2018**.

405. Heck M, Gauthier J-C, Tünnermann A, Vallée R, Nolte S, Bernier M. Long period fiber gratings for the mitigation of parasitic laser effects in mid-infrared fiber amplifiers. *Opt Express* **2019**;*27*:21347.

406. Daniel JMO, Chan JSP, Kim JW, Sahu JK, Ibsen M, Clarkson WA. Novel technique for mode selection in a multimode fiber laser. *Opt Express* **2011**;*19*:12434.

407. Liu T, Chen SP, Hou J. Selective transverse mode operation of an all-fiber laser with a mode-selective fiber Bragg grating pair. *Opt Lett* **2016**;*41*:5692.

408. Li L, Wang M, Liu T, Leng J, Zhou P, Chen JB. High-power, cladding-pumped all-fiber laser with selective transverse mode generation property. *Appl Opt* **2017**;*56*:4967.

409. Wolf AA, Dostovalov AV, Wabnitz S, Babin SA. Femtosecond writing of refractive index structures in multimode and multicore optical fibres. *Quantum Electron* **2018**;*48*:1128.

410. Babin SA, Kuznetsov AG, Sidelnikov OS, Wolf AA, Nemov IN, Kablukov SI, Podivilov EV, Fedoruk MP, Wabnitz S. Spatio-spectral beam control in multimode diode-pumped Raman fibre lasers via intracavity filtering and Kerr cleaning. *Sci Rep* **2021**;*11*:21994.

411. Maximilian H, Georg S, Ria GK, Daniel R, Thorsten AG, Christian M, Malte PS, Andreas T, Stefan N, editors. Next generation of tailored mode selective transmission gratings for fiber integrated devices. In: Proc. SPIE, **2019**.

412. Chang HX, Su RT, Long JH, Chang Q, Ma PF, Ma YX, Zhou P. Distributed active phase-locking of an all-fiber structured laser array by a stochastic parallel gradient descent (SPGD) algorithm. *Opt Express* **2022**;*30*:1089.

413. Jeong H, Lee J, Lee KH, Kim DJ, Koo J, Lee JH, Jo M. 740-watt level optical tap coupler using side-polished large-mode-area double clad fibers for a high power fiber laser. *Opt Express* **2021**;*29*:19525.

414. Vukovic N, Chan J, Codemard CA, Zervas MN, S. Keen VR, Jessett R, Botheroyd I, M. Greenwood, editors. Singlemode kilowatt fibre laser with adjustable beam profile and M². In: CLEO Europe EQEC'19; **2019**.

415. Vukovic N, Chan JS, Codemard CA, Zervas MN, Keen SJ, Chen R, Jesset R, Botheroyd I, Durkin M, Greenwood M, Armani AM, Kudryashov AV, Paxton AH, Ilchenko VS. Multi-kilowatt fibre laser with azimuthal mode output beam for advanced material processing. In: Laser resonators, microresonators, and beam control XXII, **2020**.

416. Natasha V, Jaclyn SC, Christophe AC, Michalis NZ, editors. Fibre-delivered kilowatt petal beams with self-healing properties. In: Proc. SPIE, **2021**.

417. Hochheim S, Brockmuller E, Wessels P, Koponen J, Lowder T, Novotny S, Willke B, Neumann J, Kracht D. Single-frequency 336W spliceless all-fiber amplifier based on a chirally-coupled-core fiber for the next generation of gravitational wave detectors. *J Lightwave Technol* **2021**;*1*:2136–43.

418. Donald LS, Jr., Jason DT, Daniel SS, Christina BO, Martin M, editors. KW monolithic PCF fiber amplifers for narrow linewidth and single mode operation. In: Proc. SPIE, **2012**.

419. Benjamin GW, Donald LS, Jr., Jason DT, editors. A monolithic pump signal multiplexer for air-clad photonic crystal fiber amplifiers. In: Proc. SPIE, **2010**.

420. Kim PH, Christina BO, Jes B, Kent M, Martin DN, Thomas N, Peter MWS, Mads Hoy S, Mark D, Christian J, Harald RS, editors. Airclad fiber laser technology. In: Proc. SPIE, **2008**.

421. Jakob Juul L, Claus Friis P, Guillaume V, editors. Side pumping of double-clad photonic crystal fibers. In: Proc. SPIE, **2004**.

422. Larsen JJ, Vienne G. Side pumping of double-clad photonic crystal fibers. *Opt Lett* **2004**;*29*:436.

423. Sincore A, Sipes DL, Tafoya JD, Schulz DS, Shah L, Richardson MC, editors. Integrated all-fiber thulium-doped PCF pump combiner. In: Advanced solid-state lasers congress, 2013/10/27. Paris: Optica Publishing Group; **2013**.

424. Alex S, Jason T, Donald S, Jr., Lasse L, Lawrence S, Martin R, editors. Photonic crystal fiber pump combiner for high-peak power all-fiber thulium lasers. In: Proc. SPIE, **2014**.

425. Huang G, Lv GY, Fan YY, Geng C, Li XY. Predictive optimization algorithm for beam combination systems based on adaptive fiber optics collimators. *Opt Lasers Eng* **2022**;*148*:106753.

426. Li F, Geng C, Huang G, Yang Y, Li XY. Wavefront sensing based on fiber coupling in adaptive fiber optics collimator array. *Opt Express* **2019**;*27*:8943.

427. Leonid AB, Mikhail AV, editors. Design of adaptive fiber optics collimator for free-space communication laser transceiver. In: Proc. SPIE, **2005**.

428. Leonid AB, Thomas W, Mikhail AV, Ling L, Gary WC, editors. Development of adaptive fiber collimators for conformal fiber-based beam projection systems. In: Proc. SPIE, **2008**.

429. Vorontsov MA, Weyrauch T, Beresnev LA, Carhart GW, Liu L, Aschenbach K. Adaptive array of phase-locked fiber collimators: analysis and experimental demonstration. *IEEE J Sel Top Quantum Electron* **2009**;*15*:269.

430. Vorontsov MA, Weyrauch T. High-power lasers for directed-energy applications: comment. *Appl Opt* **2016**;*55*:9950.

431. Finalists named for 2015 Prism Awards for Photonics Innovation. 2014. https://spie.org/about-spie/press-room/press-release-archive/prism-2015-finalists-11-26-2014.

432. Geng C, Li XY, Zhang XJ, Rao CH. Coherent beam combination of an optical array using adaptive fiber optics collimators. *Opt Commun* **2011**;*284*:5531.

433. Geng C, Zhao B, Zhang E, Luo W, Tan Y, Zhu Y, Yang H, Mu J, Li X, Duan K, Zhao W. 1.5 kW incoherent beam combining of four fiber lasers using adaptive fiber-optics collimators. *IEEE Photonics Technol Lett* **2013**;*25*:1286.

434. Zhi D, Ma PF, Ma YX, Wang XL, Zhou P, Si L. Novel adaptive fiber-optics collimator for coherent beam combination. *Opt Express* **2014**;*22*:31520.

435. Zhi D, Ma YX, Chen ZL, Wang XL, Zhou P, Si L. Large deflection angle, high-power adaptive fiber optics collimator with preserved near-diffraction-limited beam quality. *Opt Lett* **2016**;*41*:2217.

436. Zhi D, Ma YX, Tao RM, Zhou P, Wang XL, Chen ZL, Si L. Highly efficient coherent conformal projection system based on adaptive fiber optics collimator array. *Sci Rep* **2019**;*9*:2783.

437. Ma YX, Luo G, He SY, Chen ZL, Su RT, Ma PF, Zhou P, Si L. Cantilevered adaptive fiber-optics collimator based on piezoelectric bimorph actuators. *Appl Opt* **2022**;*61*:3195.

438. Ye J, Xu JM, Song JX, Wu HS, Zhang HW, Wu J, Zhou P. Flexible spectral manipulation property of a high power linearly polarized random fiber laser. *Sci Rep* **2018**;*8*:2173.

439. Ye J, Xu JM, Song JX, Wu HS, Zhang HW, Wu J, Zhou P. Spectrum-agile hundred-watt-level high-power random fiber laser enabled by watt-level tunable optical filter. *Appl Phys Express* **2018**;*11*:062704.

440. Ye J, Xu JM, Zhang Y, Song JX, Yong LJ, Zhou P. Spectrum-manipulable hundred-watt-level high-power superfluorescent fiber source. *J Lightwave Technol* **2019**;*37*:3113.

441. Ye J, Fan CC, Xu JM, Xiao H, Leng JY, Zhou P. 2-kW-level superfluorescent fiber source with flexible wavelength and linewidth tunable characteristics. *High Power Laser Sci Eng.* **2021**;*9*:04000e55.

442. Birks TA, Gris-Sánchez I, Yerolatsitis S, Leon-Saval SG, Thomson RR. The photonic lantern. *Adv Opt Photonics* **2015**;*7*:107.

443. Montoya J, Aleshire C, Hwang C, Fontaine NK, Velazquez-Benitez A, Martz DH, Fan TY, Ripin D. Photonic lantern adaptive spatial mode control in LMA fiber amplifiers. *Opt Express* **2016**;*24*:3405.

444. Noordegraaf D, Skovgaard PMW, Maack MD, Bland-Hawthorn J, Haynes R, Lægsgaard J. Multi-mode to single-mode conversion in a 61 port photonic lantern. *Opt Express* **2010**;*18*:4673.

445. Ryf R, Fontaine NK, Montoliu M, Randel S, Ercan B, Chen H, Chandrasekhar S, Gnauck AH, Leon-Saval SG, Bland-Hawthorn J, Salazar-Gil JR, Sun Y, Lingle R, editors. Photonic-lantern-based mode multiplexers for few-mode-fiber transmission. In: Optical fiber communication conference, 2014/03/09. San Francisco, California: Optica Publishing Group; **2014**.

446. Eznaveh ZS, Zacarias JCA, Lopez JEA, Shi K, Milione G, Jung Y, Thomsen BC, Richardson DJ, Fontaine N, Leon-Saval SG, Correa RA. Photonic lantern broadband orbital angular momentum mode multiplexer. *Opt Express* **2018**;*26*:30042.

447. Wittek S, Bustos Ramirez R, Alvarado Zacarias J, Sanjabi Eznaveh Z, Bradford J, Lopez Galmiche G, Zhang D, Zhu W, Antonio-Lopez J, Shah L, Amezcua CR. Mode-selective amplification in a large mode area Yb-doped fiber using a photonic lantern. *Opt Lett* **2016**;*41*:2157.

448. Montoya J, Hwang C, Martz D, Aleshire C, Fan TY, Ripin DJ. Photonic lantern kW-class fiber amplifier. *Opt Express* **2017**;*25*:27543.

449. Huang B, Zacarias JCA, Liu H, Fontaine NK, Chen HS, Ryf R, Poletti F, Hayes JR, Antonio-Loppez J, Zhao J, Correa RA, Li G. Triple-clad photonic lanterns for mode scaling. *Opt Express* **2018**;*26*:13390.

450. Lu Y, Liu WU, Chen ZL, Jiang M, Zhou Q, Zhang JB, Li CJ, Chai JY, Jiang ZF. Spatial mode control based on photonic lanterns. *Opt Express* **2021**;*29*:41788.

451. Chang HX, Chang Q, Xi JC, Hou TY, Su RT, Ma PF, Wu J, Li C, Jiang M, Ma YX, Zhou P. First experimental demonstration of coherent beam combining of more than 100 beams. *Photonics Res* **1943**;*2020*:8.

452. Ma PF, Chang HX, Ma YX, Su RT, Qi YF, Wu J, Li C, Long JH, Lai WC, Chang Q, Hou TY, Zhou P, Zhou J. 7.1 kW coherent beam combining system based on a seven-channel fiber amplifier array. *Opt Laser Technol* **2021**;*140*:107016.

453. Prossotowicz M, Heimes A, Flamm D, Jansen F, Otto H-J, Budnicki A, Killi A, Morgner U. Coherent beam combining with micro-lens arrays. *Opt Lett* **2020**;*45*:6728.

454. Wang N, Zacarias JCA, Antonio-Lopez JE, Eznaveh ZS, Gonnet C, Sillard P, Leon-Saval S, Schülzgen A, Li G, Amezcua-Correa R. Transverse mode-switchable fiber laser based on a photonic lantern. *Opt Express* **2018**;*26*:32777.

455. Li HX, Yan K, Zhang YM, Gu C, Yao PJ, Xu LX, Zhang R, Su JQ, Chen W, Zhu YG, Zhan QW. Low-threshold high-efficiency all-fiber laser generating cylindrical vector beams operated in LP$_{11}$ mode throughout the entire cavity. *Appl Phys Express* **2018**;*11*:122502.

456. O'dea B, Farrow RL, Victor B, Lugo J, Hawke R, Gross K, Hodges A, Brown A, Nelson M, Foley B, Chen Y, Almonte K, Dye D, Reynolds M, Kennedy K, Swenson D, Kliner D, Dudley A, Laskin AV. Variable beam high power fiber laser with optimized beam characteristics for metal cutting. In: Laser beam shaping XIX, **2019**.

457. Lu JF, Meng LH, Shi F, Liu XM, Luo ZQ, Yan PG, Huang LJ, Pang FF, Wang TY, Zeng XL, Zhou P. Dynamic mode-switchable optical vortex beams using acousto-optic mode converter. *Opt Lett* **2018**;*43*:5841.

458. Zhang XC, Zhang WD, Li CY, Mao D, Gao F, Huang LG, Yang DX, Mei T, Zhao JL. All-fiber cylindrical vector beams laser based on an acoustically-induced fiber grating. *J Opt* **2018**;*20*:075608.

459. Wu HS, Lu JF, Huang LJ, Zeng XL, Zhou P. All-fiber laser with agile mode-switching capability through intra-cavity conversion. *IEEE Photonics J.* **2019**;*1*.

460. Lu JF, Shi F, Meng LH, Zhang LK, Teng LP, Luo ZQ, Yan PG, Pang FF, Zeng XL. Real-time observation of vortex mode switching in a narrow-linewidth mode-locked fiber laser. *Photonics Res* **2020**;*8*:1203.

461. Meng L, Lu J, Shi F, Xu J, Zhang L, Yao H, Zeng X. Multi-orthogonal high-order mode converter based on acoustically induced fiber gratings. *IEEE Photonics Technol Lett* **2020**;*32*:819.

462. Shi F, Lu J, Meng L, Cheng P, Liu X, Pang F, Zeng X. All-fiber method for real-time transverse-mode switching of ultrashort pulse. *IEEE Photonics Technol Lett* **2020**;*32*:97.

463. Xu JT, Zhang LK, Liu X, Zhang L, Lu J, Wang LT, Zeng XL. Dynamic vortex mode-switchable erbium-doped Brillouin laser pumped by high-order mode. *Opt Lett* **2021**;*46*:468.

464. Wu HS, Xu JT, Huang LJ, Zeng XL, Zhou P. High-power fiber laser with real-time mode switchability. *Chin Opt Lett* **2022**;*20*:021402.

465. Yang L, Jiang Tao X, Yi Zhu C, Tian Fu Y, Yi A, Chen Chen F, Liang Jin H, Xiang Long Z, Pu Z, editors. Mode control on all-fiberized Raman fiber amplifier based on acoustically-induced fiber grating. In: Proc. SPIE, **2020**.

466. Shiraishi K, Sugaya S, Kawakami S. Fiber Faraday rotator. *Appl Opt* **1984**;*23*:1103.

467. Ballato J, Snitzer E. Fabrication of fibers with high rare-earth concentrations for Faraday isolator applications. *Appl Opt* **1995**;*34*:6848.

468. Sun L, Jiang S, Zuegel JD, Marciante JR. All-fiber optical isolator based on Faraday rotation in highly terbium-doped fiber. *Opt Lett* **2010**;*35*:706.

469. Sun L, Jiang S, Marciante JR. All-fiber optical faraday mirror using 56-wt%-terbium-doped fiber. *IEEE Photonics Technol Lett* **2010**;*22*:999.

470. Sun L, Jiang S, Marciante JR. Compact all-fiber optical Faraday components using 65-wt%-terbium–doped fiber with a record Verdet constant of −32 rad/(Tm). *Opt Express* **2010**;*18*:12191.

471. AdValue Photonics. June 11, 2014: AdValue photonics wins a second 2014 R&D 100 Award for its high power all fiber isolator. https://www.advaluephotonics.com/news-events/news-archive.

472. AdValue Photonics. 50W 1 micron high power fiber isolator. https://www.advaluephotonics.com/images/pdfs/products/AP-aISO-17-3.pdf.

473. Ju S, Kim Y, Watekar PR, Jeong S, Han W-T, editors. Development of a novel all-optical fiber isolator using a CdSe quantum dots doped optical fiber. In: Optical Fiber communication conference; 2012/03/04. Los Angeles, California: Optica Publishing Group; **2012**.

474. Ju S, Jeong S, Kim Y, Watekar PR, Han W. Demonstration of all-optical fiber isolator based on a CdSe quantum dots doped optical fiber operating at 660 nm. *J Lightwave Technol* **2013**;*31*:2793.

475. Linganna K, Ju S, Lee Y, Han WT. Development of alumino-silicate glass fiber doped with high Pr^{3+} concentration for all-optical fiber isolator application. *J Mater Sci Mater Electron* **2019**;*30*:12790.

476. Hansen KR. Transverse mode instability in high-power ytterbium doped fiber amplifiers. Lyngby: Technical University of Denmark; **2012**.

477. Ramachandran S, Khitrov V, Minelly JD, Tumminelli R, Petit V, Pooler ES. 3kW single-mode direct diode-pumped fiber laser. In: Fiber lasers XI: technology, systems, and applications, **2014**.

478. Hupel C, Kuhn S, Hein S, Haarlammert N, Nold J, Beier F, Sattler B, Schreiber T, Eberhardt R, Tünnermann A, editors. MCVD based fabrication of low-Na fibers for high power fiber laser application. In: advanced solid state lasers, 2015/10/04. Berlin: Optical Society of America; **2015**.

479. Jain D, Jung Y, Barua P, Alam S, Sahu JK. Demonstration of ultra-low NA rare-earth doped step index fiber for applications in high power fiber lasers. *Opt Express* **2015**;*23*:7407.

480. Ballato J, Petit V, Tumminelli RP, Minelly JD, Khitrov V. Extremely low NA Yb doped preforms (<0.03) fabricated by MCVD. In: Fiber lasers XIII: technology, systems, and applications, **2016**.

481. Beier F, Hupel C, Nold J, Kuhn S, Hein S, Ihring J, Sattler B, Haarlammert N, Schreiber T, Eberhardt R, Tünnermann A. Narrow linewidth, single mode 3 kW average power from a directly diode pumped ytterbium-doped low NA fiber amplifier. *Opt Express* **2016**;*24*:6011–20.

482. Kong FT, Dunn C, Parsons J, Kalichevsky-Dong MT, Hawkins TW, Jones M, Dong L. Large-mode-area fibers operating near single-mode regime. *Opt Express* **2016**;*24*:10295.

483. Beier F, Möller F, Sattler B, Nold J, Liem A, Hupel C, Kuhn S, Hein S, Haarlammert N, Schreiber T, Eberhardt R, Tünnermann A. Experimental investigations on the TMI thresholds of low-NA Yb-doped single-mode fibers. *Opt Lett* **2018**;*43*:1291–4.

484. Sidharthan R, Lin D, Jie Lim K, Li H, Huiting Lim S, Jian Chang C, Men Seng Y, Liang Chua S, Jung Y, Richardson DJ, Yoo S. Ultra-low NA step-index large mode area Yb-doped fiber with a germanium doped cladding for high power pulse amplification. *Opt Lett* **2020**;*45*:3828–31.

485. Kuhn S, Hein S, Hupel C, Nold J, Stutzki F, Haarlammert N, Schreiber T, Eberhardt R, Tünnermann A, editors. High-power fiber laser materials: influence of fabrication methods and codopants on optical properties. In: Proc. SPIE, **2019**.

486. Ma XY, Ye J, Zhang Y, Xu JM, Huang LJ, Leng JY, Pan ZY, Zhou P. Hundred-watt-level phosphosilicate Raman fiber laser with less than 1% quantum defect. *Opt Lett* **2021**;*46*:2662.

487. Ma X, Xu J, Ye J, Zhang Y, Huang L, Yao T, Leng J, Pan Z, Zhou P. Cladding-pumped Raman fiber laser with 0.78% quantum defect enabled by phosphorus-doped fiber. *High Power Laser Sci Eng* **2022**;*10*:010000e8.

488. Zhang Y, Xu J, Li S, Liang J, Ye J, Ma X, Yao T, Zhou P. Phosphosilicate fiber-based low quantum defect Raman fiber laser with ultrahigh spectral purity. *Nanomaterials* **2022**;*12*:1490.

489. Nicholson JW, Yablon AD, Ramachandran S, Ghalmi S. Spatially and spectrally resolved imaging of modal content in large-mode-area fibers. *Opt Express* **2008**;*16*:7233.

490. Flamm D, Schulze C, Naidoo D, Schroter S, Forbes A, Duparre M. All-digital holographic tool for mode excitation and analysis in optical fibers. *J Lightwave Technol* **2013**;*31*:1023.

491. Huang LJ, Guo SF, Leng JY, Lu HB, Zhou P, Cheng XA. Real-time mode decomposition for few-mode fiber based on numerical method. *Opt Express* **2015**;*23*:4620.

492. Christensen SL, Michieletto M, Johansen MM, Maack MD, Lægsgaard J. Observation of dynamical eigenmodes induced by the moving refractive index grating of TMI in a rod amplifier. *Opt Lett* **2021**;*46*:5755.

493. Simon LC, Mette MJ, Mattia M, Marco T, Martin DM, Jesper L, editors. Study of seeding mechanisms of TMI with spatially and temporally resolved imaging. In: Proc. SPIE, **2021**.

494. Jiang M, Wu HS, An Y, Hou TY, Chang Q, Huang LJ, Li J, Su RT, Zhou P. Fiber laser development enabled by machine learning: review and prospect. *PhotoniX* **2022**;*3*:16.

495. An Y, Huang LJ, Li J, Leng JY, Yang LJ, Zhou P. Learning to decompose the modes in few-mode fibers with deep convolutional neural network. *Opt Express* **2019**;*27*:10127.

496. An Y, Li J, Huang LJ, Leng JY, Yang LJ, Zhou P. Deep learning enabled superfast and accurate M(2) evaluation for fiber beams. *Opt Express* **2019**;*27*:18683.

Xiao Chen received the Master's degree in optical engineering from the National University of Defense Technology, in 2021. He is currently a Ph.D. candidate with the College of Advanced Interdisciplinary Studies. His current research interests include specialty fibers design and characterization, laser beam diagnosis and high-power fiber lasers.
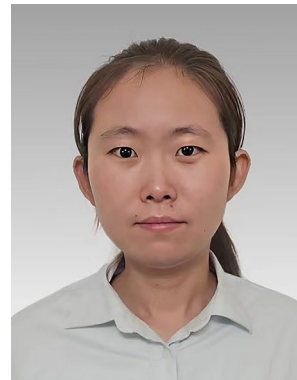
Tianfu Yao received the Doctor's degrees in optoelectronics from the Optoelectronics Research Centre, University of Southampton (UK) in 2014. She is currently an associate research fellow with the College of Advanced Interdisciplinary Studies, National University of Defense Technology. Her research interests include Raman fiber lasers and nonlinear optics for wavelength conversion. She has completed the projects of Chinese National Natural Science Foundation, China Postdoctoral Science Foundation and so on as the chief investigator. She is author or co-author of more than 50 journal papers in the field of laser physics.

Liangjin Huang received the Doctor's degree in optical engineering from the National University of Defense Technology, in 2016. He is currently an associate research fellow with the College of Advanced Interdisciplinary Studies, National University of Defense Technology. His research interests include specialty optical fibers, fiber material and fabrication, mode decomposition, and high-power fiber lasers.

Yi An received the Master's degree in optical engineering from the National University of Defense Technology, Changsha, China, in 2019, where he is a currently pursuing the Doctor's degree with the College of Advanced Interdisciplinary Studies. His current research interests include fiber design and characterization, machine learning, mode decomposition technique, and high-power fiber lasers.

Zhiyong Pan is currently a senior engineer with the College of Advanced Interdisciplinary Studies, National University of Defense Technology. He has long been engaged in the design, fabrication and application of rare-earth doped laser fibers. He has more than 20 years of experience in the research of specialty optical fibers.

Hanshuo Wu received the B.S. degree in optical engineering from the Zhejiang University in 2015, and M.S. and Ph.D. degrees in optical engineering from the National University of Defense Technology in 2017 and 2022, respectively. He is currently a research associate with the College of Advanced Interdisciplinary Studies, National University of Defense Technology. His research interests focus on specialty optical fibers design and high-power fiber lasers.

Pu Zhou is a professor in National University of Defense Technology. Currently, his research interests include High-power Fiber Lasers, Beam Combination, and AI & Laser. He has achieved a series of original results in the field of high-power fiber lasers, high-power narrow-linewidth/single-frequency fiber lasers, coherent/spectral beam combination, laser beam diagnosis, etc.